A Parametric Representation and Classification of Sandy Beach Profiles

Case Study of Narrabeen-Collaroy

CIEM0500: Master's Dissertation

M. Julseth

TUDelft

A Parametric Representation and Classification of Sandy Beach Profiles

Case Study of Narrabeen-Collaroy

by

M. Julseth

To obtain the degree of Master of Science
at the Delft University of Technology, to be defended
publicly on Friday, June 28th, 2024 at 10:00AM.

TUDelft

Acknowledgements

Summary

Coastal areas are highly dynamic systems sensitive to natural and anthropogenic change. The range of social, economic, and environmental functions served by diverse coastal environments makes understanding their geomorphology valuable. Parametric shape functions have historically been used to represent the cross shore profile of specific coastal environments. Geometric (consequential) parameters of these functions are often related to parameters representing key morphological drivers (causal parameters) to provide first order predictive capabilities. Advances in the application of data-driven modelling techniques presents opportunity to develop a unified characterization of cross shore morphology in diverse coastal environments. However, the ability to represent diverse profile geometries using a single parametric representation has not been observed. The aim of this study is therefore to evaluate the ability of parametric expressions to effectively characterize diverse coastal profile geometries. Here, a new parametric function is presented that can effectively represent key geometric attributes of diverse cross shore profiles. This function demonstrated high performance in the representation of both theoretical profile morphotypes ($\overline{SSE}$ = 0.04) and measured profile data from Narrabeen-Collaroy Beach, Australia ($\overline{RMSE}$ = 0.05 m) compared to eight existing parametric functions. Parametric values were effectively applied to group profiles with similar geometry using manual labelling and K-means clustering. The average profile of each cluster (i.e., the cluster centroid) provided a good representation of the grouped profiles, particularly when parametric grouping was used in place of empirical grouping. Correlation analyses between causal and consequential parameters demonstrated an ability to identify expected geomorphological trends using the new parametric function. Application of cluster centroids for correlation analysis provided amplified correlation strengths for expected geomorphological relationships, particularly when clustering with fitted parametric values. These results suggest that a parametric representation of the coastal profile has potential to characterize and group diverse profile geometries, and that causal-consequential parameter relationships have potential to identify geomorphological trends. The application of these results provide a foundation for the development of a predictive coastal profile model. This model could be trained using data from diverse coastal environments to predict coastal profile response to changes in the metocean climate related to human interventions and climate change.

Plain Language Summary

Coastal areas are sensitive to erosion and accretion caused by natural processes and human influence, such as extreme storms, coastal development, and climate change. Protecting and managing coastal environments is valuable because they provide economic and social opportunities to humans, and are home to a range of diverse species, such as shellfish, plants, and birds. Elevation profiles measured perpendicular to the shore (i.e., cross shore profiles) can be used to understand the geometry and behaviour of coastal environments. Mathematical functions have historically been used to represent these profiles. These functions contain parameters that represent certain aspects of the profile shape and can be adjusted to match the function shape with a measured profile. The values of these fitted parameters help give numerical meaning to the attributes of cross shore profile data, allowing scientists and engineers to understand how certain coastal environments typically behave. However, it is challenging to represent different coastal environments with a single mathematical function because the cross shore profile shapes can be very different. The aim of this study is therefore to evaluate the ability of parametric expressions to effectively characterize diverse coastal profile geometries. Here, a new mathematical function is presented that can represent cross shore profiles with a wide range in geometry. This new function was able to match the shape of different cross shore profiles from literature better than eight other existing functions, and was also able to match the shape of a large amount of measured cross shore profiles from Narrabeen-Collaroy Beach, Australia ($\overline{SSE}$ = 0.04, $\overline{RMSE}$ = 0.05 m, respectively). The numerical values of the fitted parameters from the function were then used to group the measured cross shore profiles according to their geometry, using both manually defined categories and a data grouping algorithm called K-means clustering. Analysis of the data grouping algorithm results showed that grouped measured profiles could be effectively represented using the average of the grouped profiles, especially if the profiles were grouped using the fitted parameters of the new mathematical function. Next, the fitted parameters from the function were correlated to average wave and tide conditions from the same measurement location for a series of time frames before each profile measurement. The resulting correlations showed that the relation of fitted parameters and average wave and tide statistics can effectively identify the expected coastal profile behaviour. Additionally, using the averaged group profiles in the correlation analysis resulted in stronger correlations between the fitted parameters and the wave and tide statistics. These results suggest that fitted parameters for cross shore profiles have potential to describe and group different measured profiles, and can be related to wave and tide statistics to identify trends in profile shapes. These results could be applied to make predictions of the cross shore profile shape based on measured wave and tide statistics. Collecting data from different coastal environments and using it to guide the predictions could help coastal engineers and scientists understand how certain coastal environments will react to changes associated with coastal development and climate change.

Contents

List of Figures

List of Tables

Nomenclature

Abbreviations

Term	Definition
AHD	Australian Height Datum
BFGS	Broyden-Fletcher-Goldfarb-Shanno algorithm; a minimization algorithm
L-BFGS-B	Limited Memory BFGS Bounded algorithm; a minimization algorithm
MHHW	Mean Higher High Water; the mean value of the highest observed daily high tides
MHW	Mean High Water; the mean value of all observed high tides
MLLW	Mean Lower Low Water; the mean value of the lowest observed daily low tides
MLW	Mean Low Water; the mean value of all observed low tides
MSL	Mean Sea Level; the mean value of all observed water levels
RMSE	Root Mean Square Error
RQ	Research Question
RTR	Relative Tidal Range
SED	Squared Euclidean Distance
SLSQP	Sequential Least Squares Programming; a minimization algorithm
SSE	Sum of Squared Error
TN	True North; an angular reference system where North is set to $0°$
TR	Tidal Range; the difference between the maximum and minimum observed tidal levels

Symbols

Symbol	Definition	Typ. Unit
A, $A_{1,2}$	Profile scale and shape parameters	$[m^{1-n}]$
β	Profile slope	$[°]$
B, $B_{1,2,3}$	Profile shape and scale parameters	$[m]$, $[-]$
C	Profile elevation or steepness parameter	$[m]$, $[-]$
Cg	Wave group celerity	$[m\ s^{-1}]$
$\delta_{0,1}$	Profile slope transition scale parameter	$[m]$
D_{50}	Median sediment grain size	$[mm]$
d_i	Outer depth of closure	$[m]$
d_l	Inner depth of closure	$[m]$
ϵ	Wave steepness	$[-]$
Ef	Exposure factor	$[-]$
ϕ	Wave angle of incidence	$[°]$
FI	Orthogonal fetch length	$[m]$
g	Acceleration due to gravity	$[m\ s^{-2}]$
η	Water level set-up	$[m]$
H_b	Breaking wave height	$[m]$
H_e	Effective wave height	$[m]$
H_s	Significant wave height	$[m]$
h_b, h_c, h_s, h_t	Vertical distance parameters for stated profile features	$[m]$
$h(x)$	Profile elevation observed at cross shore distance, x	$[m]$
$\bar{i}$	mean of a given variable, i	unit of i
K	Number of clusters for clustering analysis	$[-]$
k	Profile curvature parameter	$[m^{-1}]$
L	Wave length	$[m]$
$L_{0,1}$	Profile length scale parameters	$[m]$
M_s	Marginal shoal width	$[m]$

Symbol	Definition	Typ. Unit
m_0	Beach face slope	[-]
N	Number of data points in a given sample	[-]
$n, n_{1,2,3}$	Profile shape exponential parameters	[-]
Ω	Dimensionless sediment fall velocity	[-]
P	Total wave energy flux (wave power in text)	[W m^{-1}]
P_{LS}	Alongshore component of wave power	[W m^{-1}]
ρ	Density	[kg m^{-3}]
R_i	Rank of random variable, i	[-]
$r_{i,j}$	Rank correlation between random variables i and j	[-]
σ_i	standard deviation of a given variable, i	unit of i
$S_{1,2,3}$	Profile slope parameters	[-]
s	Profile slope function	[-]
T	Wave period	[s]
T_p	Peak wave period	[s]
τ_{wind}	Wind induced shear stress	[Pa]
u	Near-bed flow velocity	[m s^{-1}]
$\overline{u}$	Time-averaged component of near-bed flow velocity	[m s^{-1}]
u_{hi}	High-frequency oscillatory component of near-bed flow velocity	[m s^{-1}]
u_{lo}	Low-frequency oscillatory component of near-bed flow velocity	[m s^{-1}]
W_s	Sediment fall velocity	[m s^{-1}]
x	Cross shore distance	[m]
x_b, x_c, x_s, x_t	Horizontal distance parameters for stated profile features	[m]
y_{obs}	Measured elevation profile	[m]
y_{pred}	Predicted elevation profile	[m]
z_b	Profile bed level function	[-]
$z_{0,1}$	Profile elevation parameters	[m]

1

Introduction

Chapter Outline
In this chapter the motivation and significance of the research is presented, detailing the need for improved first order profile estimation techniques for diverse coastal environments. The scope of the study and the related research questions are then presented to provide a foundation for the development of a predictive model through parametric representation of profile geometry and driving morphological factors. A brief approach for the research is then given indicating that parametric representations will be applied to characterize diverse profile geometries in a sandy beach environment and used to identify expected geomorphological processes.

1.1. Motivation

Coastal areas are highly dynamic systems influenced by a range of natural and anthropogenic factors, including biological organisms, natural phenomena like storms and floods, changes to the global climate, and human activities like infrastructure development and recreation. The interventions that humans make to coastal environments serve a series of social, ecological, and economic functions, and include activities like beach nourishment, artificial beach construction, dike and seawall development, wetland restoration, and offshore energy production. The value of coastal environments in modern society makes the understanding of complex coastal behaviour in diverse environments important. These complexities are amplified by a changing global climate, resulting in altered hydrodynamic and wave characteristics relevant for coastal engineering. The following research aims to address this complexity through the study of coastal profile morphology. This research forms the basis for the development of tools to predict coastal profiles in diverse environments influenced by natural and anthropogenic change. Future applications of this research have potential to aid in the design of robust coastal interventions through an improved understanding of coastal profile development and response.

1.1.1. Climate Change Impacts

Climate change is defined as long-term changes to average weather patterns on local to global spatial scales (NASA, 2024). Climate change is acutely driven by the burning of fossil fuels, increasing the concentration of greenhouse gases in the atmosphere, such as carbon dioxide and methane. The result is increased global average temperatures (+1.09°C 2011-2020 from 1850-1900), increased global mean sea levels (+0.2 m 1901-2018), increased rates of sea level rise (+2.4 mm/year 2006-2018 from 1901-1971), and long term changes to average weather patterns driving more frequent and intensified extreme weather events (IPCC, 2023). In coastal regions, changes to sea levels and extreme weather events have increased the likelihood of flood and storm related damages to the natural and built environment. Given that an estimated 2.15 billion people live in near-coastal areas (Reimann et al., 2023), these damages have direct implications to human livelihood. For example, in September 2023 Hurricane Fiona caused mass destruction in Atlantic Canada, fuelled by warmer than average sea surface temperatures that allowed the storm to retain its strength while travelling North along the Atlantic coast of the USA (Snoddon, 2023). The result was Atlantic Canada's costliest extreme weather event on record, with storm surge and extreme waves causing significant erosion and coastal flooding (Figure 1.1). This event lead to three deaths and an estimated $800 million (CAD) in insured losses in Canada alone (Pasch et al., 2023).

Figure 1.1: (a) Track of Hurricane Fiona following the eastern coast of North America, making landfall in Atlantic Canada (IBTrACS, 2022); (b) Before and after photos showing significant dune erosion on Prince Edward Island, Canada following high storm surge and wave action due to Hurricane Fiona (CoastSnap, 2022).

Increases in the global mean sea level as a result of climate change allows waves to travel further nearshore before dissipating. As a result, the upper part of the shoreface is more exposed to processes driving sediment transport. Additionally, climate change has resulted in changes to the oceanic wave climate, with 0.4% per year increases in global wave power since 1948 (Reguero et al., 2019). Water levels in water bodies governed by hydrological processes will also be affected by climate change. However, the impact of climate change on these systems is not equal across geographic regions. For instance, extreme heat events leading to droughts may occur in some regions, while extreme rain events leading to flooding may occur in others. Further, extreme dry periods followed by extreme wet periods have the potential to cause major fluctuations in the water levels of inland water bodies. As cross shore coastal profiles tend to respond to their local forcing conditions, changing water levels and wave climates in discrete coastal environments have the potential to change the profile shapes within these systems. The magnitude of these changes however is uncertain, and typically requires case-specific analysis to quantify.

Past studies have applied various methods to quantify the magnitude of change expected of the coastal profile given altered water levels and wave climates. The simplest of these methods is the Bruun rule, which applies the concept of profile equilibrium to estimate shoreline position and cross shore profile changes as a function of sea level rise (Bosboom & Stive, 2021; Bruun, 1962). Despite its widespread use in both coastal engineering studies and research, the validity of the Bruun rule for natural coastlines has been largely contested given its restrictive underlying assumptions (Bosboom & Stive, 2021; Cooper & Pilkey, 2004). Despite the resulting preference for more sophisticated process based models such as xbeach and unibest, the Bruun rule continues to appear when computing first order estimates of profile shape and position. The continued use of the Bruun rule is expected to be a result of its ease of use and interpretation, long-standing presence in coastal engineering literature, and lack of equally simple alternatives (Cooper & Pilkey, 2004). The application of measured data presents a potential alternative for first order estimates of profile response to change. If the measured geometry of diverse coastal profiles can be quantitatively related to metocean statistics and physical site characteristics (i.e., sediment information), then estimates could be made about coastal profile geometry for a system with a changing metocean climate. The present study develops the basis for the construction of such a data-driven coastal profile predictive model.

1.1.2. Human Intervention Impacts

The proximity of human civilization to coastal areas and the resulting value of coastal regions for social, ecological, and economic prosperity has resulted in continued human intervention in coastal environments. These interventions are diverse and include various types of infrastructure, including offshore wind and wave farms, hard structures such as sea walls, break waters and groynes, soft structures such as artificial beaches, local beach nourishment, and mega-nourishment, and living-shoreline developments such as dune grass and mangrove planting. A human intervention is thus defined here as any meditated development or altercation made by human beings within a given coastal environment. As the present study is focused on coastal profile behaviour, so-called "hard" interventions (i.e., sea-walls, breakwaters, harbours) are less relevant here. The interventions that humans make in coastal environments are relevant to the present study for two primary reasons; human interventions can impact the natural environment, and changing natural conditions can impact the behaviour and lifespan of human interventions.

Human interventions have the ability to alter the natural characteristics and processes of coastal environments, either by design or not. For instance, a beach nourishment that employs sediment with different characteristics (i.e., grain size, density, porosity) from the local material will result in changes to the observed cross shore profile (Figure 1.2). This observation is well represented in coastal engineering and design literature through studies of profile equilibrium (Dean, 1977, 1991), empirical records (Bujan et al., 2019), and best practice guidelines (Haney et al., 2007; Schasfoort & Janssen, 2013). It is generally supported that analysis of profile response to the intended design parameters, such as nourishment sediment characteristics, is a necessary step in the design process. The development of a data-driven tool relating metocean statistics and physical site characteristics to profile geometry would allow designers to conduct thorough feasibility assessments with quantified uncertainty, and is therefore valuable. Further, a tool such as this could be applied during impact assessments for inter-

ventions indirectly related to nearshore coastal environments. For instance, studies in wave-powered marine renewable energy have demonstrated that offshore wave farms can influence the nearshore wave climate (Millar et al., 2007; Palha et al., 2010). The importance of wave characteristics to the coastal profile has been demonstrated repeatedly in the literature, and is generally accepted as a governing factor of profile geometry in a wide range of environments. As such, changes to the nearshore wave climate resulting from a human intervention can lead to further unintended changes to the coastal profile, and should therefore be studied prior to development.
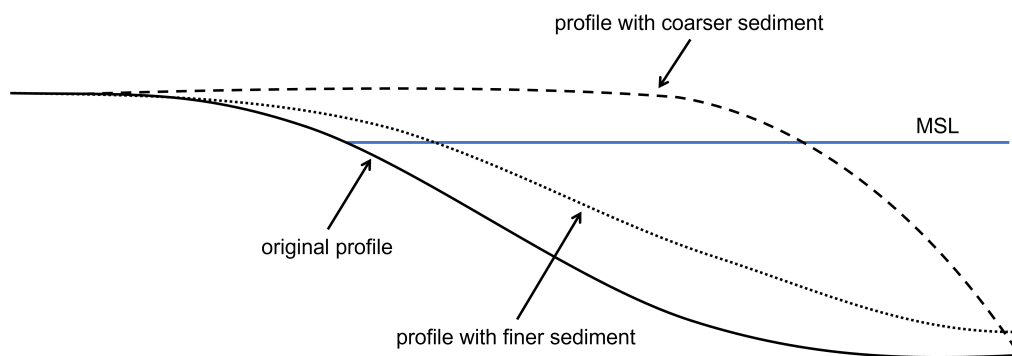
Figure 1.2: Conceptual visualization of the relative impact of sediment grain size on a nourished cross shore profile, where sediment coarser than the original profile leads to steepening and sediment finer than the original profile leads to flattening.

As discussed in Section 1.1.1, changes to the metocean climate have the potential to impact coastal profile shapes. As such, climate change has the potential to change the behaviour and lifespan of human interventions along the coast. As increasing value is placed on the use of nature-based or nature-driven coastal engineering interventions, it is important to assess the resilience of these interventions to a changing climate. In particular, consideration of the temporal and spatial scales of variability in the climate and thus the beach state is integral to the design of robust yet innovative coastal interventions which apply nature-based concepts. The temporal scale considered when assessing coastal profile response should therefore be long enough as to smooth small-scale features, but short enough as to resolve cyclical profile behaviour. The use of measured data from diverse environments may be useful for this, and can be applied using parametric representations of profile geometry to reduce small-scale complexities present in the empirical data. A suitable parametric representation is therefore required which can satisfy a series of requirements, including the ability to fit a diverse range of measured profiles and be applied to identify profile morphotypes. An ideal parametric representation would further provide a clear representation of geometric characteristics (i.e., section lengths, slopes, and key elevations) that could easily be related to relevant metocean statistics and physical characteristics (i.e., wave information, water level information, and sediment information).

1.2. Research Significance

The study of cross shore transport and coastal profile development with respect to incident metocean conditions has been an area of interest in the coastal engineering research community for some time. The first notable attempts to characterize this process came from Bowen (1980), Bruun (1954), and Dean (1977, 1991), which focused on the characterization of dynamic equilibrium profiles using both semi-empirical and analytical formulations. Following these initial formulations, various numerical models were developed using the concepts of energy and mass balance, which can describe shorter timescale coastal profile development and response of sandy, high energy systems in great detail (i.e., xbeach, unibest, Delft3D) (Reeve et al., 2016). Greater uncertainty exists in the modelling of coastal environments with diverse energy conditions and physical characteristics due to a limited understanding of low energy morphodynamic behaviour (Ton et al., 2021). Several studies (both at TU Delft and elsewhere) have aimed to address this knowledge gap to help characterize coastal profile behaviour in diverse low energy systems such as tidal flats, estuaries, and inland lakes (for instance in Bearman et al. (2010), Hanssen et al. (2022), Hegge et al. (1996), Makaske and Augustinus (1998), Ton et al. (2021), and Travers (2007)). These studies have analyzed the spatial trends in coastal profiles as well as the underlying processes effecting low energy morphological evolution.

The primary focus of coastal morphology studies is generally to characterize the morphological behaviour of a specific coastal environment. Despite the large amount of available information about the morphological response of high energy coastlines, and the growing available information about low energy coastlines, deriving general conclusions regarding the expected response of a coastal profile with unique physical characteristics and forcing conditions remains a challenge. The ability to unify the morphological behaviour of coastal environments with diverse physical and metocean conditions is valuable, as it would allow for prediction of changes to coastal profiles caused by changes in local conditions. This analysis can be reduced to focus on discrete coastal environments through quantification of a single system's response to variable forcing, as initially explored by Wright and Short (1984) when defining the concept of beach states. Several studies have since expanded on this work for low energy systems by identifying coastal profile morphotypes as a function of exposure (Hegge et al., 1996; Makaske & Augustinus, 1998; Travers, 2007). These studies demonstrate that measured profiles from diverse environments can be categorized using attributes of their profile geometry. This categorization could be made easier through profile parameterization. However, an assessment of the applicability of profile parameterizations to fit and geometrically quantify diverse profile morphotypes has not been conducted. The use of profile parameterizations is valuable given the proven capability to describe profile geometry parameters as a function of physical site characteristics and metocean conditions. The connection of coastal morphotypes from diverse environments to profile parameterizations could provide a clear pathway to establish simple yet effective profile geometry predictions.

1.3. Scope & Research Questions

1.3.1. Scope
This research project aims to study the ability to use parametric representations of coastal profile geometry and driving morphological factors to characterize diverse coastal profiles in sandy beach environments. The first goal of the research is to identify a set of parameters that effectively describe a wide range of physical site characteristics, hydrodynamic conditions (collectively the "causal" parameters), and geometric characteristics of the coastal profile (the "consequential" parameters). An example set of potential causal parameters include median sediment grain size (D50), significant wave height (Hs), peak wave period (Tp), and tidal range (TR). An example set of potential consequential parameters include the beach slope, depth of closure, and degree of profile concavity. If the profile is represented using a parametric shape function, then the consequential parameters become the set of free parameters that impact the profile shape. It is thus important for interpretation that these free parameters have a clear connection to characteristics of the profile geometry. For instance, if the Dean profile were applied (Equation 1.1) then the consequential parameters would be A and n, which are used to minimize differences between the predicted profile depth at a given cross shore position $h(x)$, and the measured depth at the same position. Figure 1.3 demonstrates an example of measured profile representation using Equation 1.1 with a vertical translation. The measured profile for fitting in this example is taken from the Narrabeen-Collaroy Beach Survey Program (Turner et al., 2016).

$$h(x) = Ax^n \tag{1.1}$$

It has been demonstrated that the consequential parameters in this example govern the profile scale and shape, and can be related to the physical processes driving coastal morphology (Bruun, 1954; Dean, 1977, 1991). However, it has also been demonstrated that these parameters are interrelated, and are challenging to relate to singular distinct geometric characteristics (for instance in Are and Reimnitz, 2008), implying potential challenges for application in the present study. More complex shape functions can include additional consequential parameters describing discrete geometric characteristics, however the potential for overdetermination increases with the complexity of the parametric representation. A further summary of several existing parametric shape functions is presented in Chapter 2.
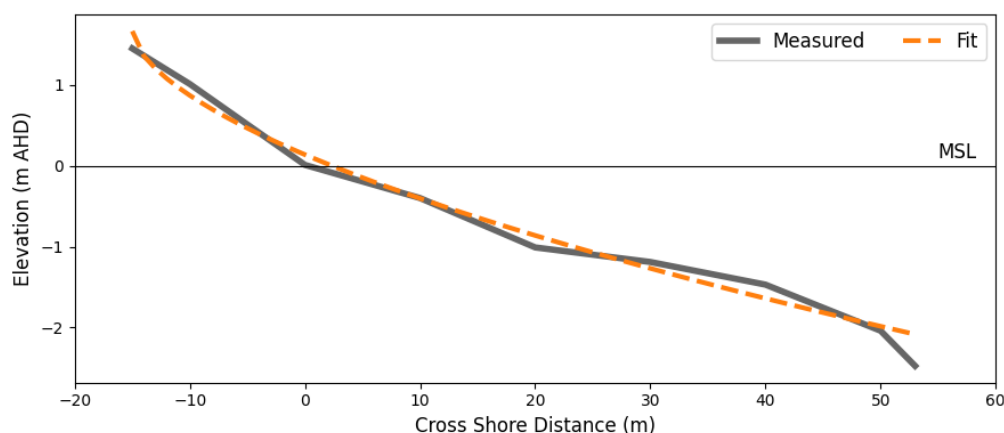
Figure 1.3: Fit to a measured cross shore profile from Narrabeen-Collaroy Beach, Australia, using Equation 1.1 (transect PF2, 1979-03-26). Fitted parametric values are A = 0.31, n = 0.59, and C = 1.66 m (where C is a vertical translation).

The second goal of the research is to use measured data to characterize the relationship between the causal and consequential parameters of a given coastal environment on timescales relevant to the assessment of engineering designs. Data collected from the Narrabeen-Collaroy Beach Survey Program is applied for this purpose. Although the use of data from a single region may be limiting in studying the full impact of causal parameter variability in diverse coastal environments, it is necessary to simplify the present study and develop a basis for future expansion of the work. Consequential parameters fit to discrete profile measurements from the study location are therefore used alongside the mean and standard deviation of causal parameters at various temporal scales to assess the relationship between the geometric attributes of the profile and morphological drivers.

The study does not include an assessment of profile development or wave transformation using existing process based and behavioural models, such as SWAN, xbeach, unibest, or Delft3D. As such, tests using these models are outside of the scope of work for the project. Comparisons to existing process based and behavioural models are considered outside of the scope of work for this project because the presently intended use case for this work is to develop a predictive model that may be used for first-order estimates of profile geometry only. It is strongly believed that process based and behavioural models remain important for coastal analyses, and should continue to be applied during more detailed studies until the proposed data-driven methods are sufficiently expanded and validated. Furthermore, the present study is limited to an analysis of sandy beach environments. Although future expansion to more diverse coastal environments is desireable, additional complexities associated with these environments (i.e., cohesive sediment, permafrost, hard-bottoms) are considered too great for the present study.

1.3.2. Research Questions
The following research questions aim to address key steps in developing a basis from which a predictive coastal profile model can be built. There are two primary research questions, each with a series of subquestions. The first primary question focuses on the representation of diverse coastal profiles using a set of consequential parameters and application of consequential parameters for profile classification. The second primary question focuses on identifying expected relationships between causal parameters and consequential parameters within measured data.

1. To what extent can coastal profile geometry of diverse coastal environments be unified using measured data and parametric shape functions?

    • To what degree of accuracy can parametric shape functions represent diverse coastal profile geometry?
    • Can a parametric shape function be used to effectively group and classify measured profile data?

2. How well can causal and consequential parameters characterize the geomorphological processes affecting cross shore profile geometry?

    • What is the impact of varying temporal scales to the distribution of causal parameters?
    • Are expected geomorphological processes identifiable through causal-consequential parametric correlation analysis?

1.3.3. Research Approach

To effectively answer the presented research questions (RQs), a series of steps were developed to clearly define the approach of the study. Step one, two, three, and four are related to RQ1, while step five and six are related to RQ2. A detailed outline of the applied approach is presented in Chapter 3.

1. Identify a set of diverse profile morphotypes previously identified in a sandy coastal environment.
2. Define a set of parametric expressions that can be used to characterize coastal profile geometry, and assess each expression's ability to fit the identified morphotypes using an optimization process.
3. Based on the results of morphotype fitting, select a parametric expression and fit the expression to a series of measured profiles using an optimization process, resulting in a set of fitted consequential parameters.
4. Group and classify the measured profile data using both parametric values and the empirical data itself, allowing for the identification of representative profiles for each profile group.
5. Identify a set of causal parameters that influence profile shape, and compute these causal parameters from available observations at the study location on multiple time scales.
6. Assess relationships between causal and consequential parameters using rank correlations. Compare observed correlations for the entire dataset to those of representative profiles with group mean causal parameters.

1.4. Thesis Outline

Chapter 2 presents the relevant background information for coastal profile development and characterization. Chapter 3 defines the methodology applied during the study, and provides a summary of the data which was used for the study's completion. Chapter 4 presents the results of the study. Chapter 5 provides a discussion of the results of this study and its applicability for future development. Finally, Chapter 6 presents a summary of the study, its relevant findings, and recommendations. Supplementary and supporting material is included in the appendices as directed within the text.

2

Background

Chapter Outline

In this chapter relevant background information is presented. Key background knowledge required for the interpretation of the following research includes an understanding of the processes driving nearshore sediment transport and thus cross shore morphology. Additionally, existing strategies for characterization of the cross shore profile are presented, including classification of common profile states and the parameterization of profile geometry and morphological drivers.

2.1. Cross Shore Morphology

A coastal profile is an elevation profile of the coast following a linear cross shore transect, typically extending from a subaerial reference point into the water. The cross shore profile can be divided into different zones according to the magnitude of the average incident metocean conditions and the water depth. Three primary zones of the coastal profile were described by Hallermeier (1981); the littoral zone or upper shoreface, the shoal zone or lower shoreface, and the offshore zone or shelf (Figure 2.1). The position of the boundaries between these zones are quantified using the concept of depth of closure. The landward boundary depth may be referred to as the inner depth of closure, and is defined as the maximum depth for nearshore erosion by annual extreme wave conditions (i.e., the wave height exceeded for 12 hours per year, or the effective wave height, H_e). The effective wave height, H_e, and inner depth of closure, d_l, can be approximated using Equation 2.1 and 2.2 (Birkemeier, 1985; Brutsche et al., 2016; Hallermeier, 1978).

$$H_e = \overline{H}_s + 5.6\sigma_s \tag{2.1}$$

$$d_l = 1.57 H_e \tag{2.2}$$

Where $\overline{H}_s$ is the annual mean significant wave height, and σ_s is the associated standard deviation (Brutsche et al., 2016). The region of the profile landward of the inner depth of closure composes the majority of seasonal profile variability. Processes effecting this region are thus the primary focus for the present study. The outer boundary depth is referred to as the outer depth of closure, and is defined as the maximum water depth for sediment motion initiation by annual median wave conditions (Hallermeier, 1978, 1981). The region beyond the outer depth of closure is considered stable relative to annual wave-driven hydrodynamics, and thus has negligible interannual geomorphological variability.
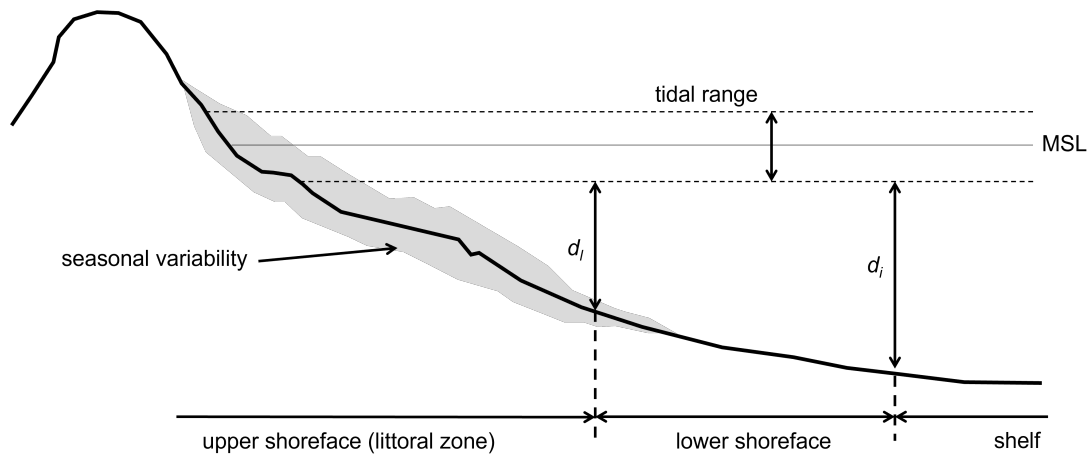
Figure 2.1: Nearshore coastal profile spatial boundaries. Depth limits d_i and d_l correspond to the outer and inner closure depth, respectively, as defined by Hallermeier (1978, 1981). Dynamic profile behaviour primarily occurs on the upper shoreface (adapted from Bosboom and Stive, 2021; Hallermeier, 1981).

Measurement and quantification of coastal profiles and their principle geometric features (i.e., consequential parameters) can be used to understand coastal geomorphology and sediment dynamics within a system of interest. Measurement of coastal profiles in a range of coastal systems and during different seasons has resulted in an understanding of expected profile shapes under varying conditions. The following section aims to explore the processes governing the cross shore profile geometry. These processes may be broken into several primary components; cross shore sediment transport, alongshore sediment transport, and tidal influence. Despite their importance to the present research, the study of these topics is extensive and thus the following sections are constrained to a summary of the key underlying principles. It should be noted that focus is placed on subaqueous processes for the present study, and thus aeolian transport is neglected here.

2.1.1. Cross Shore Transport

Cross shore sediment transport in the upper shoreface consists of a mix of suspended and bed load, attributed to multiple components contributing to the flow velocity and direction near the bed, and turbulence within the water column. These components include undertow (return flow), steady streaming, bound and free long waves, and short-wave transformation and breaking induced turbulence (Bailard, 1982; Roelvink & Stive, 1989). The velocity near the bed, u, thus contains a time-averaged component, $\overline{u}$, a wave-group scale oscillatory component, u_{lo}, and a short-wave scale oscillatory component, u_{hi} (Equation 2.3, Bosboom and Stive, 2021). These flow components must be considered alongside the characteristics of the sediment itself to characterize sediment transport and profile development.

$$u = \overline{u} + u_{lo} + u_{hi} \tag{2.3}$$

Time-Averaged Flow

The time-averaged component of the flow can be further decomposed into two primary mechanisms that govern time-averaged transport; return flow and steady streaming. Return flow may be described as a balancing offshore mass flux in the lower part of the water column driven by an onshore mass flux in the upper part of the water column. The onshore mass flux that drives return flow is governed by a combination of hydrodynamic and wave driven processes. Hydrodynamic onshore mass flux can be observed as a change in the nearshore water level resulting from atmospheric forcing (i.e., wind and atmospheric pressure differentials) and is commonly seen in nature as wind set-up and storm surge. In the case of a shore-normal wind, wind-driven shear stress on the water, τ_{wind}, force surface waters to be move towards the coast. The shoreline forms a natural boundary for the moving layer, causing it to accumulate until the increase in water level, $\overline{\eta}$, creates an equal and opposing hydrostatic pressure to the wind shear (Equation 2.4). The increased water level drives a circulation current near the bed, as water that is "trapped" against the coast returns offshore (Figure 2.2a).

$$\rho g h \frac{d\overline{\eta}}{dx} = \tau_{wind,x} \tag{2.4}$$

When considering elevations above the wave trough, a positive (in the direction of propagation) time averaged net mass flux exists. This is the only part of the water column that observes a non-zero wave-driven mass flux, as water velocity below the wave trough varies harmonically in time (Bosboom & Stive, 2021). In the surf zone, this mass flux is magnified by the so-called surface roller present in breaking waves. Since water cannot continually pile up against the closed boundary of the coastline, a net mass flux in the form of a current must exist below the trough level. This current opposes the wave driven mass flux above the trough level. In the surf zone, the magnitude of the onshore wave driven mass flux is large, driving a strong offshore return current near the bed (Figure 2.2b). It should be noted that return currents can indeed be three dimensional, but are described solely in the 2D-vertical frame of reference here for simplicity. This return current can drive offshore sediment transport if sediment is already in motion or the offshore flow velocity exceeds that which is necessary to initiate sediment transport (i.e., the critical velocity). The critical velocity is obtained theoretically through a balance of forces acting upon a single grain of sediment, and is thus a function of the sediment properties (relative density, size, and friction, interlocking, or cohesion with surrounding sediment).
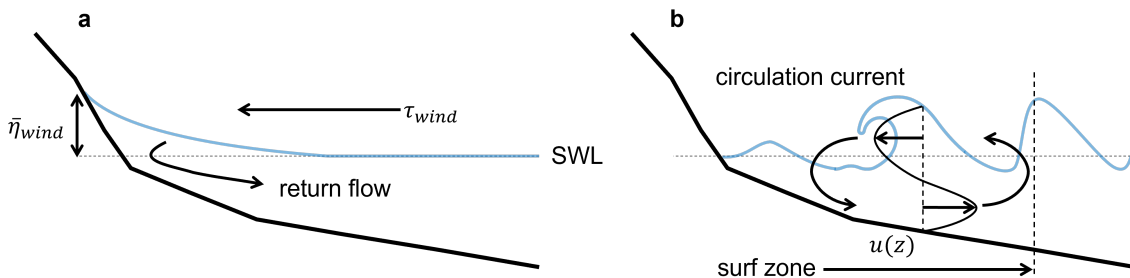
Figure 2.2: (a) Wind set-up balancing wind shear stress and driving a return current near the bed; (b) Wave mass-flux driving a circulation current (adapted from Bosboom and Stive, 2021).

Steady streaming may be described as a non-zero wave-averaged horizontal flow in the direction of wave propagation between the bed and the wave boundary layer (Longuet-Higgins, 1953). The wave boundary layer is the transition layer between the bed and the region of normally oscillating flow in the water column (Bosboom & Stive, 2021). If the magnitude of waves are large, the resulting return current typically dominates the flow velocity near the bed, particularly in the surf zone. This process results in offshore sediment transport and thus erosion of the coastal profile. However, steady streaming may dominate the horizontal flow near the bed in regions outside of the surf zone or when wave magnitudes are small. Steady streaming can therefore contribute towards onshore sediment transport and accretion of the coastal profile if sediment is already in suspension or the critical velocity is exceeded.

Low-Frequency Oscillatory Flow
The low-frequency oscillatory component of the flow is primarily related to variations in the surface wave height on the spatial scale of wave groups. The waves in the centre of wave groups are affected by constructive interference and thus have large wave heights, while the waves at the edges of wave groups are affected by destructive interference and thus have smaller wave heights. Radiation stress (depth averaged momentum flux) is proportional to the wave height, resulting in greater radiation stresses in areas where the wave height is large and lower radiation stresses in areas where the wave height is small. A balance of forces in the cross shore direction demonstrates that small changes in pressure associated with changes in water level are required to counteract the changes in radiation stress associated with spatially varied wave heights at the length scale of wave groups. The resulting variability in water level can be visualized as low-frequency oscillations. Before the surface waves interact with the coast and dissipate energy through breaking, these low-frequency oscillations remain out of phase with the wave groups and are referred to as bound long waves. Bound long waves contribute to offshore sediment transport, as the sediment brought into suspension by the largest free-surface waves occurs during the offshore directed component of the low-frequency oscillation (i.e., the bound wave trough). When free-surface waves break, the low-frequency oscillations are "set free", as the breaking criteria for these waves is different than the waves inside the wave groups to which they were previously bound. At this point the low-frequency oscillations become free long waves, that are approximately in phase with free-surface wave groups nearshore of the surf zone. The sediment brought into suspension by the largest free-surface waves now occurs during the onshore directed component of the low-frequency oscillation (i.e., the free wave peak), and the free wave thus contributes towards onshore sediment transport. An example of the phase relationships between free-surface wave groups, bound long waves, and free long waves is presented in Figure 2.3.
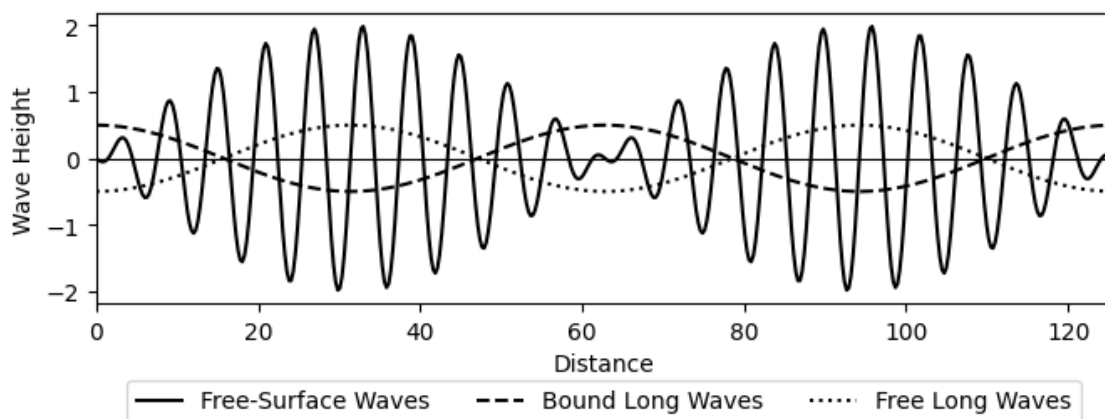
Figure 2.3: Phase relationships between free-surface waves, bound long waves, and free long waves.

Both the magnitude and period of free surface waves are important when considering long wave development. Since long waves are initially bound to the wave group and the associated wave height differential, more clearly defined wave groups will result in more distinct long waves. These wave groups are typically well defined during swell dominated conditions. Since waves are dispersive, waves generated from the same storm (non-locally) with different periods will arrive at the coast at different moments. If swell from multiple storms reaches the coast simultaneously, then the interference pattern will have a

more clear signal compared to that of a locally generated sea. As a result, swell dominated conditions give way to stronger long wave signals.

High-Frequency Oscillatory Flow
High frequency oscillatory flow may be described as surface-wave induced velocity oscillations. These oscillations have two primary mechanisms contributing to sediment transport; suspension of sediment from the bed, and contribution to sediment transport through net mass flux during wave transformation. In deep water, free-surface waves may be approximated with a sinusoidal function, resulting in a symmetrical horizontal velocity signal and thus a negligible net contribution to the flow velocity. As these waves approach the shore they transform, becoming first asymmetric about the horizontal axis (positively skewed) and then asymmetric about the vertical axis, before eventually breaking. In the case of positive skewness, the free-surface waves have a larger mass flux above the still water level than below the still water level, resulting in stronger velocities under the wave crest than under the wave trough (Bosboom & Stive, 2021). This velocity differential implies an onshore contribution to the net flow and thus onshore sediment transport (Seymour, 2005). The magnitude of this contribution along different regions of the cross shore profile is governed by the free-surface wave magnitude. As free-surface waves propagate further nearshore, the increased velocity at the wave crest results in asymmetry about the vertical axis. Similar to skewed waves, asymmetric waves have strong onshore directed velocities, contributing to both onshore transport and suspended sediment concentration (Bosboom & Stive, 2021; Seymour, 2005). As free-surface waves break, the resulting turbulence greatly increases the suspended sediment concentration which is subsequently transported according to the net flow direction and magnitude.

2.1.2. Alongshore Transport
Alongshore transport may be defined as sediment transport parallel to the coast resulting primarily from wave driven alongshore currents within the surf zone. Breaking waves with a non-orthogonal angle of incidence result in a cross shore gradient of the shear component of the radiation stress, generating a shore-parallel water mass flux (i.e., a current). The magnitude of the mass flux is proportional to the wave angle of incidence and energy flux in the surf zone (Bosboom & Stive, 2021). This proportionality generally implies that energetic waves that dissipate significant amounts of energy during breaking will drive a strong alongshore current. This current can transport sediment that is suspended through high-frequency oscillatory flow and breaking induced turbulence. The result of alongshore sediment transport on cross shore profile geometry includes structural gains and losses (i.e., changes in total sediment volume within a given cross shore transect) and development of alongshore features that are resolvable in the cross shore profile (Bosboom & Stive, 2021; Seymour, 2005). The contribution of alongshore transport to the sediment volume and geological features within a cross shore transect was well demonstrated in Ashton and Murray (2006). This study investigated the development of coastal features such as flying spits, sand waves, and capes using a process based numerical model with high angle wave forcing, and identified a strong sensitivity of coastal feature development to high angle waves. The observations derived from this study are supported by beach state observations made by Wright and Short (1984), who demonstrated variability in cross shore profile geometry on the scale of plan-view coastal features such as mega-cusps and rips (e.g., Figure 2.4c).

2.1.3. Tidal Influence
In sandy beach environments, coastal profile behaviour is typically dominated by wave driven processes nearshore of the outer surf zone edge. Wave-dominance is particularly notable in environments where the tidal range is small because near-constant water levels result in near-stationary shoaling, surf, and swash zone positions. As the tidal range increases relative to the wave conditions however, the position of the shoaling, surf, and swash zones observe increased spatial variability. As a result, a given section of the profile is exposed to fluctuating wave processes on the timescale of the local astronomical tide period (Masselink & Short, 1993). This tide-driven variability acts to increase the horizontal spatial scale of geometric features on the profile, preventing the development of distinct wave driven morphology (i.e., bar-trough beach states) (Masselink & Short, 1993). Offshore of the outer surf zone edge and in deep water (i.e., on the lower shoreface and shelf), surface waves have limited-to-no interaction with the bed. In these areas the cross shore tidal velocity is important for the development of features such as tidal ridges (Bosboom & Stive, 2021). This portion of the profile however is not

typically of interest for coastal development and management in sandy systems, and is therefore neglected in the present study. Further, sediment transport on tidal flats is governed by ebb versus flood tidal dominance, and high-water versus low-water slack duration (Bosboom & Stive, 2021). Although these processes do contribute toward the development of nearshore coastal profiles, they are primarily important in muddy, tide-dominated environments, which are outside the scope of the present study.

2.2. Profile Characterization

2.2.1. Profile States

As mentioned in Section 2.1, measurement of coastal profiles in a range of coastal environments with diverse forcing conditions has resulted in an understanding of expected profile shapes under varying conditions. One of the first study campaigns used to understand and categorize coastal profile shapes was conducted by Wright and Short (1984) for sandy open coast systems in Australia. This campaign resulted in the definition of six sandy beach states differentiated based on profile geometry, presence of distinct morphological features, and differences in the driving hydrodynamic processes and sediment characteristics. At the extremes of the defined beach states are fully dissipative beaches and highly reflective beaches, characterized by mild sloped, shallow beaches with large subaqueous sand volumes, and steep sloped, deep beaches with limited subaqueous sand volume, respectively (Figure 2.4) (Wright & Short, 1984). Dissipative beaches tend to indicate erosional behaviour and are found in high energy environments, whereas reflective beaches tend to indicate accretional behaviour and are found in low energy environments. A series of intermediate beach states were also identified, representing transitional phases of sandy beaches from one extreme to the other. The definitions of sandy beach states by Wright and Short (1984) continue to have relevance in modern coastal engineering, being commonly used to study coastal morphology processes and to categorize natural beaches (for instance in Grasso et al. (2009) and Ranasinghe, Symonds, et al. (2004)).

Although beach state definition is useful, several studies have identified shortcomings of using the highly reflective beach state to describe all sandy beaches in low energy environments. Hegge et al. (1996), Makaske and Augustinus (1998), and Travers (2007) indicated various levels of concavity associated with beach profiles in low energy environments depending on the amount of wave exposure. The proposed profile shapes resulting from these studies differed, but generally agreed that a subaqueous terrace was present and became more pronounced as the degree of sheltering increased. This observation was highlighted by Ton et al. (2021), where the expected depth of the subaqueous terrace was quantified using the theoretical formulation for depth of closure from Hallermeier (1981). The result of each of these studies was the definition and classification of various profile states (morphotypes). An example of this classification method may be taken from Travers (2007), who identified four primary morphotypes for a series of sandy, low energy beaches in Australia. This study classified morphotypes according to both profile geometry and common incident conditions at each beach, providing an example of how to quantitatively classify beach states. To classify morphotypes, an exposure factor (Ef) was defined as a function of the direct fetch length (FI, the fetch length orthogonal to the shoreline), and the marginal shoal width (Ms, the distance between MLW and MLW - 2 m) (Equation 2.5).

$$Ef = log(\frac{FI}{Ms})$$ (2.5)

Larger values of Ef therefore imply larger exposure to incident conditions, as demonstrated by inverse proportionality with Ms and proportionality with FI. These proportionality relationships indicate decreased dissipation when Ms is small, due to reduced wave transformation and breaking length, and increased wave energy when FI is large. The importance of wave energy and potential for dissipation is therefore integral to profile morphology and morphotype classification in this study. The exposure factor was applied alongside trends in profile geometry to identify common morphotypes and classify beaches accordingly (Figure 2.5).
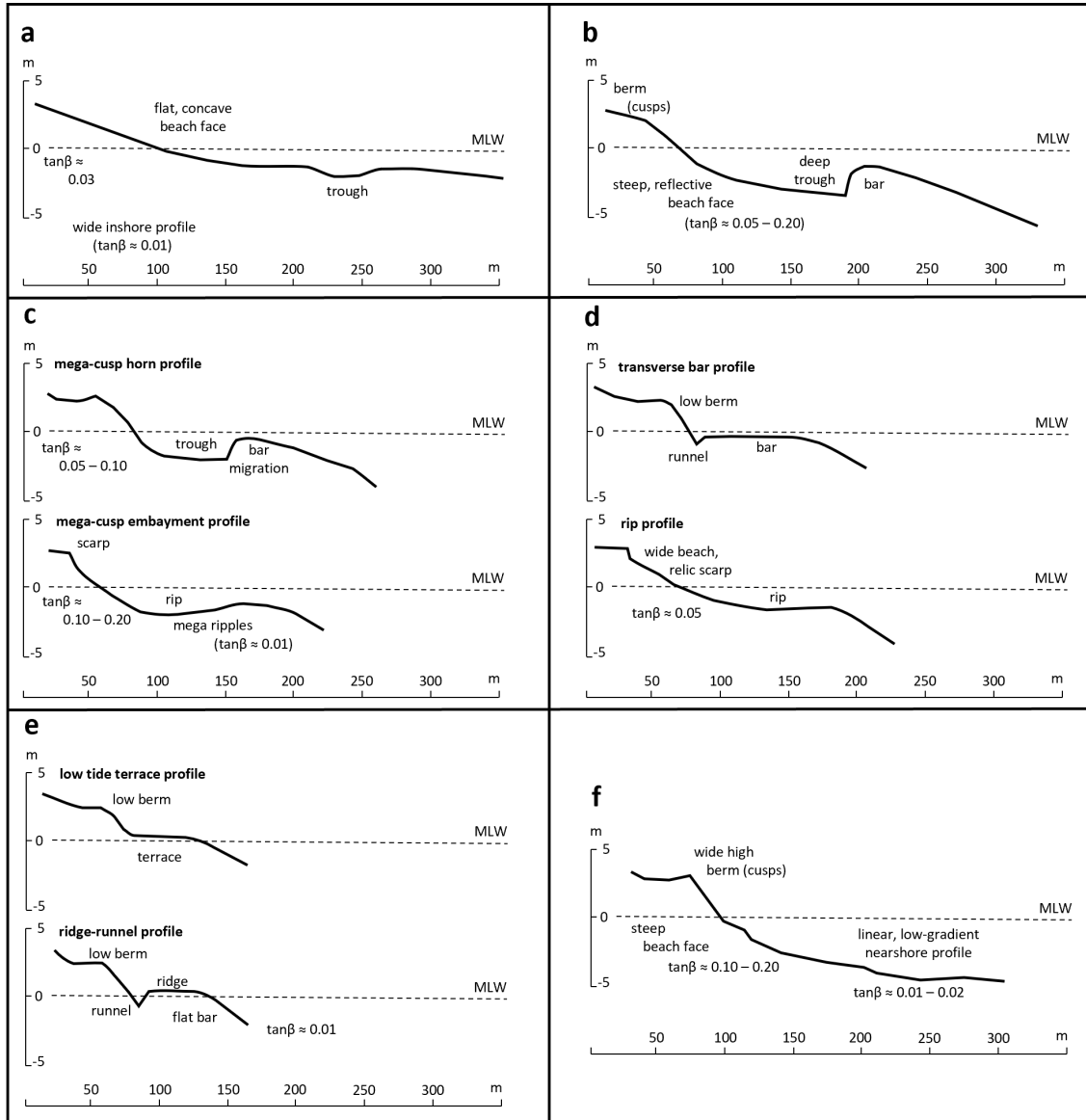
Figure 2.4: (a) Typical profile for a dissipative beach state; (b) Typical profile for an intermediate alongshore bar-trough beach state; (c) Typical profiles for an intermediate rhythmic bar and beach state with example cross sections at the beach cusp horn (top) and beach cusp embayment (bottom); (d) Typical profiles for an intermediate transverse bar and rip beach state with example cross sections at the transverse bar (top) and rip (bottom); (e) Typical profiles for an intermediate ridge-runnel or low tide terrace beach state with example cross sections at the low tide terrace (top) and ridge runnel (bottom); (f) Typical profile for a reflective beach state (adapted from Wright and Short, 1984).
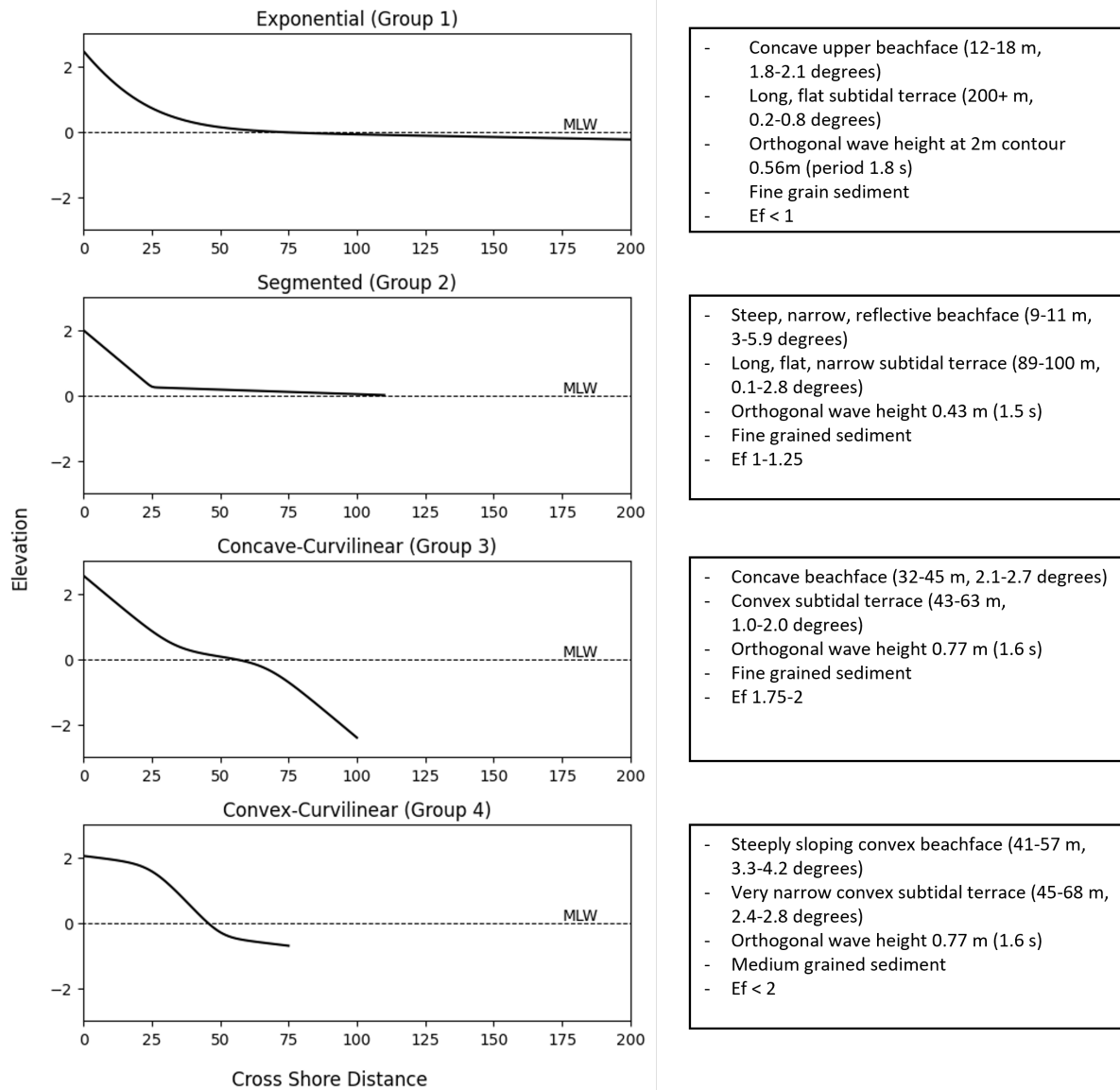
Figure 2.5: Attributes of low energy beach morphotypes (adapted from Travers, 2007).

2.2.2. Profile Parameterization

The methods used to predict coastal geomorphology can be divided into three categories; process based models (including hybrid models), data-driven or probabilistic models, and profile shape functions (i.e., parametric functions). Process based models use analytical representations of the physical processes in coastal systems to describe their collective interaction and influence on coastal morphology (Reeve et al., 2016). Data driven models and probabilistic models use measured observations and probabilistic techniques to make inferences about statistically significant patterns and trends describing coastal morphology and quantify the related uncertainties (Reeve et al., 2016). Profile shape functions are equations used to represent the coastal profile on short term (several months to years) to long term equilibrium (several years to decades) timescales, through the application of consequential parameters (Section 1.3.1). The present study focuses on the application of profile shape functions with data.

Profile shape functions are based primarily on the theory of profile equilibrium. The theory of profile equilibrium states that under constant forcing conditions, the beach profile will eventually reach an equilibrium geometry at which point it will no longer observe morphological change. Given that forcing conditions in nature are not constant, the profile must therefore tend towards changing equilibrium states. As such, measured profiles can represent a combination of equilibrium states which the beach has tended towards during past and present forcing. It should then be possible to predict geometric traits of the coastal profile given information about past forcing and the physical traits of the environment in consideration (i.e., sediment characteristics). Profile shape functions leverage this strategy by applying parameters to control the function shape. These parameters may be geometrically fit to observed or averaged profiles and empirically related to the physical processes present in the environment under consideration. These functions are valuable because of their simplistic nature, typically requiring limited computations to provide estimates of coastal profiles. As a result, they can serve as valuable first order estimates of profile geometry and expected response. However, due to the diversity of coastal profiles in nature, different profile shape functions are required to study different profile geometries and timescales. A collection of shape functions from previous studies are presented in Table 2.1. The identified existing shape functions may be divided into three primary categories by their form and typical characteristics: Logarithmic and Exponential (Log/Exp) functions, Polynomial functions (Poly.), and Hyperbolic and Trigonometric functions (Trig.). Logarithmic and exponential functions are those which contain logarithmic and exponential operators, typically resulting in convergence of the function to a horizontal asymptote. These functions are smooth and monotonic, and thus are unable to resolve coastal features such as steps and sand bars. Polynomial functions are those that use a single polynomial or piecewise combination of polynomials to represent the profile. A piecewise combination of polynomials allows these functions to become non-monotonic as needed to resolve more complex profile geometry, however transitions between sections may be sharp. Hyperbolic and trigonometric functions are those containing hyperbolic or trigonometric operators, allowing for smoother non-monotonicity compared to piecewise polynomial functions. At the time of this review, a comprehensive study of profile function applicability in a range of diverse coastal environments was not identified.

Table 2.1: Summary of several profile functions from previous studies (expanded from Hsu et al., 2006; Türker and Kabdaşli, 2009).

Source	Shape Function	Remark
Bruun (1954) and Dean (1977)	$h(x) = Ax^n$	**Poly.** Equilibrium profile considering uniform wave energy dissipation, where $h(x)$ is depth at a specified cross shore distance, A is a profile scale parameter, and n is a profile shape factor. This profile was shown to fit well to sandy beaches on the Dutch and Danish North Sea.

Table 2.1 – *Continued from previous page*

Source	Shape Function	Remark
Powell (1990)	$h(0 < x < x_s) = -h_s(\frac{x-x_s}{x_s})^{n_1}$, $h(x_s < x < x_t + x_s) = -h_t(\frac{x-x_s}{x_t})^{n_2}$, $h(x_t + x_s < x < x_b + x_s) =$ $-(h_b - h_t)(\frac{x-x_s-x_t}{x_b-x_t})^{n_3} + h_t$	**Poly.** Tri-parabolic profile defined for shingle beaches considering three profile sections, where x_s is the horizontal distance from the origin to the SWL, h_s is the beach crest elevation, x_t is the beach terrace position, h_t is the beach terrace elevation, x_b is the horizontal distance from the origin to the wave base, h_b is the wave base elevation, and n_i are fitting parameters related to wave steepness.
Bodge (1992)	$h(x) = B(1 - e^{-kx})$	**Log/Exp** Equilibrium profile based on goodness of fit to Atlantic US sandy beaches, introducing an exponential for offshore sediment grading, where B is the depth reached asymptotically offshore, and k is profile curvature defined as a distance.
Inman et al. (1993)	$h(0 < x < x_s) = A_1 x^n$, $h(x_s < x < x_c) = A_2 (x - x_s)^n$	**Poly.** Bi-parabolic profile considering two sections representing the outer shorerise profile ($x_s < x < x_c$) and inner bar-berm profile ($0 < x < x_s$), connected at the bar-berm edge. Here the shoreline is assumed to be located at $x = 0$.
Komar and McDougal (1994)	$h(x) = \frac{m_0}{k}(1 - e^{-kx})$	**Log/Exp** Equilibrium profile considering beach face slope with concavity due to tidal effects, where m_0 is the beach face slope. This profile is a direct extension of Bodge (1992).
Lee (1994)	$h(x) = (\frac{1}{B})ln(1 + \frac{x}{A})$	**Log/Exp** Equilibrium profile considering linear wave theory, where B is a parameter related to the wave length and A is a length scaling parameter.
Hsu et al. (2006)	$\frac{h}{h_c} =$ $A_1[1 - e^{-B_1 \frac{x}{x_c}}] - A_2 e^{-B_3(1-\frac{x}{x_c})} sech(B_2(1 - \frac{x}{x_c})) + A_2 e^{-B_3} sech(B_2)$	**Trig.** Barred profile with free parameters used to scale the beach face slope (A_1), bar height (A_2), profile concavity (B_1), bar width (B_2), and bar asymmetry (B_3), for dimensionless depth ($\frac{h}{h_c}$) and cross shore position ($\frac{x}{x_c}$). h_c and x_c represent the measured bar crest height and position, respectively.

Table 2.1 – *Continued from previous page*

Source	Shape Function	Remark
Dai et al. (2007)	$h(x) = Ae^{Bx} + C$	**Log/Exp** Equilibrium profile for sub-aerial and subaqueous profiles, defined to represent upward-concave (U-EBP), downward-concave (D-EBP), and medium characteristic (M-EBP) beach states as identified in South China. Here A is a scaling parameter, B is a parameter of beach concavity, and C is a coefficient of the mean slope.
Hanssen et al. (2022)	$h(x) = z_0 + 0.5\delta_0(S_1 - S_2)(\frac{x-L_0}{\delta_0} - ln(cosh(\frac{x-L_0}{\delta_0})) - ln(2)) + S_2(x - L_0)$	**Trig.** Two-sloped flexible profile defined to represent profiles with varied concavity. Distinct slopes are smoothly connected using a hyperbolic tangent, where S_1 is the nearshore slope, S_2 is the offshore slope, z_0 is the elevation of the $S_1 - S_2$ point of intersection, L_0 is the horizontal distance from the origin to the $S_1 - S_2$ point of intersection, and δ_0 is the width of the hyperbolic tangent transition.

The profile parameterization provided in Hanssen et al. (2022) demonstrates high flexibility, clear parametric meaning, and effective representation of two sloped profiles similar to the Group 1 and Group 2 morphotypes described by Travers (2007) (Figure 2.5). However, it is expected that the expression provided by Hanssen et al. (2022) may struggle to fit profiles with more complex geometry or more then two distinct slopes, as seen in Group 3 and Group 4 morphotypes described by Travers (2007). This observation provides incentive for the expansion of the Hanssen et al. (2022) expression to three slopes so that profiles with increased complexity may be effectively represented with clear parametric meaning. This expansion will be explored in the present study.

2.2.3. Morphological Driver Parameterization

A set of representative causal parameters must be selected in order to characterize the processes related to the geometry of a given cross shore profile measurement. According to the theory of equilibrium, any given profile measurement is a representation of combined equilibrium states from past and present forcing. As such, the selected causal parameters must be computed for a duration which can resolve the influence of long term forcing and short term variability that drive profile development. The impact of varying temporal scales on beach dynamics has been demonstrated in several studies, including Anderson et al. (2018), who demonstrated that littoral cells can respond to fluctuations in both interannual and multidecadal forcing, resulting in multiple beach rotation periods. This study provides indication that several temporal scales driving spatial variability may be important for engineering design, and as such several temporal scales should be considered when relating causal and consequential parameters.

To select representative causal parameters, reference may be made to past works defining relationships between key geometric features and the underlying forcing. Frequently, these relationships are outlined in the works that present parametric shape functions, as summarized in Table 2.1. These papers, and the theoretical understanding presented in Section 2.1, indicate that the key drivers of subaqueous cross shore morphology are most clearly related to wave conditions, water levels, and sediment characteristics. Discrete representations of each of these processes can be applied as causal parameters. Most commonly, the selected parameters used to represent these processes are the significant wave height, H_s, the tidal range, TR, and the median sediment grain size D_{50}. It has however

been demonstrated that the wave magnitude alone is not the only wave characteristic that influences profile geometry. For instance, both the wave magnitude and wave period are important for the development of wave groups and the resulting low-frequency oscillatory flow. These characteristics (wave height and period) may be represented individually, or together using wave energy flux, referred to here simply as wave power, P (Equation 2.6).

$$P = \frac{\rho g}{8} H_s^2 Cg \tag{2.6}$$

Where ρ is the water density (assumed 1025 kg m^{-3} for seawater), g is acceleration due to gravity (assumed 9.81 m s^{-2} on Earth), and Cg is the wave group celerity (m s^{-1}). The alongshore component of the wave power, P_{LS}, may also be determined using the wave angle of incidence, ϕ, to assess the influence of alongshore processes on profile geometry (Equation 2.7, following Senechal and Coco, 2024).

$$P_{LS} = P cos\phi sin\phi \tag{2.7}$$

In addition to parameters that include the influence of low-frequency oscillatory flow, parameters including the influence of high-frequency oscillatory flow may also be computed. The primary parameter for this purpose is the wave steepness, ϵ, which can be used to provide an indication of wave transformation, leading to sediment stirring and contributing to the net onshore flow (Equation 2.8) (Bosboom & Stive, 2021; Seymour, 2005).

$$\epsilon = \frac{H_s}{L} \tag{2.8}$$

Where L is the wave length associated with H_s (m).

Two common dimensionless parameters derived for the purpose of beach state classification in wave dominated environments are the dimensionless fall velocity, Ω, and the relative tidal range, RTR (Equations 2.9 and 2.10, respectively) (Masselink & Short, 1993; Wright & Short, 1984).

$$\Omega = \frac{H_b}{W_s T} \tag{2.9}$$

$$RTR = \frac{TR}{H_b} \tag{2.10}$$

Where H_b is the breaking wave height, W_s is the sediment fall velocity, T is the associated wave period, and TR is the mean spring tidal range. The dimensionless fall velocity aims to indicate the dominance of reflective, intermediate, or dissipative surf zone conditions, while the relative tidal range aims to indicate the relative importance of swash, surf zone, and shoaling wave processes (Masselink & Short, 1993). Despite their application in numerous studies to classify wave dominated beaches, the usefulness of these parameters in more diverse coastal environments is reduced, particularly when considering coastal environments with large tidal ranges (Levoy et al., 2000). Additionally, both of these parameters are functions of the breaking wave height, and thus rely on the application of nearshore wave propagation when measured breaking wave heights are not available. Although this can be completed effectively using process based wave models, uncertainty in beach classification ultimately increases when additional transformative steps are required. The limitations of these parameters and the use-case upon which they are founded indicate a need for refinement prior to application in diverse coastal environments. As such, for the purpose of the present study it may be more intuitive to apply direct statistical representations of measured metocean and sediment data, and computations of simple causal relationships (i.e., wave power) for comparison with consequential parameters.

3

Methodology

Chapter Outline

In this chapter the methodology applied for the completion of the research is presented alongside a description of the applied data. First, measured data is processed such that only profiles between MLW $\pm$ 2 m and within the same period of record as corresponding metocean data are considered. Next, so-called causal parameters are selected to characterize wave and water level conditions for four time scales preceding profile measurements. A new parametric expression for the profile geometry is then defined, and performance assessment methods are outlined for the use of parametric expressions to represent diverse profile shapes. The best performing expression according to testing will be fit to measured data using parameters governing the profile geometry (consequential parameters). Strategies for the identification of profile morphotypes in measured data are then presented, including the use of manual labelling, empirical clustering, and parametric clustering. Finally, a strategy to identify geomorphological processes is detailed through the application of causal-consequential parameter rank correlations. A summary of the applied research approach is presented in Figure 3.1.
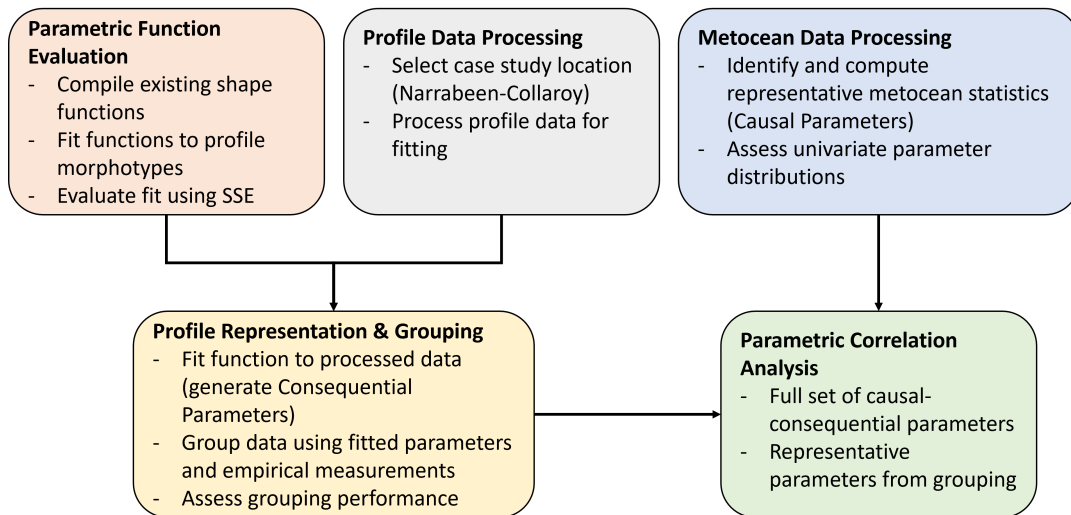
Figure 3.1: Summary of the applied research approach, demonstrating the connections between processed data, parameterization, and correlation analysis.

3.1. Data Summary

Data from the Narrabeen-Collaroy Beach Survey Program was applied for the purpose of this study. This dataset consists of monthly coastal profile measurements along five distinct transects (N = 3241), hourly hindcast nearshore wave observations at the -10 m AHD contour of each transect, and 15-minute interval hindcast astronomical tide levels. All elevation data in the dataset is measured relative to the Australian Height Datum (AHD), which is approximately equal to mean sea level (MSL) in Australia (Turner et al., 2016). The profile data period of record is from April 1976 until November 2019, and the nearshore wave and tidal data period of record is from January 1979 until December 2014. The five profile measurement transects were defined during the formative years of the survey program, and are labelled PF1, PF2, PF4, PF6, and PF8, with PF1 at the northern extent of the beach, PF8 at the southern extent of the beach, and the remaining profiles spaced approximately 900 m apart between these boundaries (Figure 3.2a). Reference locations for each transect are constant throughout the period of record and are located in the stable dune area (Turner et al., 2016). The cross shore resolution of each profile is 10 m for measurements made prior to May 2005, and 1 m thereafter. Further, the mean maximum depths of measurement prior to and post May 2005 were -2.14 m AHD and -0.59 m AHD, respectively. The change in measurement resolution and maximum measurement depth is a reflection of changes made to the transect surveying technique to apply RTK-GPS technology in place of the Emery method. The available nearshore wave data consists of significant wave heights, peak periods, and mean wave directions hindcast using data from a directional waverider buoy at the -80 m AHD depth contour near Sydney (Figure 3.2b), and transformed to each transect using a nearshore SWAN model (Turner et al., 2016). The astronomical tide data was derived using the tide analysis software, T_Tide, with the application of externally collected water level measurements at the HMAS Penguin tide gauge, located approximately 10 km south of Narrabeen-Collaroy beach. Sediment characteristics are approximately uniform along the beach, consisting of fine to medium grained sand ($D_{50} \approx 0.3$ mm). Given that sediment characteristics are uniform for the study location and that transect-specific sediment data is not publicly available, influence of sediment characteristics will be neglected for the present study. A complete description of the Narrabeen-Collaroy dataset, including information on the employed surveying methodologies, the associated measurement accuracy, and wave hindcast and transformation validation is available in Turner et al. (2016).
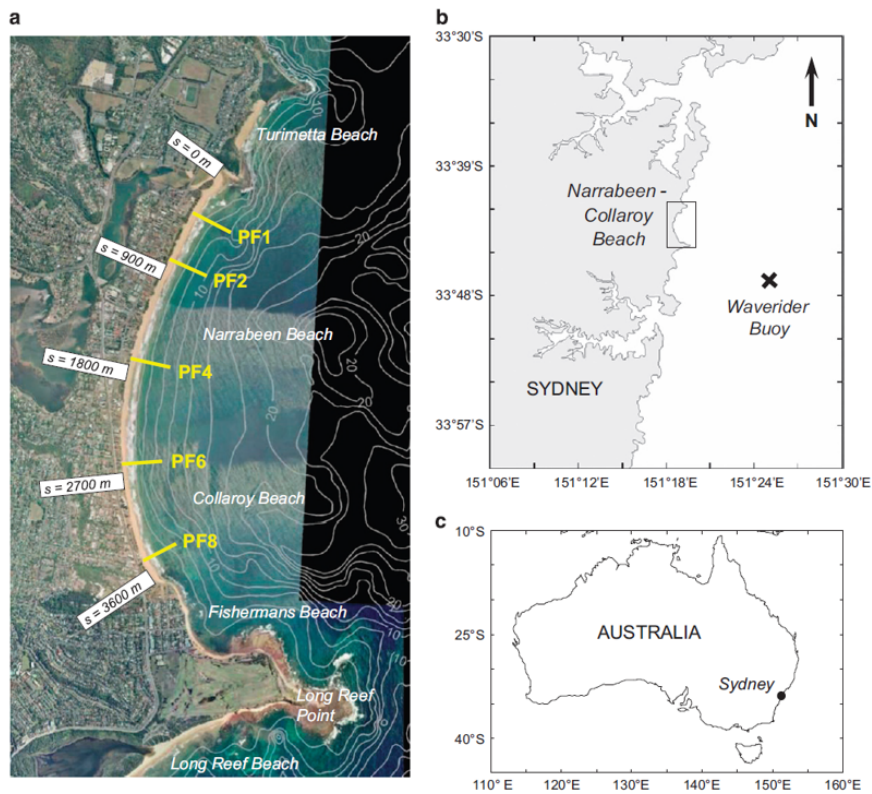
Figure 3.2: (a) Aerial photo of Narrabeen-Collaroy Beach indicating the monthly survey transects, 2.5 m interval depth contours, and local alongshore distance relative to the northern headland; (b) Narrabeen beach relative to the Sydney coastline and the Sydney waverider buoy location; (c) map of Australia showing the location of Sydney (as presented in Turner et al., 2016).

Univariate analysis of the available astronomical tide and nearshore wave data was completed to develop a foundational understanding of the metocean characteristics of the Narrabeen-Collaroy system. Nearshore waves at the study location have a mean significant wave height of 0.98 m and mean period of 9.6 s. Assessment of nearshore waves per transect indicate generally decreasing mean significant wave heights from PF1 to PF8 ($\Delta \overline{Hs} \approx 0.36$ m from PF1 to PF8). The dominant nearshore wave direction can be determined using a joint probability of occurrence table, demonstrating that waves primarily approach the beach from 67.5° to 135° TN, with the largest waves approaching from 112.5° to 135° TN (Figure 3.3). This observation supports the observed difference in mean wave conditions per transect, given the ESE dominant wave direction and the southern headland protecting more southern transects from direct wave exposure. This observation aligns with the per-transect and offshore wave analysis completed in Turner et al. (2016). Astronomical tide statistics are presented in Table 3.1, resulting in the classification of the Narrabeen-Collaroy system as mesotidal.

Table 3.1: Tidal statistics computed using the astronomical tide hindcast for Narrabeen-Collaroy. All measurements are provided in meters relative to Australian Height Datum (AHD).

Tidal Statistic	Water Level (m AHD)
MHHW	0.67
MHW	0.52
MSL	0.00
MLW	-0.53
MLLW	-0.59
Max. TR	2.05
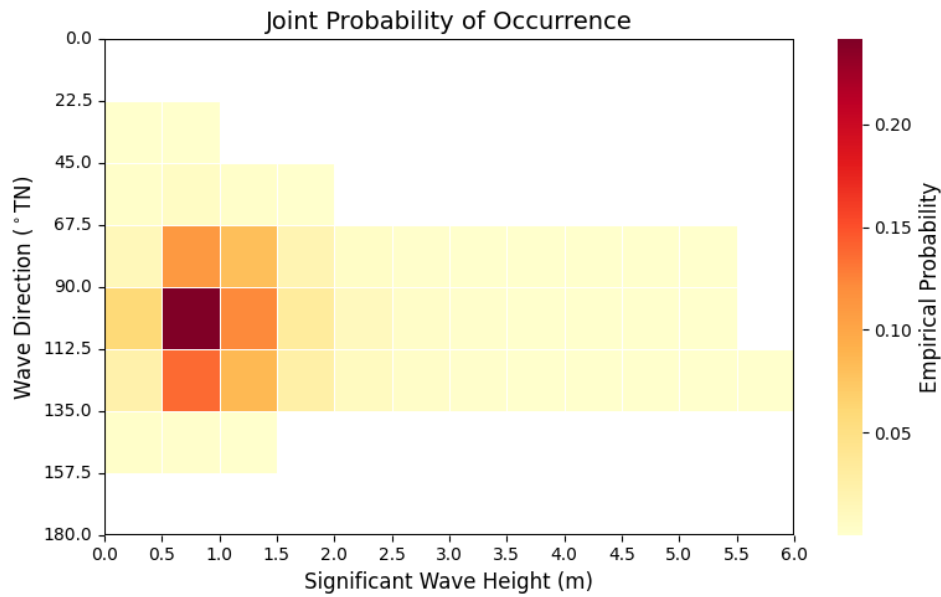
Figure 3.3: Joint probability of occurrence table for significant wave height and wave direction.

Turner et al. (2016) and Wright and Short (1984) indicate that dissipative to intermediate beach states govern the northern beach extent, while intermediate to reflective beach states govern the southern beach extent. This classification was completed using both visual observations and the dimensionless sediment fall velocity presented by Wright and Short (1984). Analysis of this classification technique indicates that when all variables except the breaking wave height are held constant, beaches with smaller breaking waves will observe lower dimensionless fall velocities and thus will be more reflective. Additionally, several studies have indicated the presence of decadal scale beach oscillation and rotation (Harley et al., 2011; Ranasinghe, McLoughlin, et al., 2004). These studies indicate strong alongshore wave energy gradients resulting in alongshore sediment transport and beach rotation. This rotation contributes to the overall beach width on longer term (inter-annual) timescales, while shorter term (intra-annual) beach width oscillations are generally attributed to erosion and recovery from storm events (Harley et al., 2015; Short, 2009; Turner et al., 2016). This expected behaviour will be considered when selecting causal parameters and interpreting observations in subaqueous profile geometry. For further reading on the dynamics and morphology of Narrabeen-Collaroy beach, the reader is referred to the works of M.D. Harley, I.L. Turner, and A.D. Short.

3.2. Data Processing

3.2.1. Profile Data

Prior to conducting analysis of profile geometry behaviour, the data had to be processed such that discrete profile measurements were directly comparable to each other and their related morphological drivers. The period of record for profile measurements is eight years longer than that of nearshore wave data and astronomic tide data, with wave and tide data missing for 1976 to 1979 and 2014 to 2019. The profile sample size was thus immediately reduced to the period of record of available wave and tide data, resulting in 2244 remaining profile measurements. Next, all profiles were re-gridded to a one-meter cross shore resolution to allow for comparison of measured profiles with different cross shore resolutions. Since all profiles measured after May 2005 have an existing resolution of 1 m, this step only affected data with a 10 m resolution collected prior to May 2005. Linear interpolation was applied to this data to obtain elevation values at a 1 m resolution between each 10 m cross shore measurement point.

Following re-gridding, the remaining sample size was further reduced to consider only profiles containing data within a standardized range of elevations, since the measured profile length is not standardized. This implies that full measured profile lengths are a poor indication of profile behaviour and should be

limited to eliminate measurement bias. The selection of this elevation range considered both the ability to include desireable geometric characteristics and the need to maintain a representative dataset of profile behaviour (i.e., prevent sample size degradation). Ideally, the lower elevation threshold would be set to the inner depth of closure defined by Hallermeier (1981), as this would allow for assessment of the entire region of annual profile variability. Equations 2.1 and 2.2 were applied to assess this elevation as a potential lower threshold. Unfortunately, the minimum estimated inner depth of closure using these equations was -4.53 m, resulting in only 61 profiles for consideration should this threshold be selected. The study of Travers (2007) was thus referenced for identification of a shallower lower elevation threshold that would less significantly degrade the sample size. The elevation bounds used in that study were MLW $\pm$ 2 m. Although these bounds were selected for that study based on profile activity observations in low energy environments, application of these bounds did result in an acceptable sample size for the present study (N = 483). In order to mitigate further sample size degradation, this elevation range was selected for application in the present study under the pretense that any subsequent spatial trends or observations may not be representative of the entire active profile. The resulting dataset contained at least 25 measurements per month, with the least monthly measurements during the month of June (25) and the most monthly measurements during the month of March (56). No significant trend was found between the month of measurement and number of measurements made. The reduced dataset consists of measurements made between 1979 and 1990, implying that all of the data to be used in the present study was collected using the Emery method, as was standard during this period.

Once profile data was filtered, re-gridded, and trimmed to within the specified elevation bounds, a horizontal translation was applied such that the beginning of each profile measurement was located at the point [x = 0 m, y = MLW+2 m]. This translation ensures that each profile measurement began at the same cross shore position, and placed the data in a standardized format for parametric fitting. Further processing of measured profile data was completed for specific analyses, and are described further in the following sections. It should be noted that for the purpose of profile visualization, profiles were horizontally translated so that the intersection of the profile with MSL (0 m AHD) was located at the origin.

3.2.2. Metocean Data

As presented in Section 2.2.3, the available wave and tidal data must be represented with a set of causal parameters associated with each profile measurement. 11 distinct causal parameters were computed from the available data for comparative analysis with the profile geometry (Table 3.2). Each of these causal parameters were computed for four arbitrary time frames preceding the measurement date of each measured profile within the reduced sample size. The selected computation time frames were seven days, three months, six months, and one year. These time frames aimed to investigate the relative importance of several different temporal scales on profile geometry. A causal parameter was assigned as the time averaged value and standard deviation of each computed wave statistic to investigate the relative influence of long term conditions versus short term variability. The standard deviation in this scenario aimed to represent the occurrence of storms during the computation period, where larger standard deviations in the computed statistics indicate a larger range in wave conditions.

Table 3.2: Selected causal parameters for comparative analysis with profile geometry.

Parameter Symbol	Parameter Meaning
TR_{max}	Maximum tidal range observed during the computation period [m]
$\overline{H_s}$	Time averaged significant wave height for the computation period [m]
σ_{H_s}	Significant wave height standard deviation during the computation period [m]
$\overline{T_p}$	Time averaged peak period for the computation period [s]
σ_{T_p}	Peak period standard deviation during the computation period [s]
$\overline{P}$	Time averaged wave power for the computation period [W m^{-1}]
σ_P	Wave power standard deviation during the computation period [W m^{-1}]
$\overline{P_{LS}}$	Time averaged alongshore wave power for the computation period [W m^{-1}]
$\sigma_{P_{LS}}$	Alongshore wave power standard deviation during the computation period [W m^{-1}]
$\overline{\epsilon}$	Time averaged wave steepness for the computation period [-]
σ_ϵ	Wave steepness standard deviation for the computation period [-]

3.3. Profile Parameterization

3.3.1. A New Parametric Expression

The flexibility, parametric meaning, and effective representation of two-sloped profiles by the parametric expression of Hanssen et al. (2022) provides incentive for the expansion of the expression for three-sloped profiles. The methodology used for derivation of the Hanssen et al. (2022) expression was referenced to develop a three-sloped version of this expression, hereafter referred to as the Julseth (2024) expression. The Hanssen et al. (2022) profile expression was derived through the integration of a slope function, s, consisting of two distinct slope values connected using a hyperbolic tangent. The parameters included in this slope function are the first slope magnitude, S_1, the second slope magnitude, S_2, the horizontal distance from the origin to the slope transition, L_0, and the length scale of the slope transition, δ_0 (Equation 3.1) (Figure 3.4).

$$s = \frac{1}{2}(S_1 - S_2)(1 - \tanh \frac{x - L_0}{\delta_0}) + S_2 \tag{3.1}$$

Expanding the slope expression to three slopes introduces three new parameters; the third slope magnitude, S_3, the horizontal distance from the origin to the second slope transition, L_1, and the length scale of the second slope transition, δ_1. The resulting slope function is presented in Equation 3.2.

$$s = \frac{1}{2}(S_1 - S_2)(1 - \tanh \frac{x - L_0}{\delta_0}) + \frac{1}{2}(S_2 - S_3)(1 - \tanh \frac{x - L_1}{\delta_1}) + S_3 \tag{3.2}$$

Following the methodology of Hanssen et al. (2022), the slope function may be integrated to obtain a bed-level function. This integration is summarized here.

$$\int s\,dx = z_b$$

$$z_b = \int (\frac{1}{2}(S_1 - S_2)(1 - \tanh \frac{x - L_0}{\delta_0}) + \frac{1}{2}(S_2 - S_3)(1 - \tanh \frac{x - L_1}{\delta_1}) + S_3)dx$$

$$z_b = \frac{1}{2}(S_1 - S_2)x - \frac{1}{2}(S_1 - S_2)\delta_0(\ln\cosh\frac{x - L_0}{\delta_0} + \ln 2) +$$
$$\frac{1}{2}(S_2 - S_3)x - \frac{1}{2}(S_2 - S_3)\delta_1(\ln\cosh\frac{x - L_1}{\delta_1} + \ln 2) + S_3 x + C \tag{3.3}$$

We may then solve for the constant, C, using the understanding that when $x = L_1$ and $\delta_1 \to 0$, $z_b = z_1$, where z_1 is the vertical distance from the x-axis to the point of intersection between S_2 and S_3. To maintain consistency with the bed level expression form presented in Hanssen et al. (2022), z_1 may be expressed as a function of the point of intersection between S_1 and S_2 (z_0), S_2, L_0, and L_1 (Equation 3.4). This gives the solution for the constant presented in Equation 3.5

$$z_1 = z_0 + S_2(L_1 - L_0) \tag{3.4}$$

$$C = -\frac{1}{2}(S_1 - S_2)(L_1 - \delta_0\ln\cosh\frac{L_1 - L_0}{\delta_0} - \delta_0\ln 2)$$
$$-\frac{1}{2}(S_2 - S_3)(L_1) - S_3 L_1 + S_2(L_1 - L_0) + z_0 \tag{3.5}$$

Substituting the solution for C back into Equation 3.3 and simplifying gives the final expression form, presented in Equation 3.6.

$$z_b = \frac{1}{2}(S_1 - S_2)\delta_0(\frac{x - L_1}{\delta_0} - \ln\cosh\frac{x - L_0}{\delta_0} + \ln\cosh\frac{L_1 - L_0}{\delta_0}) +$$
$$\frac{1}{2}(S_2 - S_3)\delta_1(\frac{x - L_1}{\delta_1} - \ln\cosh\frac{x - L_1}{\delta_1} - \ln 2) +$$
$$S_3(x - L_1) + S_2(L_1 - L_0) + z_0 \tag{3.6}$$

An example comparison of the Hanssen et al. (2022) expression and the Julseth (2024) expression is presented in Figure 3.4. The Julseth (2024) expression contains eight parameters for fitting which may be used to interpret the profile geometry. Given the clear connection of each parameter to the profile geometry itself, parameters may also be combined to represent discrete aspects of the profile. For instance, the depth of the second slope transition may be computed using Equation 3.4. Comparison of this value to the value of z_0 may provide indication of features such as sand bars or mega-ripples. Additionally, the length of the second slope can be directly calculated by subtracting L_0 from L_1. The resulting value may provide indication of subaqueous terrace lengths when fitted to profiles with geometry similar to the Group 1, 2, and 3 morphotypes presented in Travers (2007).
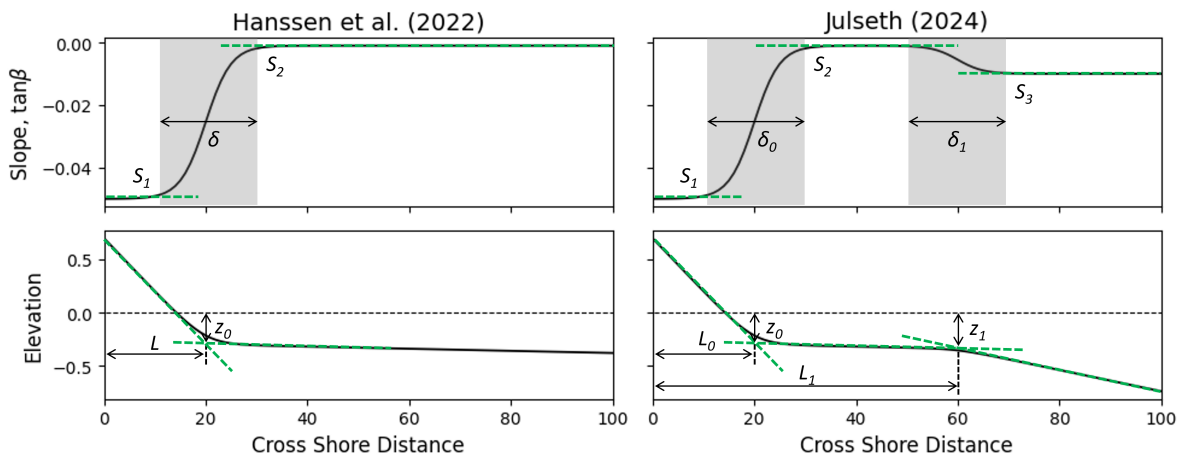

Figure 3.4: A comparison of the Hanssen et al. (2022) and Julseth (2024) slope functions and bed level functions, with labelled parameters. Parameter values used to develop these slopes are S_1=0.05 S_2=0.001, S_3=0.01, L_0=20, L_1=60, δ_0=5, δ_1=5, z_0=-0.3.

3.3.2. Expression Evaluation & Parametric Fitting

Nine parametric functions were assessed on their ability to represent diverse coastal profile geometries. The parametric functions that were tested were those presented in Table 2.1, with the exception of the function presented in Bodge (1992), since the expression provided in Komar and McDougal (1994) is a direct extension of this function with apparently increased parametric meaning. The Julseth (2024) expression was also included in the assessment. The morphotype groups presented in Travers (2007) were applied to represent diverse profile geometry. As such, artificial profiles were developed to match those presented by Travers, using the Hanssen et al. (2022) expression for Group 1 and Group 2 morphotypes and the Julseth (2024) expression for Group 3 and Group 4 morphotypes (refer to Figure 2.5). A minimization problem was solved in Python for each morphotype group and parametric function pair. An objective function for each parametric function was defined which allowed input of parameter values related to a given parametric function, the cross shore measurement points of the profile to be fit, and the associated elevations values. Each function was defined to return the sum of squared error (SSE) between the parametric profile and the profile to be fit, evaluated at the input cross shore points (Equation 3.7).

$$SSE = \Sigma(y_{obs} - y_{pred})^2 \tag{3.7}$$

Where y_{obs} is the morphotype elevations to be fit, and y_{pred} is the predicted elevations based on the input parameters. A minimization process was then completed, where the parameter values were adjusted through Newton iteration until the returned value of the objective function was minimized or the maximum number of iterations was reached. Parametric function performance was assessed using the minimized value of the objective function for comparison. A balance of clear parametric meaning and ability to represent all four of the tested profile shapes (i.e., minimum overall SSE) was used to select a parametric function for fitting to measured data.

It should be noted that minimization performance can be sensitive to the initial parameter input. Given the complexity of the evaluated parametric functions and the often interrelated impact of each parameter on the function shape, it is possible that more than one combination of parametric values can result in an objective function output that is close to the best fit. These solutions may be referred to as local minima of the objective function, and can be challenging to identify for complex minimization problems. Constraints and boundaries placed on the values of the fitted parameters can help to mitigate the output of local minima through preservation of expected parametric relationships. Through testing of each of the evaluated parametric functions, recommended initial guesses and boundaries were identified which appeared to result in minimization of the objective function without loss of parametric meaning due to the output of unrealistic parametric values. A full list of the applied parameter initializations and boundaries is presented for each parametric function in Appendix B. To mitigate potential bias in the selection of a minimization algorithm, the default algorithms within the SciPy.optimize.minimize Python package were applied. The default algorithms of this package are Sequential Least Squares Programming (SLSQP), Broyden-Fletcher-Goldfarb-Shanno algorithm (BFGS), and Limited Memory BFGS Bounded algorithm (L-BFGS-B). The primary difference between these minimization algorithms is the representation of the Hessian matrix (i.e., a matrix of second derivatives of the objective function), which is used to determine the correct descent direction during Newton iteration. Generally, little difference in performance was observed while using the default minimization algorithms with the recommended initializations and boundaries. For further information regarding these algorithms, the reader is referred to the relevant SciPy documentation.

Using the defined minimization process with the recommended initial parameter values and constraints, the selected parametric function was fit to each of the 483 profiles present in the filtered and processed profile dataset. This process resulted in the development of a dataframe containing the fitted parameters for each measured profile (i.e., a set of consequential parameters). The measured profile length was added to this dataframe to provide information regarding the total length scale of the fitted profile. Maintaining the measured profile length in the parametric dataframe primarily allows for seamless development of profile-specific cross shore discretizations when visualizing the fitted parametric function. The root mean squared error (RMSE) was applied to assess the ability of the selected parameterization to represent the measured profile data (Equation 3.8).

$$RMSE = \sqrt{\frac{\Sigma(y_{obs} - y_{pred})^2}{N}} \tag{3.8}$$

Where N is the number of points compared between y_{obs} and y_{pred}, which given the one-meter discretization of each profile is equal to the total profile length. The RMSE was used to replace the SSE here simply to maintain the unit of comparison between the observed and predicted profiles. It should be noted that this statistic is a direct function of the SSE, and thus the information gained from it is the same.

3.4. Profile Characterization

3.4.1. Profile Grouping

Using the fitted parameter values, labels may be manually defined to group similar parametric values and inter-parametric relationships. These labels can be used to identify common geometric trends in the measured profile data. For example, a label of "mild" or "steep" may be defined to describe the foreshore slope based on whether a parameter representing this geometric characteristic is above or below a given threshold. A clear connection between consequential parameters and the profile geometry is therefore valuable, since direct relationships will propagate the development of clear, meaningful data labels.

Although the use of manually defined labels can be helpful to identify general geometric trends, the definition of these labels and the selection of the related grouping boundaries is subjective to expert judgment and the characteristics of the data in question. If data from multiple diverse coastal environments is included in the analysis, then parametric distributions will likely not be single peaked. As a result, the use of standardized statistical indicators for differentiation between labels (i.e., parametric median values) may simply group data from different sources. This may be undesirable, as more subtle geometric trends may exist that may be characterized by smaller differences in parametric values. To resolve more subtle profile states, an increased number of bins is required to group the parametric data. The resulting labels will become increasingly complex. For instance, if labels were defined based on three parameters and each parameter is divided into two bins, then eight potential labels would exist by combining each single-parameter label. This number of labels is manageable, but may not provide enough information regarding more subtle differences in profile geometry. If each parameter is divided into 3 bins however, then 27 possible labels now exist. This increase affects the difficulty and time required to analyze the labels and interpret geometric trends. Furthermore, the method selected for differentiation between labels may become subjective when more divisions are made. As such, the resulting labels themselves could lose quantitative meaning. Incentive therefore exists for the application of an objective grouping algorithm that relies primarily on quantitative analysis and less on expert judgment. One such objective grouping algorithm is cluster analysis. For clarification, a summary of key terms related to cluster analysis is presented in Table 3.3. Cluster analysis uses the principle of object dissimilarity to partition data into groups with the largest inter-sample similarity.

Table 3.3: Summary of terms used to describe cluster analysis (adapted from Scott et al., 2020).

Cluster Analysis Term	Definition	This Study
Sample	Input into the algorithm to be clustered	Cross shore profile
Feature	Attribute of the sample	Cross shore elevation measurements, profile length, consequential parameters
Cluster	Groups of samples	Grouped cross shore profiles
K	Number of clusters	Number of profile clusters
Centroid	Representation of cluster group	Mean of profile features within a single cluster
Inter-cluster	Between two clusters	-
Intra-cluster	Within a single cluster	-

The most common algorithm used for cluster analysis is K-means clustering, which represents the cluster centroid as the mean value of respective features in each sample (Hartigan, 1975). The process followed for K-means clustering is as follows:

1. Initial cluster centres are selected. In the present study the K-means++ algorithm was applied to select initial cluster centres. This algorithm applies probabilistic techniques to strategically select initial cluster centres, improving the quality of the final solution (Arthur & Vassilvitskii, 2007).

2. The squared-euclidean distance (SED) is computed between samples and cluster centres.

3. Each sample is assigned to the closest cluster centre.

4. The mean of the samples in each cluster is computed and applied as the new cluster centre.

5. Steps 2 to 4 are repeated until the maximum number of iterations is reached or the cluster assignment of samples remains constant.

A visual representation of this process in 2D and with K = 3 is presented in Figure 3.5. This figure demonstrates the initial centroid selection (upper left), the initial cluster assignment and data partitioning (upper right), the centroid assignment and partitioning following the second iteration (bottom left), and the centroid assignment and partitioning following 20 iterations (bottom right).
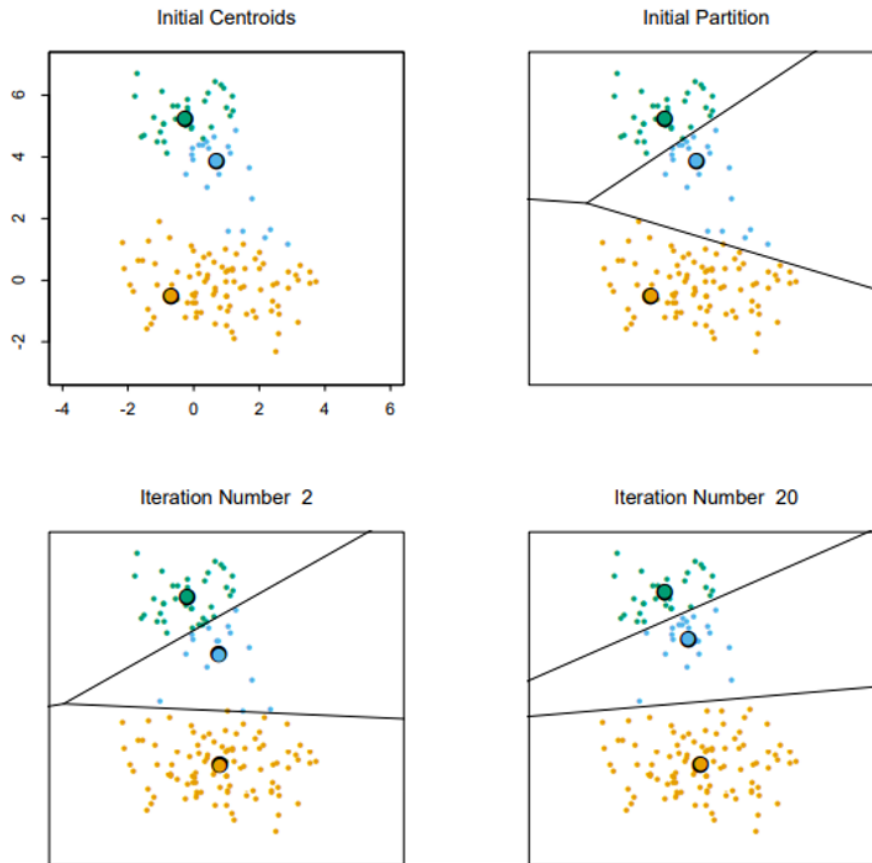
Figure 3.5: Successive iterations of the K-means clustering algorithm (Source: Hastie et al., 2001).

Two versions of K-means clustering were completed for the present study. The first version used profile elevation values at normalized cross shore positions and the total profile length as the features comprising each sample, and thus is an application of the empirical profile data (empirical clustering). The second version used the parametric values fitted to each measured profile as the features comprising each sample, and thus is an indirect application of the empirical data through parametric representation of the profile geometry (parametric clustering). Conducting clustering analysis with both empirical and parametric features allowed for comparison of K-means clustering performance using empirical profile data versus parametric profile representations. The following subsections describe the methodology followed to conduct cluster analysis for each dataset.

The number of clusters, K, was determined by analyzing the mean variance represented by each cluster and the SSE between the clustered processed measured data (i.e., the empirical samples) and the cluster centres. This analysis was completed for 4, 9, 16, 25, 36, 49, 64, 81, 100, 121, 144, 169, and 196 clusters. It was determined through this assessment that the amount of variance in each cluster tends approximately linearly towards zero when the number of clusters is increased, particularly for more than 49 clusters. This observation was expected since more clusters result in fewer profiles per cluster. Although decreasing the number of profiles per cluster reduces the amount of intra-cluster variance, increasing the number of clusters towards the number of measured profiles results in loss of value in the analysis. As such, minimizing intra-cluster variance is not necessarily desireable. The SSE was thus used as a comparative statistic to help select the desired number of clusters. This statistic demonstrated marginal gains when considering more than nine clusters. 49 clusters were therefore selected to balance reduction of intra-cluster variance and minimization of observed SSE.

Empirical Clustering
The empirical clustering analysis applied the direct profile elevation data and the total profile lengths to identify groups of profiles with similar geometric features. To compare elevation values directly, each

profile was normalized by interpolating the measured elevations to 101 evenly spaced points along its length. This normalization resulted in loss of information regarding the spatial scale of each profile. To mitigate this, the total profile length was included as a feature in each sample. Elevation values and profile lengths were then scaled to take values between zero and one, ensuring clear interpretation of relative differences by the clustering algorithm and reducing potential for misleading results. In this case, the maximum observed elevation was assigned a value of one and the minimum observed elevation was assigned a value of zero, with the remaining measurements scaled to maintain the relative elevation differences. This scaling was completed separately for the profile length feature. Finally, the features were weighted to ensure that the length scale of each profile was adequately represented in the analysis, assigning 50% weight to the profile length feature and distributing the remaining 50% weight between each of the 101 cross shore elevation values (i.e., $\sim$0.5% per value). Following clustering, the samples and their corresponding cluster centroids were unweighted and descaled to conduct statistical and visualize assessment. Assessment of clustering performance was completed using the mean intra-cluster variance and RMSE, providing information regarding the amount of variance represented by each cluster and the similarity of each cluster centroid to its corresponding samples.

Parametric Clustering
The parametric clustering analysis applied the fitted parametric values to the measured dataset to identify groups of profiles with similar geometric features. Unlike the empirical clustering, cross shore normalization was not required for parametric clustering, since each feature represented a distinct geometric characteristic. As such, each feature was scaled individually to take values between zero and one, relative to the maximum and minimum value of that feature. The scaled features were used for clustering. Following clustering, the samples in each cluster and the corresponding cluster centroids were descaled. Representative profiles were developed by evaluating the parametric function with fitted parameter values at the same cross shore positions as the processed profile data. Assessment of clustering performance was completed using the same methodology for the empirical clusters (intra-cluster variance and RMSE). Use of the same assessment methodology allowed for direct comparison of performance between empirical and parametric clustering.

3.4.2. Parametric Correlation Analysis
An analysis of correlations between the computed causal parameters and the fitted consequential parameters from a selected parametric shape function was completed to assess the ability to identify expected geomorphological trends in a measured dataset using a parametric representation of the profile geometry. Correlation strength was assessed using the Spearman Rank Correlation Coefficient, $r_{i,j}$, where i and j represent two random variables (Equation 3.9).

$$r_{i,j} = \frac{cov(R_i, R_j)}{\sigma_{R_i}\sigma_{R_j}} \tag{3.9}$$

Where R_i and R_j are the ranks of the values in i and j, and $cov(R_i, R_j)$ is the covariance of the ranks of i and j. This correlation coefficient varies between -1 and 1, where a value of -1 implies a perfect negative rank correlation and a value of 1 implies a perfect positive rank correlation (Zwillinger & Kokoska, 2000). Rank correlation is an assessment of a monotonic relationship between two parameters. A positive monotonic correlation thus implies that increased (decreased) values of one parameter are correlated to increased (decreased) values of another parameter. This correlation differs from the well-known Pearson Correlation in that non-linear monotonic correlations can be identified. The rank correlation is therefore considered to be more versatile than the Pearson Correlation when assessing trends in proportionality, but does not indicate the order of identified correlations (e.g., linear, quadratic, exponential). Spearman correlation significance was assessed using a p-value for a hypothesis test with the null hypothesis that two given parameters have no ordinal correlation (Zwillinger & Kokoska, 2000). Correlations were deemed significant for p-values less than or equal to 0.05 (i.e., 95% confidence in an ordinal correlation).

Rank correlation matrices were computed for three different cases. The first case considered correlations between the computed causal parameters for each of the processed profiles and the consequential parameters obtained through parametric fitting to each profile. This analysis thus provides an

indication of potential correlations in the full processed dataset. The second case considered correlations between the consequential parameters of the empirical cluster centroids and the mean causal parameters associated with the profiles within each cluster. The consequential parameters of cluster centroids were obtained by taking the mean parametric values for each profile within each cluster. The third case considered correlations between the consequential parameters of the parametric cluster centroids and the mean causal parameters associated with the profiles within each cluster. As with the empirical cluster centroids, the consequential parameters of centroids were obtained by taking the mean parametric values for each profile within each cluster. It should be noted that clusters obtained using the empirical features are expected to be different than those obtained using parametric features. The second and third correlation cases apply the cluster centroids in order to represent a portion of the data and its associated variance. In doing so, less profiles and thus less noise is expected during these correlation analyses. Differences in correlation strength between the full processed dataset and the clustered representations may therefore provide an indication of ability to use cluster centroids to represent grouped geometrically similar profiles and amplify correlation signals.

It should be noted that the provided analyses do not intend to identify cause-and-effect relationships between so-called causal and consequential parameters. Instead, this analysis aims to determine if expected geomorphological trends can be observed in measured data using a given profile parameterization. This analysis provides a basis for future studies to identify cause-and-effect relationships which may be applied for predictive capability.

4

Results

Chapter Outline
In this chapter the results of the completed research are presented. Parametric function evaluation is first shown, demonstrating that higher complexity functions are generally able to fit more diverse geometries. The highest performing expression is the new expression defined in this study ($\overline{SSE}$ = 0.04). Application of this function with measured data indicates its ability to provide a clear representation of profile geometry ($\overline{RMSE}$ = 0.05 m), and applicability for grouping of profiles with similar geometric attributes (mean inter-cluster variance = 0.07 for both empirical and parametric clustering). Next, analysis of causal parameters is presented, indicating increased influence of parametric variability when the shortest considered computation time scale is used, demonstrated by narrowed inter-quantile range values for longer time scales. Finally, causal-consequential correlation analyses are shown, suggesting that analyses with all fitted profiles provides weak significant correlations (max $r_{x,y}$ = 0.41) that align with expected geomorphological trends. Representation of profile groups using empirical and parametric cluster centroids demonstrates an ability to amplify correlation signals (max $r_{x,y}$ = 0.80 and 0.76, respectively), however correlations using parametric cluster centroids appear to be more similar to correlations made with the full dataset compared to representation using empirical cluster centroids.

4.1. Profile Parameterization
To what degree of accuracy can parametric shape functions represent diverse coastal profile geometry?

4.1.1. Expression Evaluation
Several parametric functions exist which are able to provide reasonable fits to the profile morphotypes presented in Travers (2007). To fit both simple and complex profile geometry, parametric functions should have a high degree of flexibility, while maintaining a clear connection of each parameter to the profile geometry itself. This connection ensures that fitted parameters can be effectively interpreted and used to represent characteristics of the measured profile. Ability for each parametric function to represent diverse profile geometry was compared by computing the SSE from the fitted parametric function to artificial profiles representing each morphotype. SSE for each profile parameterization are presented in Table 4.1.

Table 4.1: Sum of squared error observed between profile morphotypes and fitted parametric functions.

Parametric Function	Sum of Squared Error			
	Exponential (Group 1)	Segmented (Group 2)	Concave-Curvilinear (Group 3)	Convex-Curvilinear (Group 4)
Komar and McDougal (1994)	0.22	0.56	23.94	26.84
Lee (1994)	5.00	2.77	5.43	4.25
Dai et al. (2007)	0.22	0.56	5.43	4.25
Bruun (1954) and Dean (1977)	8.75	4.30	5.11	4.15
Powell (1990)	0.14	<0.01	2.17	0.16
Inman et al. (1993)	0.24	0.45	0.75	1.62
Hsu et al. (2006)	0.04	0.37	0.23	0.01
Hanssen et al. (2022)	<0.01	<0.01	4.17	3.08
Julseth (2024)	0.12	<0.01	<0.01	<0.01

The results in Table 4.1 demonstrate that Group 1 and Group 2 morphotypes can be well represented by most of the considered parametric functions. This representation is attributed to the monotonic, simplified geometry of these morphotype groups. Group 3 and Group 4 morphotypes were best represented by polynomial-type shape functions (i.e., biparabolic functions) and hyperbolic-type shape functions. Generally, the hyperbolic-type functions outperformed the other function types when considering ability to fit all four morphotype groups. Plots showing the fit of each tested parametric expression are presented in Appendix A.

The parametric functions constrained to single concavity are those presented by Bruun (1954), Dai et al. (2007), Hanssen et al. (2022), Komar and McDougal (1994), and Lee (1994). These expressions generally demonstrate ability to represent Group 1 and Group 2 morphotypes well. It is noted that the Lee (1994) and the Bruun (1954) expressions have reduced ability to represent Group 1 and Group 2 morphotypes. In the case of the Lee (1994) expression, its logarithmic form results in challenges fitting gradual offshore slopes without overcompensating through increased concavity, and gradual nearshore slopes without overcompensating through increased scale. This behaviour results in a weaker fit to profiles with long, gradual geometry. In the case of the Bruun (1954) expression, the function also struggles with parametric overcompensation in order to fit larger sections of the profile. This behaviour creates localized sections with increased error. As expected, the ability of single concavity expressions to fit Group 3 and Group 4 morphotypes is weak compared to more complex expressions. Typically, the single concavity expressions appear to fit the Group 3 and Group 4 morphotypes using a relatively straight line, resulting in similar SSE for each expression. The exception to this observation is the expression presented by Komar and McDougal (1994), which is the worst performing single concavity expression

for Group 3 and Group 4 fitting. The poor performance of this expression is attributed to the tendency of this expression to be strongly concave-up, resulting in large error when fitting to profiles with both concave-up and convex-up sections.

The parametric functions with increased geometric complexity are those presented by Hsu et al. (2006), Inman et al. (1993), and Powell (1990), as well as the newly derived expression from this study, referred to as Julseth (2024). These expressions demonstrate ability to represent all morphotype groups well, however loss of meaning of parameter values may be present when fitting expressions with increased complexity to simple profiles (i.e., Group 1 and Group 2). The Julseth (2024) expression is the strongest performing of the considered expressions, with a SSE of <0.01 for morphotype Group 2, 3, and 4, and the third smallest overall SSE for Group 1, resulting in a mean SSE of 0.04. The next best overall performing expression is that of Hsu et al. (2006), with the second smallest SSE for morphotype Group 1, 3, and 4, and the third smallest overall SSE for Group 2, resulting in a mean SSE of 0.16. Since the fitting profiles were developed using the Hanssen et al. (2022) and Julseth (2024) expressions, it is reasonable to assume that the Hsu et al. (2006) expression is equally able to represent all four morphotype groups compared to the Julseth (2024) expression. With that said, the meaning of the seven parameter values used to fit the Hsu et al. (2006) expression ($h_c, x_c, A_1, A_2, B_1, B_2, B_3$) are challenging to interpret given the direct connection of these parameters to barred profiles. Understanding the meaning of these parameters when fitted to non-barred profiles is thus ambiguous, and requires further study. Conversely, the eight parameters used for fitting in the Julseth (2024) expression ($S_1, S_2, S_3, \delta_0, \delta_1, L_0, L_1, z_0$) describe attributes of the profile geometry more plainly, which is beneficial when fitting to coastal profiles with diverse geometry. As a result, the Julseth (2024) expression was further applied to measured data to test its ability to accurately represent and group measured profiles. Analysis of the distribution of the fitted geometric parameters was performed to identify morphotype groups in the measured data, and observed parametric distributions were compared to the expected behaviour of the Narrabeen-Collaroy system. This analysis was completed alongside a univariate analysis of the selected causal parameters at Narrabeen-Collaroy, as presented in Section 4.2.

4.1.2. Parametric Fitting
The Julseth (2024) expression was fit to the processed profile data in order to represent geometric characteristics and identify spatial trends. This expression was able to fit the measured data with a high degree of accuracy, resulting in a maximum RMSE of 0.33 m and a mean RMSE of 0.05 m. The profile with the maximum RMSE has a shape similar to the ridge-runnel state described by Wright and Short (1984) (Figure 4.1). The profile length in this case is dominated by the ridge profile, with a short (<10 m) foreshore slope and relatively deep (1.5 m) runnel. This is expected to result bias towards fitting of the convex-up ridge slope, largely ignoring the complex nearshore geometry and increasing the RMSE. The inter-quantile range was applied to determine if the maximum observed RMSE fit was an outlier, as presented in Equation 4.1.

$$Max.Outlier > Q3 + 1.5(|Q1| + |Q3|) \tag{4.1}$$

Where $Q1$ is the 25th percentile, and $Q3$ is the 75th percentile. This conditional test indicated that fit values with RMSE greater than 0.16 were likely maximum outliers. The maximum RMSE profile was the only profile with an RMSE value significantly greater than the computed threshold. This profile was therefore removed to mitigate its influence on the interpretation of geometric trends. The subsequent maximum observed RMSE was 0.18.

Distributions of the remaining fitted consequential parameters were visualized and descriptive statistics computed to understand the general geometric characteristics of the measured profiles. S_1, S_2, and S_3 were observed to have single peaked distributions (μ = 6.75°, 0.87°, 3.10°, σ = 1.98°, 1.92°, 1.96°, respectively). The magnitude of the mean slope values indicate that the measured profile between MLW$\pm$2 m typically has a concave-up nearshore curvature and a convex-up offshore curvature. The standard deviation of S_2 indicates potential for negative slopes, indicating resolution of features such as bars, mega-ripples, and ridges. This geometry is further supported by the observation that mean values of z_0 and z_1 are within a single standard deviation of each other, indicating likelihood of profiles where z_0 is deeper than z_1 (μ = -0.86 m, -1.41 m, σ = 0.65 m, 0.54 m, respectively). The length parameters derived from the Julseth (2024) expression (L_0, L_1, L_{total}) are all single peaked and tend to have a small
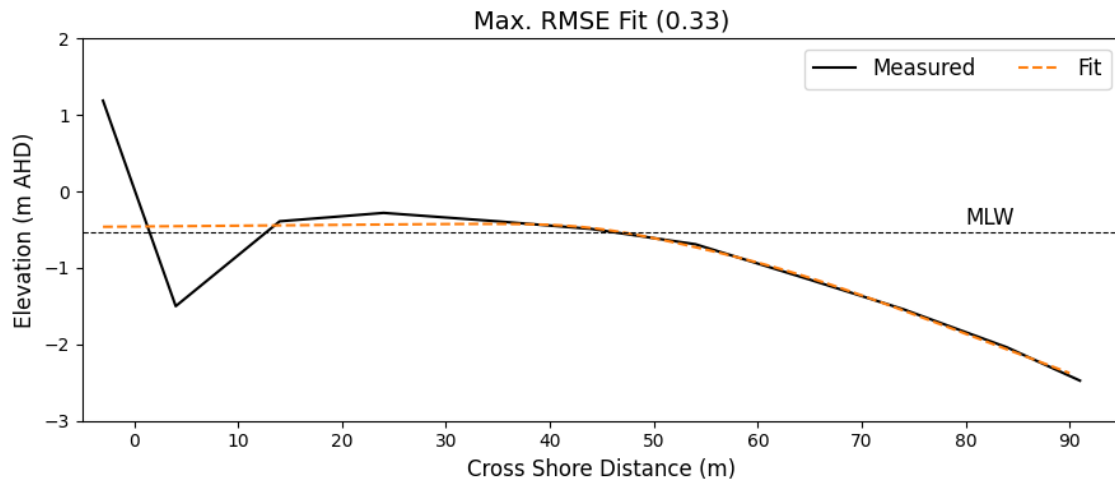
Figure 4.1: Fit to measured data with the largest observed RMSE using the Julseth (2024) expression.

positive skewness (μ = 20.29 m, 55.55 m, 79.40 m, σ = 7.67 m, 14.96 m, 16.79 m, respectively). The fitted δ parameters in the Julseth (2024) expression show double peaked distributions, with a narrow distribution centred around 1 m and a wider distribution centred around approximately 6 m. This double peaked distribution indicates the presence of both gradual and sharp profile transitions which may be related to the presence of geological features (i.e., mega-ripple and low-barred profiles would be expected to have larger values of delta indicating smoother transitions). Univariate histograms of each consequential parameter are presented in Appendix A. When comparing the general characteristics of the fitted data to the approximate bounds presented for beach states in Wright and Short (1984), the observed values indicate the mean measured profile represents an intermediate beach state (refer to Figure 2.4). This classification aligns with the classification presented in Wright and Short (1984) for Narrabeen-Collaroy beach, indicating that the Julseth (2024) parameterization provides a good representation of the measured profiles.

4.2. Profile Characterization
4.2.1. Metocean Parametric Analysis
What is the impact of varying temporal scales to the distribution of causal parameters?

Empirical univariate distributions of the computed causal parameters were assessed to understand the general characteristics of each causal parameter and the impact of different time periods for computation. As discussed in Section 3.2.2, the time frames for computation were seven days, three months, six months, and one year preceding each profile measurement. Univariate distributions of each causal parameter are presented in Figure 4.2 and Appendix A. Analysis of the inter-quantile range for univariate distributions of time-averaged causal parameters shows narrowed distributions for longer computation periods. This observation indicates greater influence of variability in the mean causal parameter values when a shorter computation period is applied, demonstrating that the effect of large variability (such as storms) is most clearly visible for shorter computation periods. This observation is supported by an increased inter-quantile range in the causal parameter standard deviations for shorter computation periods. As a result, correlations with causal means are expected to be larger for time scales of less than one year, assuming that storms are the dominant drivers of profile geometry. Analysis of univariate distributions of time-averaged wave height and power shows decomposition of single peaked distributions into two-peaked distributions for longer computation periods. This observation is expected to be a result of the relationship between dominant wave angles and transect orientation, as more southern transects are observed to generally have smaller wave heights, resulting in the development of a second peak for longer averaging periods. However, this observation could also be an indication of fully developed sea dominance versus swell dominance of the incident wave conditions, leading to a second peak development when longer time scales are considered. Visual analysis of the alongshore power

distributions shows that the alongshore wave power is generally about one order of magnitude smaller than the total wave power and has positive skewness (mean > median). Observed positive skewness indicates increased alongshore power for waves travelling northward, as expected given the dominant wave direction. Finally, the maximum astronomical tidal range demonstrates tendency towards the mean maximum tidal range of the entire dataset for longer time averaging periods, as expected given the cyclical nature of this statistic.
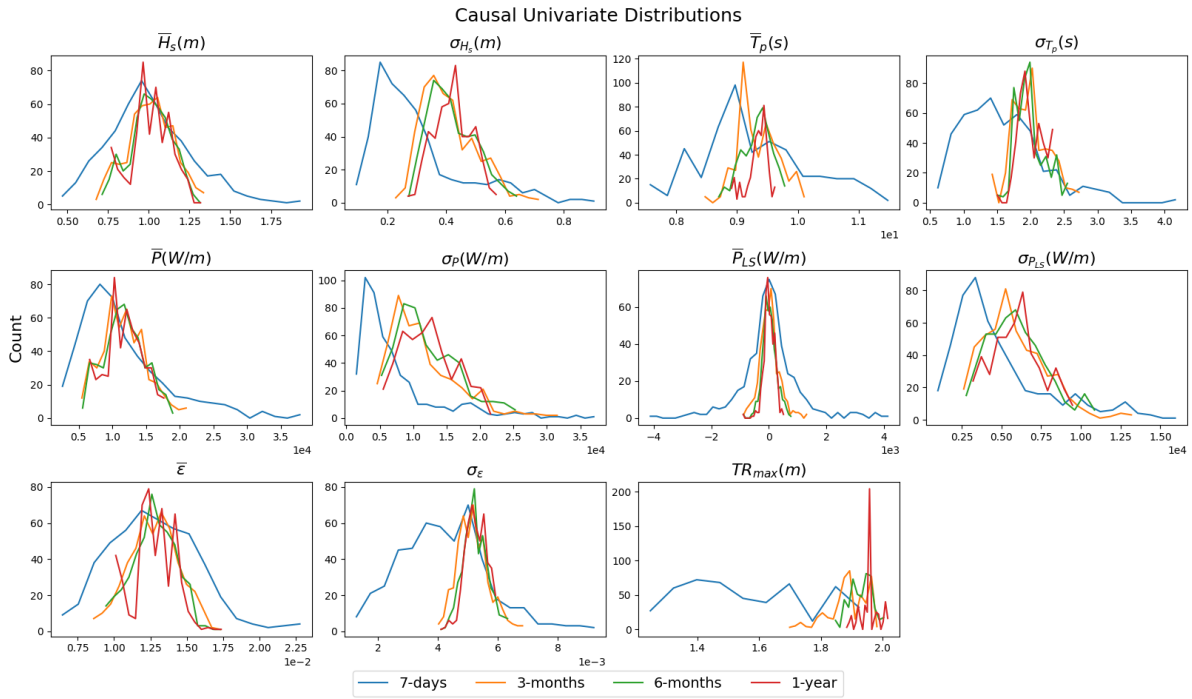
Figure 4.2: Causal parameter distributions for each computation time scale.

4.2.2. Profile Grouping
Can a parametric shape function be used to effectively group and classify measured profile data?

Fitted parameters of the Julseth (2024) expression were used to create labels for the measured profile data to test the ability to identify discrete profile morphotypes using the geometric parameterization. For simplicity, labels were constrained to three keywords to describe the profile using five of the eight available consequential parameters. A description of these keywords and their meaning is presented in Table 4.2. It should be noted that alternate labels could be developed depending on the geometric properties of interest. The following classifications aim to demonstrate the capability to use the Julseth (2024) parameterization to identify trends in measured profile geometry, with emphasis placed on the foreshore slope, subaqueous terrace length, and presence of bars. The presented conditional values are the 50th quantile of the associated parametric relationship. Based on the defined labels, there are eight possible profile classifications. Plots of the measured profiles for each classification and the associated mean parametric representation demonstrate that classification of measured data using the Julseth (2024) parameterization is possible (Figure 4.3). Additional labelling examples are presented in Appendix A.

The limitation of this strategy is the subjective nature of the classification condition. In this case, median values were used to differentiate between profile classes associated with a single parameter. Given that a single beach was assessed during the present study, this method is considered effective to identify varying profile states. However, if data from multiple diverse locations is considered, finding conditional values that can represent discrete profile states both between measurement locations and

Table 4.2: Consequential parameters used for labelling of measured profiles, and the associated conditions and keywords applied.

Parameters	Condition	Keyword
S_1	$S_1 < 6.56°$	"Mild"
	$S_1 > 6.56°$	"Steep"
L_0, L_1	$L_1 - L_0 < 34.55m$	"Short"
	$L_1 - L_0 > 34.55m$	"Long"
z_0, z_1	$z_0 < z_1$	"Barred"
	$z_0 > z_1$	"Unbarred"
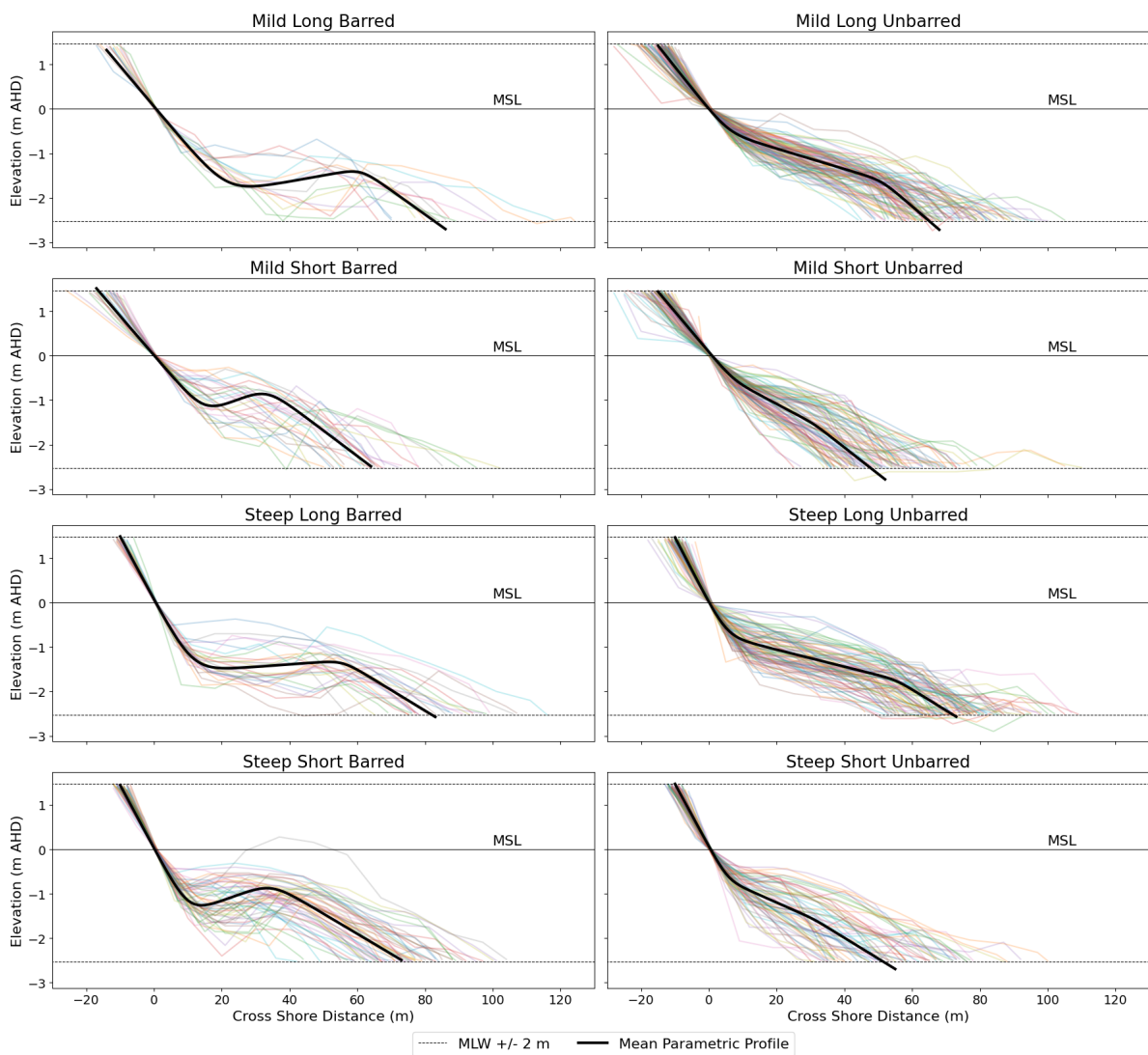
Figure 4.3: Classified measured profiles using the labels defined by the Julseth (2024) parameterization. Coloured lines represent measured profiles, while black bold lines represent the mean parameterized profile associated with each profile class.

within single measurement locations becomes increasingly subjective. K-means clustering was therefore tested as an objective classification method to categorize measured profiles with diverse geometry.

Clustering was completed on the processed measured data as well as the fitted parameter values to assess the capability of clustering using both empirical and parameterized representations of the profile. The mean intra-cluster variance and RMSE were computed as metrics for comparison of each clustering method's ability to reduce variance in the dataset. The mean intra-cluster variance for the empirical clustering had a mean value of 0.07 with a standard deviation of 0.03, while the parametric clustering had a mean of 0.07 with a standard deviation of 0.05. The mean intra-cluster RMSE for the empirical clustering was 0.23 m with a standard deviation of 0.05 m while parametric clustering had a mean RMSE of 0.24 with a standard deviation of 0.07. These metrics indicate that empirical and parametric clustering provide similar variance reduction capabilities, however empirical clustering appears to slightly outperform parametric clustering using these metrics. Although these statistical indicators are useful for comparison of overall variance representation, they provide little information about grouping of profiles with similar geometric characteristics, which is ultimately the primary goal of clustering. Through visual assessment, parametric clustering appears to outperform empirical clustering when considering groupings of profiles with similar geometric characteristics. This observation is demonstrated through comparison of Figure 4.4 and Figure 4.5. These figures present the processed measured profiles within the 49 clusters obtained through empirical and parametric clustering. The colour of the presented profiles corresponds to the label that each respective profile was assigned using Table 4.2. It should be noted that a cluster in a given position of Figure 4.4 does not correspond to the cluster in the same position of Figure 4.5. Given that the cluster analysis is completed using different features, the resulting clusters are inherently different and thus only general visual observations can be made. These figures demonstrate that despite having more average variance per cluster, the parametric clustering appears to outperform empirical clustering when grouping profiles based on geometric characteristics. This observation is made by considering the homogeneity of colours in each cluster, where increased homogeneity indicates classification of profiles in a more similar fashion to the manual parametric labelling. One example of this which is clear in Figure 4.4 and Figure 4.5 is the grouping of barred versus unbarred profiles. While empirical clusters tend to combine barred and unbarred profiles, the parametric clusters appear to group barred and unbarred profiles more effectively. This demonstrates that the Julseth (2024) parametric function can be applied alongside K-means clustering to effectively identify geometric profile trends.

4.2.3. Parametric Correlation Analysis
Are expected geomorphological processes identifiable through causal-consequential parametric correlation analysis?

The first case for causal consequential rank correlation analysis considered the computed causal parameters for each of the processed profiles and the consequential parameters obtained through parametric fitting to each profile. This analysis presented significant but relatively weak correlations between fitted consequential parameters and computed causal parameters, with a maximum observed significant rank correlation of 0.41 between the six-month total wave power standard deviation and the full profile length. The maximum observed significant rank correlation considering only the parameters in the Julseth (2024) parameterization was -0.32 between the three-month total wave power standard deviation and the most offshore slope parameter (S_3) (Figure 4.6).

Positive rank correlations are observed between S_1 and several causal parameters related to wave characteristics, with increased correlation strength between those parameters representing variability in wave conditions for a six-month computation period. The inverse correlation is observed between these causal parameters and S_2 and S_3, with similar magnitude. A positive correlation between the wave power parameters and the length parameter indicate longer profiles between MLW $\pm$ 2 m and longer subaqueous terraces are correlated to more energetic wave conditions, while the negative correlation with the nearshore depth parameter indicates deeper profiles are correlated to more energetic wave conditions. Further, a positive correlation with total wave power and δ_0 indicates that more gradual transitions between the first and second slopes are correlated to increased wave energy. Correlations with mean wave power and mean wave height have marginal variations in strength for different time

Figure 4.4: Measured profiles clustered using empirical measurements, coloured using manual labels. Homogeneity of profile colours per cluster here indicates ability to identify expected profile morphotypes using empirical cluster analysis.
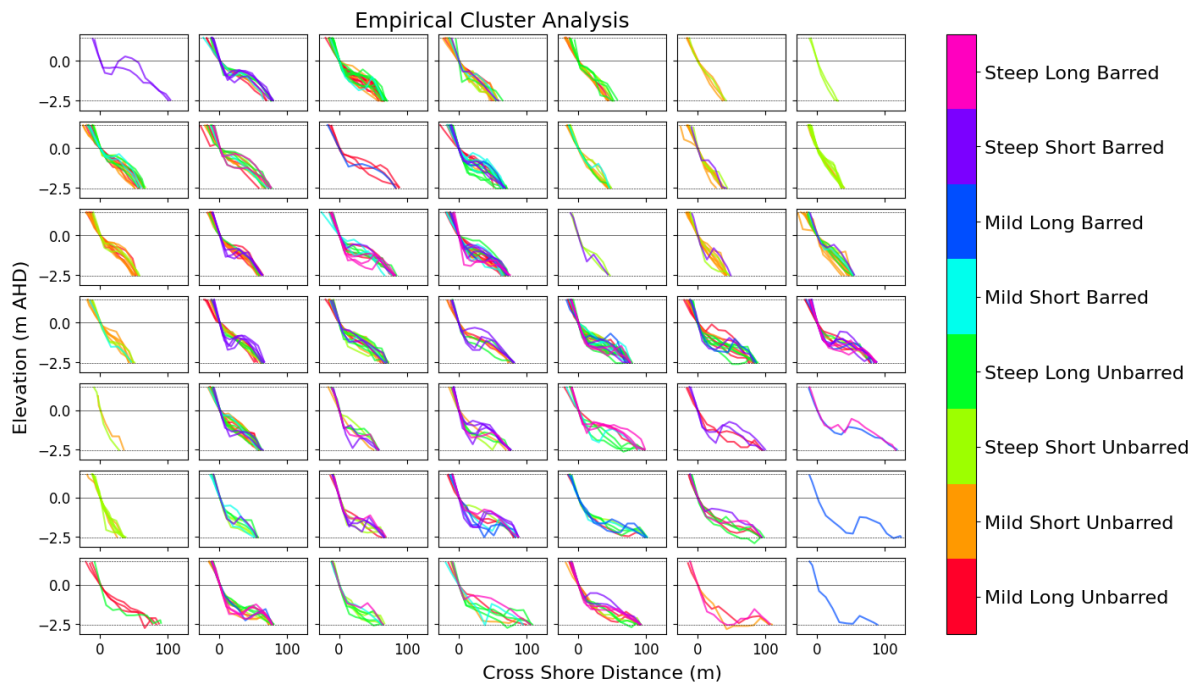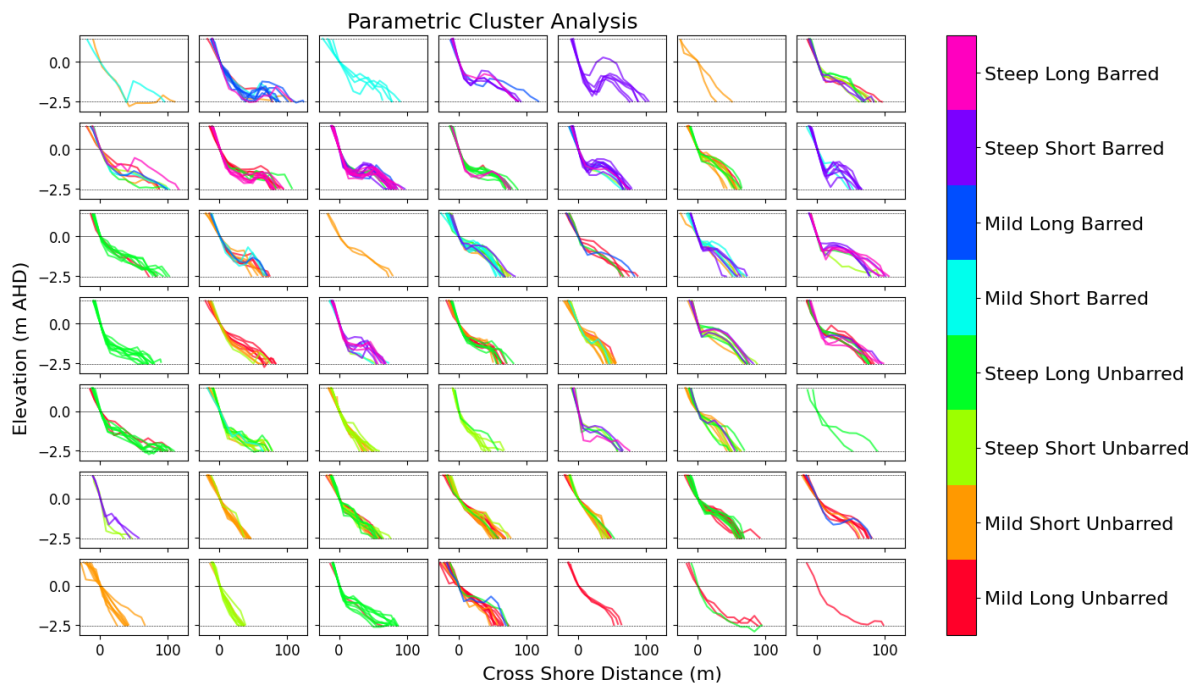

Figure 4.5: Measured profiles clustered using parametric representation, coloured using manual labels. Homogeneity of profile colours per cluster here indicates ability to identify expected profile morphotypes using parametric cluster analysis.

Figure 4.6: Observed Spearman rank correlations between fitted consequential parameters and computed causal parameters for all measured profiles. Only significant correlations are provided.

scales, indicating importance of different time scales for different geometric features (e.g., correlation strength with $\overline{H}_s$ and L_{total} decreases for longer time periods, but increases with z_0 for longer time periods). Correlations observed between consequential parameters and the causal parameters related to tidal range and wave period are generally more scarce. The strongest correlations observed with the tidal range are between the seven-day tidal range and the total profile length (0.19), and the one-year tidal range and the most offshore slope (-0.17). These correlations indicate that short-term tidal variability is weakly correlated to lengthening of the profile between MLW $\pm$ 2 m, and long term tidal variability is correlated to flattening of the offshore profile. The strongest correlations with the wave period are between one-year mean period and the total profile length (0.30) and the one-year mean period and the most offshore slope (-0.24). These correlations indicate that longer term time scales generally dominate over shorter term time scales when considering the effect of wave period on profile geometry. Correlations with the alongshore component of the total wave power are observed primarily with the standard deviation of this causal parameter, and have similar correlation trends to the total wave parameter standard deviation. A positive monotonic relationship is observed between the standard deviation in the alongshore wave power and S_1, L_1, δ_0, and L_{total}. A negative monotonic relationship is observed with S_2, S_3, and z_0. These correlations suggest importance of wave direction variability on the geometry of the cross shore profile.

The second and third cases for causal consequential rank correlation analysis aimed to assess the ability for empirical and parametric cluster centroids to effectively match and amplify correlations in the full dataset. Empirical clustering demonstrated strong ability to amplify correlation signals, resulting in a maximum significant rank correlation of 0.80 between the mean one-year peak period and the total profile length. The maximum observed significant rank correlation considering only the parameters in the Julseth (2024) parameterization for the empirical clustering was 0.70 between the six-month wave steepness standard deviation and L_1 (the length from the origin to the intersection of S_2 and S_3) (Figure 4.7). A key observation here is the change observed in the causal parameter computation time period for the strongest observed correlations compared to the full dataset, and the difference in parameters found with the strongest correlation. Empirical clustering resulted in an increased number of significant causal-consequential correlations. Additional correlations generally match the trends observed for the full dataset correlation analysis, but do have some differences. First, all significant correlations with the nearshore slope are lost in the empirical clustering case. Second, significant positive correlations are now identified between causal parameters related to significant wave height, peak period, and wave power, and the δ_1 consequential parameter. This observation indicates that empirical clustering results in some variance to the causal-consequential relationships previously identified in the full dataset.
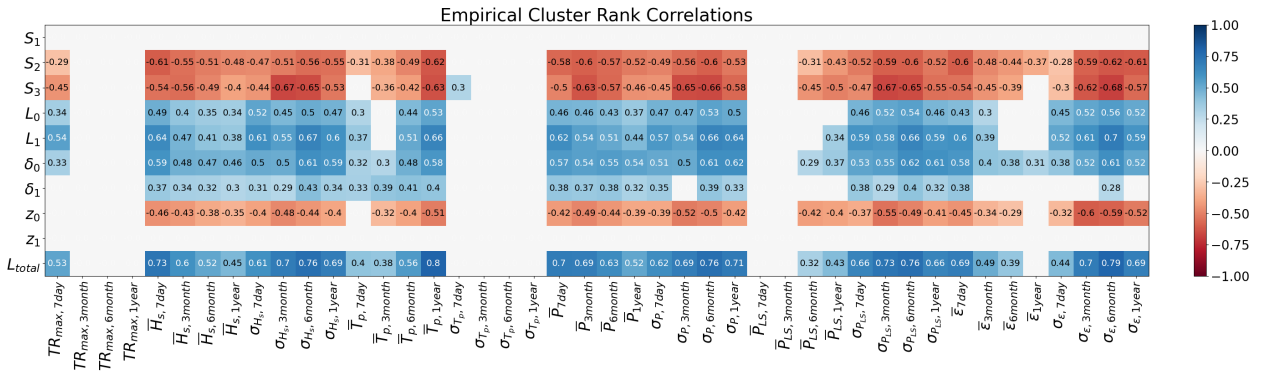
Figure 4.7: Observed Spearman rank correlations between fitted consequential parameters and computed causal parameters for empirical cluster centroids. Only significant correlations are provided.

Parametric clustering also demonstrated a strong ability to amplify correlation signals, however the amplification was not as strong as with empirical clustering. The maximum significant rank correlation observed in the parametric clustering correlation analysis was 0.76 between the six-month significant wave height standard deviation and the total profile length. The maximum observed significant rank correlation considering only the parameters in the Julseth (2024) parameterization for the parametric clustering was 0.70 between the three-month significant wave height standard deviation and the most offshore slope parameter, S_3 (Figure 4.8). It should be noted that these maximum correlations are more similar to the full data case compared to the empirical clustering case.
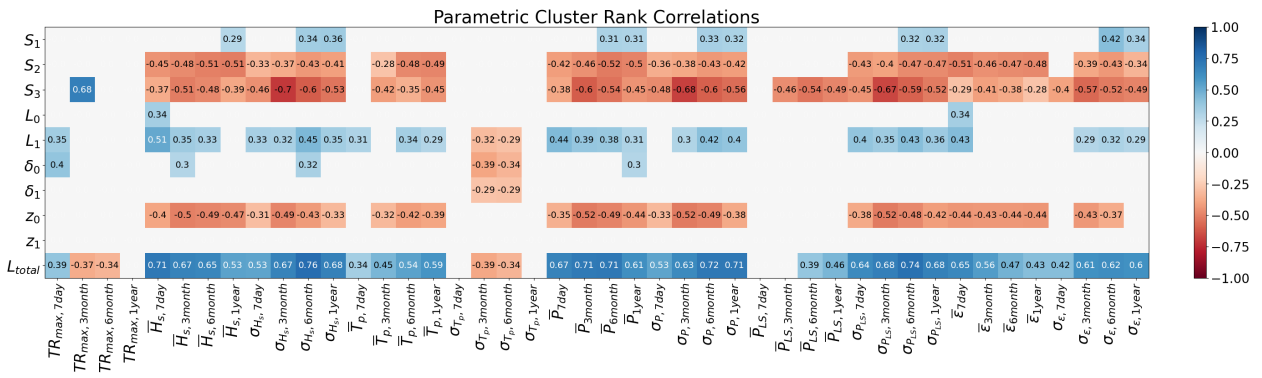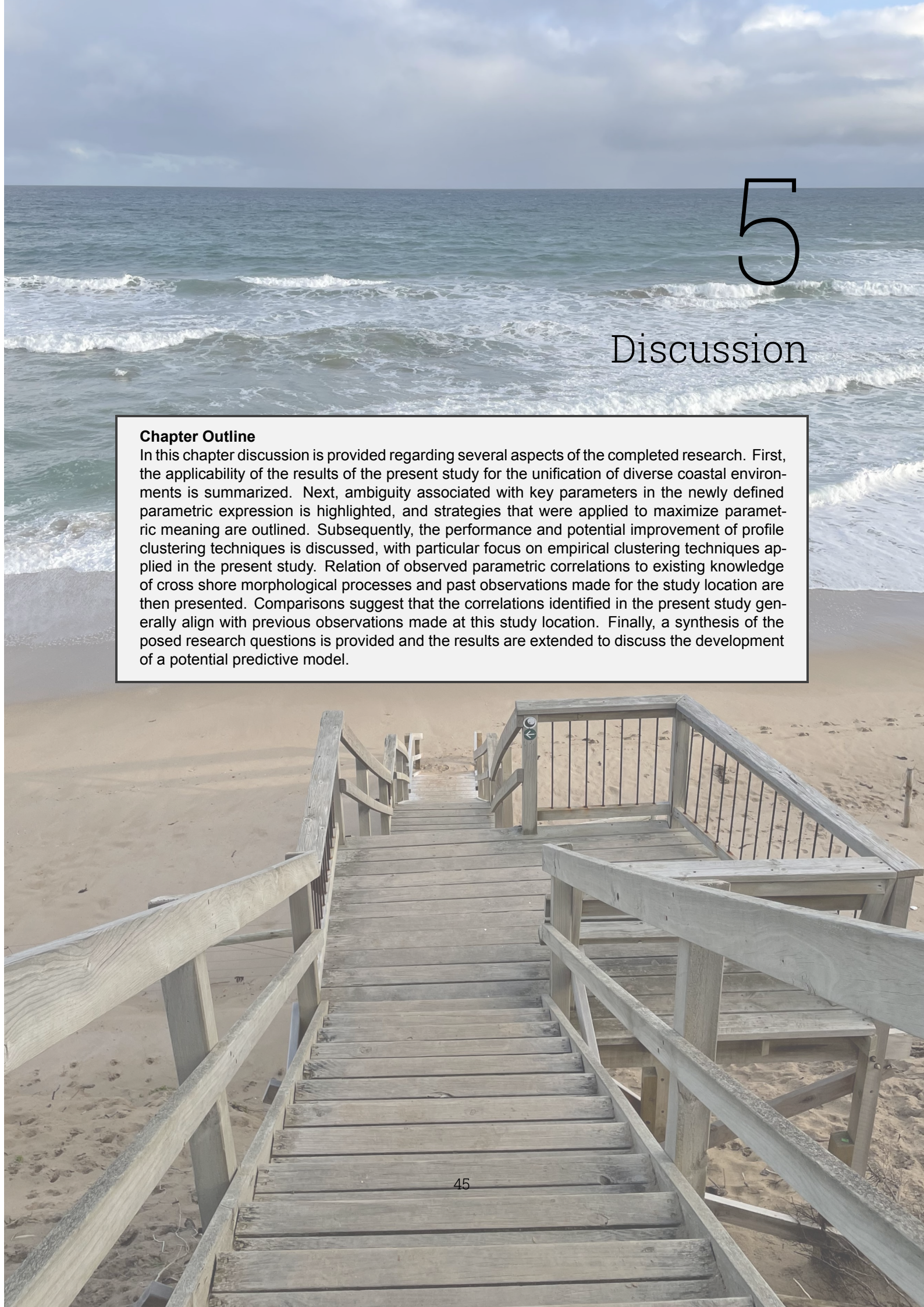

Figure 4.8: Observed Spearman rank correlations between fitted consequential parameters and computed causal parameters for parametric cluster centroids. Only significant correlations are provided.

Conversely to empirical clustering, parametric clustering results in fewer observed significant causal-consequential rank correlations compared to the full data case. The primary correlations that were lost through parametric clustering were between L_0 and the time averaged significant wave height and wave power parameters. Additionally, the majority of significant correlations with δ_0 were lost. Despite these lost correlations, the strongest observed correlations in the full data case are generally preserved and amplified in the parametric clustering case.

5

Discussion

Chapter Outline

In this chapter discussion is provided regarding several aspects of the completed research. First, the applicability of the results of the present study for the unification of diverse coastal environments is summarized. Next, ambiguity associated with key parameters in the newly defined parametric expression is highlighted, and strategies that were applied to maximize parametric meaning are outlined. Subsequently, the performance and potential improvement of profile clustering techniques is discussed, with particular focus on empirical clustering techniques applied in the present study. Relation of observed parametric correlations to existing knowledge of cross shore morphological processes and past observations made for the study location are then presented. Comparisons suggest that the correlations identified in the present study generally align with previous observations made at this study location. Finally, a synthesis of the posed research questions is provided and the results are extended to discuss the development of a potential predictive model.

5.1. Unification of Diverse Environments

The initial aim of this study was to explore the ability to use parametric representation of coastal profile geometry and driving morphological factors to characterize diverse coastal profiles. Given that a single case study location was applied for the research, consideration regarding the applicability of the findings herein to diverse coastal environments must be discussed. It is believed that the findings of the present study are relevant for the unification of diverse coastal environments primarily because the parametric function testing morphotypes were representative of low energy, fetch-limited sandy environments, while the data used for parametric representation was from an open-ocean sandy coastal environment. Given that the parametric function derived in this study was able to represent profile shapes from both low-energy beaches and open-ocean beaches with a high degree of accuracy, it is inferred that this parametric expression is applicable in sandy coastal environments with energy conditions along the full range between the considered extremes. This applicability implies that direct, quantified comparisons can be made between distinct geometric attributes of sandy coastal systems with a wide range of metocean conditions. Potential for direct and quantified comparison of diverse coastal environments, as well as the proven ability to preserve geometric meaning of consequential parameters and relate them to causal parameters, provides opportunity to refine the existing understanding of coastal profile behaviour.

A key requirement to directly compare measured profiles from different coastal environments is consistent profile data processing, such that the considered profiles have consistent morphological bounds. Consistent morphological bounds ensure that the considered profile is constrained to the same extent, where the applied boundaries are defined using attributes of the coastal environment itself. For instance, comparison of the active profile could be completed by setting the upper profile bound as the elevation of the highest observed tidal level, and the lower profile bound as the elevation of the inner depth of closure. The elevation bounds applied in the present study thus present a limitation for future comparison since a standard distance around a given elevation level was applied. If the same elevation bounds were applied to a different coastal environment, it would be challenging to ensure that an equal relative profile extent was considered and thus geometric comparisons may not have significance. Despite this limitation of the present study, the methodology applied to represent measured profiles and the resulting performance of the profile parameterization are considered valid, given the range of profile complexities and lengths that were considered during fitting. The proposed parameterization is thus considered applicable for representation, classification, and comparison of measured profiles from diverse coastal environments, provided that the considered profile extents are comparable.

5.2. Managing Parametric Ambiguity

Parametric meaning in the present study refers to the ability for a given parameter in a parametric expression to represent a distinct attribute of the coastal profile, such as its slope or length. Parametric ambiguity is therefore when the meaning of a given parameter with respect to the geometry of the profile is ambiguous, making it challenging to relate the parameter to physical processes governing the profile morphology. As demonstrated in Chapter 4, the Julseth (2024) parameterization demonstrated a high degree of flexibility and clear parametric meaning, allowing it to effectively fit diverse coastal profile morphotypes, and accurately represent and group measured coastal profile data. The strong parametric meaning of the Julseth (2024) expression refers to the direct relation that each parameter has to an attribute of the profile geometry based on the expression's derivation. As a result, each parameter should control a distinct attribute of the profile function's geometry. For instance, the L_0 parameter controls the location of the point of intersection between the first and second profile slopes, S_1 and S_2, and therefore can be used as a discrete representation of the foreshore slope length.

Despite these strengths, a limitation of the Julseth (2024) parametric expression is the effect of the δ_0 and δ_1 parameters on the truth of the fitted slope parametric values. Testing of the expression demonstrated increased error between the actual slope taken by the parametric function and the fitted parametric slope values when the magnitude of the δ parameters were increased. This observation implies that these parameters are not fully independent, resulting in ambiguity of the fitted slope parameters if the δ parameters are large relative to the total profile length. The effect of the δ parameters were noted to have a particular impact on the middle slope parameter, S_2. The largest errors in this

parameter were observed when the δ parameter lengths overlapped each other (i.e., $L_1 - L_0 \leq \frac{\delta_0 + \delta_1}{2}$, Figure 5.1).
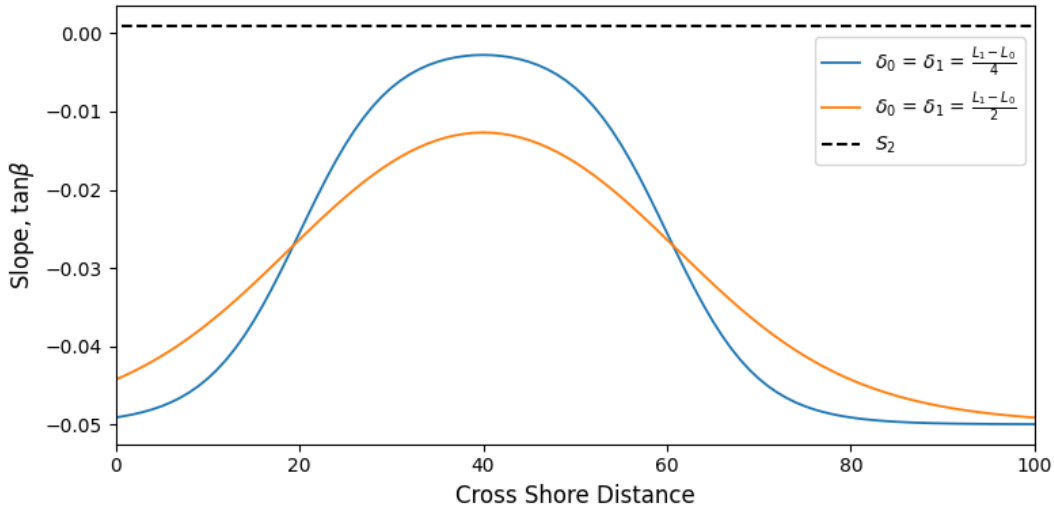

Figure 5.1: Slope function of the Julseth (2024) expression demonstrating the influence of the δ parameter relative magnitude on observed error in S_2. All parametric values used for figure generation were held constant, except for δ_0 and δ_1.

To mitigate the influence of the δ parameters on the meaning of the other parameters, constraints were applied to this parameter during the minimization process. First, each δ parameter was constrained to values between the mean cross shore resolution of the fitted profile and $\frac{1}{12}$ of the total fitted profile length. The applied lower boundary ensures that the delta parameter cannot take values less than the measured resolution of the profile, which would lead to unrealistically sharp transitions between slopes. The upper boundary ensures that the δ parameters cannot dominate the full profile length, resulting in lost parametric meaning of the slopes. Next, an inequality constraint was applied, forcing $(L_1 - L_0) - \frac{\delta_0 + \delta_1}{2}$ to take only positive values. This constraint ensures that the width of each δ parameter does not overlap, and therefore limits the influence of the δ parameters on the observed middle slope, such that S_2 may be used as an accurate representation of the related geometric characteristic. Although the application of these constraints ultimately ensures that the slope parameters retain their intended meaning, it also introduces some ambiguity to the meaning of the δ parameters since the fitted values may be unrepresentative of the measured profile. Despite this ambiguity, no impact was observed to the overall quality of fit to the processed profile data when applying the specified constraints. The maximum RMSE between the measured data and the parametric representation without constraints occurred for the same measured profile and resulted in the same RMSE value (0.33). The applied constraints are therefore considered integral to preservation of parametric meaning, and are expected to have negligible impacts on overall profile fitting performance. It is advised that care be used when interpreting fitted values of the δ parameters.

5.3. Clustering Performance

Clustering performance in the present study refers to the ability for the objective clustering algorithm to effectively group measured profiles with similar geometric attributes, such as slope and curvature. Strong clustering performance is desireable because if profiles can be effectively grouped, then similarities in the associated morphological drivers can be assessed, allowing for the unification of discrete profile measurements and potentially diverse coastal environments. Visual assessment of Figure 4.4 and 4.5 suggests that parametric clustering is more effective than empirical clustering at grouping measured profile data with similar geometric attributes. This observation is expected given the strong representation of profile geometry given by the Julseth (2024) expression, and the clear relation of each parameter to a geometric feature of the profile. Clustering using these fitted parameters should therefore result in groups of measured data indicative of key profile states, as observed. Visual analysis demonstrates that empirical clustering struggled to group profiles with similar concavity, as shown

by presence of convex-up and concave-up profiles within multiple clusters. It is believed that this observation may be a function of either the applied weighting during clustering, or the selected clustering algorithm and the features being used to cluster the empirical data (i.e., K-means and cross shore elevations).

The weights applied to each feature in the empirical cluster analysis were assigned based on the perceived relative importance of profile length scales compared to measured elevations. This assignment was ultimately subjective, and a thorough investigation regarding the impact of different weighting formats was not completed. As such, it is recommended that this analysis be completed to identify the influence of weighting on the output profile clusters. The influence of the applied weights on clustering performance should be considered when interpreting the results of further applications made using the empirical cluster analysis. With that said, it is expected that certain characteristics of the empirical cluster analysis would not significantly change through the application of different weight schemes. One such characteristic is the grouping together of convex-up and concave-up profiles.

The K-means clustering algorithm uses the SED as its sample dissimilarity metric, which is an absolute distance measurement. Clusters defined through empirical clustering are therefore those with similar absolute dissimilarity in elevations from the cluster centroid. This means that both concave-up and convex-up profiles can be assigned to the same cluster if the absolute distance from the cluster centroid is similar. This error is not observed in parametric clustering because the concavity of the profile is intrinsically represented by the relative values of each feature within the samples (i.e., the relative value of each parameter). In order to improve the performance of the empirical clustering, an alternate clustering algorithm could be applied to try and improve the treatment of each sample and the calculation of the cluster centroid. Scott et al. (2020) completed a comparison of clustering performance of four different clustering algorithms to group coral reef cross shore profiles using normalized cross shore elevation and wave celerity as the clustering features. In that study, K-medians was demonstrated to produce the most similar cluster groups, according to the inter-quantile range of distance of clustered profiles to the cluster centroid. This clustering algorithm has two primary differences compared to K-means. First, the cluster centroid is represented by the median of the clustered profiles instead of the mean. Second, the sample dissimilarity metric for K-medians is different than that of K-means (city-block versus SED, respectively). The result of using K-medians compared to K-means was found to be decreased sensitivity to outliers and increased robustness to variance in the data. The results of Scott et al. (2020) indicates that the application of K-medians in place of K-Means could yield improved representation of profile data through empirical clustering.

5.4. Parametric Correlation Analysis

The first correlations completed were between the full set of fitted consequential parameters from each profile and the associated causal parameters computed for four time frames preceding the profile measurement. This analysis resulted in generally weak correlation strengths. Despite this, the observed correlations do appear to align with expected geomorphological trends. Numerous previous studies of sediment transport dynamics at Narrabeen-Collaroy Beach provide a strong source of comparative material. The observed correlations between causal and consequential parameters for the full processed dataset suggest that cross shore sediment transport is governed by magnitude and variability in wave energy. This observation is implied by the positive correlation of significant wave height mean and standard deviation, total wave power mean and standard deviation, and wave steepness mean and standard deviation with profile length parameters and the foreshore slope steepness, and negative correlations of these parameters with offshore slopes and the foreshore slope transition depth, z_0. These correlations imply that increased wave energy results in strong wave-driven return currents, driving erosion of the foreshore slope, and accretion of the offshore slope. Similarly, these correlations imply that onshore transport occurs during periods of limited wave variability and low wave energy, resulting in shallower nearshore depths (steps / berms) and shortened profile lengths between MLW $\pm$ 2 m. The dominance of wave energy on cross shore processes of the Narrabeen-Collaroy system is supported by Harley et al. (2011, 2015), who demonstrated that wave energy variability is a primary driver of cross shore sediment dynamics, and that these cross shore dynamics dominate variability in the shoreline position and berm slope of this system. The geometric characteristics indicative of these parametric

correlations also align with transitions between intermediate beach states as defined by Wright and Short (1984). Assuming constant sediment characteristics, these beach states indicate that raising of the transition between the first and second slopes between MLW $\pm$ 2 m and shortening of the profile between these elevation limits is a function of decreased breaking wave height and increased wave period, characterized by the development of barred, ridge-runnel, low tide terrace, and stepped profiles. This implies that as the incident wave energy decreases, the net flow transitions from offshore to on-shore directed, as supported by the relative importance of cross shore processes defined in Section 2.1.

Correlations identified with the wave steepness parameters are similar to those of the total wave power and significant wave height. The relative weakness of correlations between the steepness parameter and the consequential parameters however may be a result of contradicting processes related to the wave steepness. On one hand, the wave steepness is expected to contribute to sediment stirring, allow-ing for larger sediment transport by processes dominating the net flow (typically return current during high energy conditions). Conversely however, the wave steepness can be used as an indication of an onshore contribution to the net flow (Bosboom & Stive, 2021; Seymour, 2005). This onshore contribu-tion may oppose the dominating flow direction and thus may contradict the observed geomorphological processes, resulting in reduced correlation strength.

Correlations with the alongshore portion of total wave power suggest importance of wave direction vari-ability on the geometry of the cross shore profile, demonstrating that increased variability in alongshore wave power may contribute towards offshore sediment transport. Despite this, correlations between mean alongshore wave power and profile geometry are scarce, despite the expected contribution of alongshore processes to the coastal profile geometry. The scarcity of these correlations may be par-tially attributed to dependence between the considered transects. As demonstrated in Harley et al. (2015) and Ranasinghe, McLoughlin, et al. (2004), the Narrabeen-Collaroy system observes northerly alongshore sediment transport driven by the dominating ESE wave direction, contributing toward pe-riodic clockwise rotation. Clockwise rotation of the beach is indicative of net sediment volume loss from the southern beach extent (erosion) and net sediment volume gain to the northern beach extent (accretion). As such, it is expected that erosion of some transects corresponds with accretion of other transects, depreciating potential correlations between alongshore processes and profile geometry. Fu-ture analysis of individual transects are recommended to assess this behaviour.

Correlations with the maximum tidal range demonstrate lengthening and smoothing of the profile asso-ciated with larger seven-day tidal ranges, as shown through positive correlations with L_1, δ_0, and L_{total}, and negative correlations with S_3. These correlations suggest that if the seven-day tidal range is large, then the measured profile will be long, will have a more gradual transition between the first and second slopes, and will be flatter offshore. This observation generally aligns with the expected influence of tidal flow as presented in Chapter 2, and is characteristic of the more dissipative beaches generally associ-ated with sandy tide-dominated environments (Masselink & Short, 1993). Interpreting correlations with maximum tidal range for longer computation timescales however presents interpretation challenges, as for longer computation periods this causal parameter largely converges to the maximum tidal range for the entire period of record. As such, differences in tidal ranges for longer computation times are reduced and interpreting correlations with respect to the underlying geomorphology becomes increas-ingly challenging. It is believed that expansion of the dataset to coastal environments with different tidal characteristics could aid in the geomorphological interpretation of longer computation period maximum tidal range correlations.

Wave energy variability and climate has been demonstrated to dominate cross shore geomorphology on time scales of hours to decades, supporting the observed correlations given the considered time scales for causal parameter computation in the present study (Stive et al., 2002). Wright et al. (1985) demonstrated that profile geometry is primarily a function of antecedent conditions rather than instanta-neous conditions at the time of profile measurement, as shown in the present study through significant parametric correlations at multiple time scales. However, Wright et al. (1985) also indicated that a 30 day period of time averaging was the most important for classification of profiles using the dimen-sionless fall velocity. The present study however suggests that temporal importance should be further assessed on the scale of individual geometric attributes of the profile, as correlation strength fluctu-

ates with different temporal scales for different consequential parameters. The importance of multiple time scales on beach dynamics is not a new concept for the Narrabeen-Collaroy system. However, at the time of this study, published analyses appear to focus on shoreline position and beach rotation rather than attributes of the subaqueous profile. For instance, Harley et al. (2011) and Ranasinghe, McLoughlin, et al. (2004) indicate the presence of annual and interannual periods of oscillation for beach rotation, and suggest influence of basin scale processes (i.e., El Niño) on the observed longer term oscillations. These observations have been further supported by Anderson et al. (2018), who demonstrated response of littoral cells to fluctuations in metocean processes on interannual and multidecadal time scales. These observations indicate that geomorphological processes can respond to fluctuations in forcing conditions on multiple timescales, indicating a need for assessment of profile geometric attributes on multiple timescales. The consideration of multiple timescales in coastal analysis and the design of coastal interventions could allow for the implementation of more robust solutions.

Comparison of observed significant correlations between the full data correlation analysis and the analysis conducted on clustered data indicated several discrepancies. First, loss of correlations in the empirical clustering with the nearshore slope suggests that empirical cluster centroids may represent this parameter poorly. This is supported by analysis of the empirical clusters (Figure 4.4), which demonstrates mixed grouping of profiles with foreshore slopes both greater and less than the median foreshore slope. Additionally, emergence of numerous significant correlations that were not identified in the full data correlation case also presents concerns regarding the ability for empirical cluster centroids to accurately represent the grouped profiles. Despite these concerns, the significant amplification of correlation signal using empirical clustering provides incentive for further investigation of its application using an alternate object dissimilarity metric. Parametric clustering resulted in the loss of significant correlations with the foreshore slope length, L_0, and the foreshore slope transition length, δ_0. As with empirical clustering, these lost correlations may represent poor representation of these parameters by parametric cluster centroids. Despite this, parametric clustering observed more similar correlation trends to the full data correlation case than the empirical clustering case. This suggests that parametric clustering provides a better representation of key profile states in the processed data compared to empirical clustering, and may be used to effectively amplify observed correlations in the full dataset with limited emergence of unexpected trends.

5.5. Application for Predictive Capability

The research questions presented at the beginning of the present study aimed to provide key steps towards the development of a predictive coastal profile model. Two primary research questions were posed which addressed (1) the unification of coastal profile geometry from diverse coastal environments using parametric shape functions, and (2) the characterization of geomorphological processes using causal and consequential parameters. Each of these research questions were subdivided into two further questions aimed at guiding the present study and providing a unified answer to their parent research question.

The first research question was broken into the following two subquestions:

1. To what degree of accuracy can parametric shape functions represent diverse coastal profile geometry?
2. Can a parametric shape function be used to effectively group and classify measured profile data?

Analyses conducted in the present study indicated that parametric shape functions can be used to represent diverse coastal profile shapes with a high degree of accuracy. In particular, the new parametric expression derived herein demonstrated high flexibility and potential for fitting of diverse profile states, as supported by the maximum SSE of 0.13 for the considered testing morphotypes. Alternatively, the parametric expression provided by Hsu et al. (2006) also demonstrated a high level of flexibility, with a maximum SSE of 0.37 for the considered testing morphotypes. Next, the parametric expression derived in this study was applied to measured data, resulting in a mean RMSE of 0.05 m. The fitted parameters were subsequently used to define data labels and to conduct parametric clustering. These methods demonstrated a strong ability to classify the considered data using both subjective and objective grouping techniques. In particular, clustering using the parametric data showed a strong ability to

represent varied profile geometries in the measured data, with fitting statistics comparable to empirical clustering methods. These results indicate that the first research question may now be answered. It is believed from the findings of the present study that coastal profile geometry of diverse coastal environments can be unified to a high degree of accuracy through parametric representation using the Julseth (2024) parametric shape function.

The second research question was broken into the following two subquestions:

1. What is the impact of varying temporal scales to the distribution of causal parameters?
2. Are expected geomorphological processes identifiable through causal-consequential parametric correlation analysis?

Analyses conducted in the present study indicate that computation of causal parameters at varying temporal scales results in measurable changes to the distribution of causal parameters. It was highlighted that causal parameter distributions typically observed a decrease in the interquantile range when considering longer temporal scales. It was therefore implied that the relative influence of fluctuations in metocean conditions was stronger when considering shorter time scales, while the relative influence of mean conditions was stronger when considering longer timescales. These observations provide important considerations for coastal engineers and designers when selecting causal parameter computation scales and when assessing expected geomorphological activity for a given site. Next, causal-consequential correlation analysis were conducted. Significant correlations using causal and consequential values from the entire dataset were generally weak, but showed alignment with the expected geomorphological trends presented in literature. The primary observed correlations implied offshore sediment transport is driven by increased total wave energy and increased wave energy fluctuation at all time scales. This morphological trend was implied through parametric values indicating steepening of the foreshore profile, flattening of the offshore profile, elongation of the profile between MLW $\pm$ 2 m, and deepening of the nearshore profile when more energetic wave conditions preceded profile measurement (i.e., larger H_s and P). Amplification of the correlation signals from the full dataset was observed through profile representation with cluster centroids. Correlation preservation was particularly clear using parametric clustering, and is expected to be a result of more representative grouping using this clustering method compared to empirical clustering. These observations provide incentive for the application of parametric clustering to group and represent measured profile data. These results indicate that the second research question may now be answered. It is believed from the findings of the present study that the relation of causal and consequential parameters can be used to identify dominant geomorphological processes of the considered coastal environment.

Given the provided answers to the research questions from this study, it is believed that data-driven predictions of coastal profile geometry may be completed using causal-consequential parametric relationships. In order to do this, it is first recommended that cause-and-effect analysis of causal and consequential parameters be completed, and compared with observed correlations presented in the present study and expected geomorphological trends from past literature. This analysis may be completed using techniques such as regression analysis, which provides a more direct relation of variables in comparison to correlation analysis. Further, it is recommended that the relative importance of causal parameters be assessed in greater detail, with particular focus on importance of time scales for different geometric attributes. The present study has determined plainly that diverse coastal profiles can be represented with a high level of accuracy using the Julseth (2024) parametric expression. Further, the use of parametric clustering has been highlighted as an effective tool to group profiles with similar geometric features, amplify causal-consequential correlations, and identify representative profiles for a given cluster. Predictive capability could be obtained by leveraging causal-consequential relationships within the clustered data. The envisioned predictive model would be made up of clustered consequential parametric data. Causal data related to each of the parameterized profiles would be contained as an attribute of each profile, but would not be used explicitly for clustering. To make a prediction, the user would input the key causal parameters related to their site of interest. Using a dissimilarity algorithm, the model could map these causal parameters to the cluster containing the most similar causal parameter statistics. As an output, the user would be provided with the consequential parameter values of the cluster centroid from which the input causal parameters were mapped. To quantify uncertainty in the provided prediction, the model could also output the consequential parameters of the profiles within

the mapped cluster that are most dissimilar to the cluster centroid. A simplified theoretical framework of a model such as this is outlined in Figure 5.2.
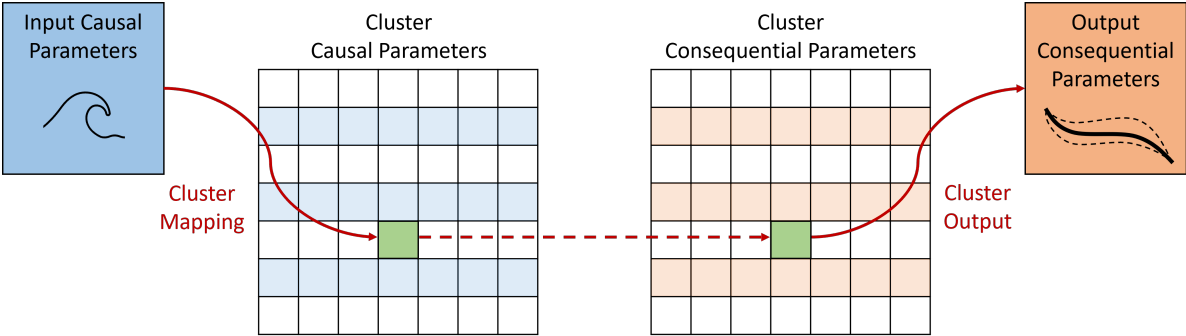

Figure 5.2: Simplified theoretical framework for a predictive model leveraging the results of the present study. In this framework, computed causal parameters are input and mapped to a consequential cluster group whose associated causal parameters are the most similar to the user input. The consequential parameter cluster centroid is then returned as the most likely coastal profile given the provided causal parameters.

6
Conclusions

Conclusions

- The newly defined parametric shape function can be used to represent diverse profile geometry with a high degree of accuracy.
- Fitted parametric values can be used to effectively identify groups of measured profiles with similar geometric attributes through manual labelling and K-means clustering.
- Increasing the computation time scale of causal parameters results in increased influence of long term mean conditions, while reduced time scales observe increased influence of short term variability.
- Rank correlation analysis between causal and consequential parameters reflects expected geomorphological processes for the study location.
- Representation of grouped profiles with parametric cluster centroids can effectively amplify correlations observed in the full dataset.
- Parametric representation of profile geometry and metocean conditions holds potential for application in a data-driven predictive model.

Recommendations

- A more precise definition of the profile elevation thresholds is needed. The applied thresholds should be related to universal features of any given coastal profile to ensure consistency in parameterization of diverse coastal environments.
- The influence of temporal variability in causal parameters on profile geometry should be defined to identify the most important temporal scales for causal parameter computation.
- A clear definition of best practices for clustering of coastal profiles is needed. Testing of various clustering algorithms and feature weighting schemes should therefore be completed to quantify their influence on the performance of empirical and parametric clustering.
- The methodology presented in the present study should be expanded to alternate study locations to assess the ability to unify diverse coastal environments using a single parametric representation of geometric features and morphological drivers.
- The influence of sediment characteristics should be included in future studies in new coastal environments through the introduction of an additional causal parameter.
- Application of the newly defined parametric function with causal parameters for predictive capability.

6.1. Conclusions

Two primary research questions were posed at the beginning of the present study. The answers to these research questions are presented below. The answers to these research questions indicate that parametric representation of diverse coastal systems using measured data has potential for predictive application. Predictive application could be used to provide improved first order estimates of profile geometry using measured data.

1. *To what extent can coastal profile geometry of diverse coastal environments be unified using measured data and parametric shape functions?*

    Identification of nine previously defined parametric shape functions demonstrated a range in complexity of existing expressions, resulting in a range of suitability for representation of diverse coastal profiles. Flexibility and clear parametric meaning of the two-sloped parametric expression from Hanssen et al. (2022) provided incentive for extension of this expression to three slopes in order to fit more diverse profile geometries. A new parametric expression was therefore derived and tested in comparison to eight of the previously defined expressions using four distinct profile morphotypes based on those identified by Travers (2007). This testing demonstrated that the newly defined expression maintained the flexibility and parametric meaning valued in the Hanssen et al. (2022) expression, while increasing the ability to represent a range of diverse profile geometries. The new expression provided the best overall fit to the four testing profiles ($\overline{SSE}$ = 0.04, the next best $\overline{SSE}$ = 0.16). The new function was subsequently fit to processed profile data from Narrabeen-Collaroy beach, for the subaqueous profile between MLW $\pm$ 2 m. The fitted parameters from the parametric expression demonstrated high performance in representing measured profiles ($max(RMSE)$ = 0.18 m) and were applied to effectively group profiles with similar geometric attributes, both using manually defined labelling and objective grouping with K-means clustering. These results demonstrate that coastal profile geometry from diverse coastal environments can be unified with a high degree of accuracy through parametric representation using the newly defined parametric function.

2. *How well can causal and consequential parameters characterize the geomorphological processes affecting cross shore profile geometry?*

    Eleven causal parameters were selected to represent the water level and wave characteristics of the study location. Each parameter was computed for four time scales prior to the measurement of each measured profile considered for the analysis (seven-days, three-months, six-months, and one-year). Assessment of causal distributions demonstrated net decreases in the inter-quantile range for each parameter when longer time scales were considered. This observation suggests increased influence of variability on causal parameters computed for shorter time scales, and increased influence of mean conditions on causal parameters computed for longer time scales. Rank correlations were computed between the causal parameters and the consequential parameters fit to measured profile data, demonstrating weak relationships ($max(r_{x,y})$= 0.41, p<0.05) suggestive of dominance of wave energy mean and standard deviation on cross shore profile geometry. Causal-consequential correlations generally aligned with previous studies completed at Narrabeen-Collaroy, and suggested that different temporal scales have varied importance on the development of different geometric features, as previously identified by Anderson et al. (2018), Harley et al. (2011), and Ranasinghe, McLoughlin, et al. (2004) for beach rotation and shoreline position. Correlations between causal and consequential parameters of empirical cluster centroids and parametric cluster centroids indicated ability to amplify observed correlations through grouped representation of measured profile data ($max(r_{x,y})$= 0.80, p<0.05 and $max(r_{x,y})$= 0.76, p<0.05, respectively). However, care is advised when assessing cluster centroid correlations given uncertainty surrounding the ability of cluster centroids to accurately represent key geometric features of the profile, particularly when employing empirical clustering techniques. These results demonstrate that geomorphological processes affecting cross shore profile geometry can be characterized through assessment of inter-parametric relationships.

6.2. Recommendations

The present study has demonstrated the ability to use parametric data representation for the characterization of coastal environments, and provides indication that similar methods may be applied for predictive capability. The following recommendations aim to provide opportunity for improvement and expansion of the present for future application.

1. *Clear definition of elevation thresholds*

   The present study outlined an analysis of the subaqueous profile between MLW $\pm$ 2 m. The selection of these elevation thresholds was based on the need to mitigate measurement bias in the data while reducing sample size degradation that occurred when deeper thresholds were selected (i.e., the inner depth of closure). Although the selection of the elevation threshold used in the present study is believed to be well founded, it is acknowledged that the resulting section of the profile considered in the analysis may not be representative of the entire active profile. This ultimately results in increased uncertainty regarding whether cross shore profile dynamics can be fully characterized using these boundaries. It is therefore recommended that further assessment of potential elevation thresholds is conducted, and that elevation thresholds be selected that are more closely related to common geometric attributes of the profile. Selection of elevation thresholds related to common geometric attributes will ensure that new data may be easily incorporated into future analyses, and that profile measurements made following the definition of these elevation thresholds will have a clear measurement depth target.

2. *Definition of causal parameter temporal influence*

   Although the selected causal parameter computation time scales for this study were ambiguous, and therefore only demonstrate general trends, the present study has demonstrated the relative impact of various computation time scales on the distribution of the selected causal parameters and the resulting correlation strength with consequential parameters. It is believed that a more rigorous study is required to assess the relative importance of causal parameter computation time scales on the behaviour of specific geometric attributes of the profile. A potential methodology for this study may be the use of time series analysis for the fitted consequential parameters of a given coastal transect. Temporal variability in fitted parameters may be related to temporal variability in metocean conditions, providing an indication of the dominant time scales for the behaviour of key geometric attributes of the profile.

3. *Definition of clustering best practices*

   The present study demonstrated that using K-means clustering, parametric clustering outperformed empirical clustering when considering the ability for cluster centroids to represent key geometric attributes of the profile. It must be considered that the selected clustering algorithm and the corresponding steps taken to process both empirical and parametric data may have influenced the resulting clustering performance. This has been demonstrated in past literature, where K-medians was shown to minimize cluster variance for empirically clustered reef profiles (Scott et al., 2020). As a result, it is recommended that in depth testing with multiple clustering algorithms be completed to determine the influence of the selected algorithm on the performance of profile grouping and representation using the cluster centroid. Additionally, the weights applied to the empirical clustering were subjective to the perceived importance of profile length scale compared to elevation values at normalized cross shore locations. It is therefore also recommended that detailed testing of the influence of feature weighting on empirical clustering performance is completed. The completion of these test will result in the quantification of uncertainty surrounding clustering performance and subsequently the conclusions made in the present study, and can be used to develop a set of guidelines for future studies that wish to apply clustering techniques to cross shore profile data.

4. *Expansion to alternate coastal environments*

One of the limitations of the present study was that data from a single coastal environment was used (Narrabeen-Collaroy beach). Although the profile of this beach does observe temporal and spatial fluctuations resulting in a range of possible states, the study of a single system presents limitations in the application of the findings herein for diverse coastal systems. As a result, it is recommended that the analysis presented in the present study be repeated using data from several alternate coastal environments. Preferably, alternate environments would be measurably different in their profile geometry and metocean conditions compared to the present study. By diversifying the analyzed dataset, geomorphological trends in a wider range of coastal environments may be unified using a single geometric parameterization. In doing so, the value of a data driven model would be increased, as it would be applicable in a wider range of coastal environments worldwide. Two potential coastal profile datasets that may be used for the expansion of the present study include the JarKus dataset for the Dutch North Sea coast, and the SEDMEX dataset for the Prins Hendrik Zanddijk, Texel, the Netherlands.

5. *Inclusion of sediment related causal parameters*

Given that the present study focuses on a single study location with near-uniform sediment characteristics, the influence of sediment on coastal profile geometry was neglected. Despite this, numerous studies indicate that sediment characteristics play a major role in the development of the coastal profile, as clearly indicated in Bruun (1954) and Dean (1977) for the development of equilibrium profiles. As such, it is strongly recommended that causal parameters related to sediment characteristics be included in future expansions of the present work, particularly as data from multiple locations is amalgamated to provide a unified characterization of the coastal profile.

6. *Application for Predictive Capability*

Parameterization of measured coastal profiles using the Julseth (2024) expression demonstrated an ability to effectively represent and group profiles with similar geometric characteristics. Given the ability to correlate the fitted parameters with causal parameters, it is believed that potential exists for the application of this parameterization in a predictive model. In Chapter 5 a framework for a predictive model that applies the concepts of the present study was shown. Alternative methods for the application of the presented parameterization of the coastal profile and morphological drivers do exist however. These methods include Bayesian Networks and Vine Copulas, which rely on parametric rank correlations to infer probable parametric values given a set of input parameters. Additionally, an Artificial Neural Network could be developed to relate causal parameters to the consequential parameters in the Julseth (2024) expression. It should be noted however that further testing of causal parameter importance and causal parameter temporal scale importance is expected to be needed for such a predictive model to be truly effective.

In conclusion, parameterizations of coastal profiles and metocean conditions are useful tools in the characterization of coastal profile development. The application of these methods with data partitioning and machine learning techniques such as clustering provides a foundation for the development of a data-driven predictive model. Such a model holds value in helping to understand the impact of changing metocean conditions on the coastal profile, and can help coastal engineers design robust and innovative coastal interventions.

References

Anderson, D., Ruggiero, P., Antolínez, J., Méndez, F., & Allan, J. (2018). A climate index optimized for longshore sediment transport reveals interannual and multidecadal littoral cell rotations. *Journal of Geophysical Research: Earth Surface*, *123*(8), 1958–1981. https://doi.org/https://doi.org/10.1029/2018JF004689

Are, F., & Reimnitz, E. (2008). The a and m coefficients in the bruun/dean equilibrium profile equation seen from the arctic. *Journal of Coastal Research*, *24*(sp2), 243–249. https://doi.org/10.2112/05-0572.1

Arthur, D., & Vassilvitskii, S. (2007). K-means++: The advantages of careful seeding. *Proc. of the Annu. ACM-SIAM Symp. on Discrete Algorithms*, *8*, 1027–1035. https://doi.org/10.1145/1283383.1283494

Ashton, A., & Murray, A. (2006). High-angle wave instability and emergent shoreline shapes: 1. modeling of sand waves, flying spits, and capes. *Journal of Geophysical Research: Earth Surface*, *111*(F4). https://doi.org/https://doi.org/10.1029/2005JF000422

Bailard, J. (1982). Modeling on-offshore sediment transport in the surfzone. *Coastal Engineering Proceedings*, *1*(18), 87. https://doi.org/10.9753/icce.v18.87

Bearman, J., Friedrichs, C., Jaffe, B., & Foxgrover, A. (2010). Spatial trends in tidal flat shape and associated environmental parameters in south san francisco bay. *Journal of Coastal Research*, *26*(2), 342–349.

Birkemeier, W. (1985). Field data on seaward limit of profile change. *Journal of Waterway, Port, Coastal, and Ocean Engineering*, *111*(3), 598–602. https://doi.org/10.1061/(ASCE)0733-950X(1985)111:3(598)

Bodge, K. (1992). Representing equilibrium beach profiles with an exponential expression. *Journal of Coastal Research*, *8*(1), 47–55. Retrieved January 18, 2024, from http://www.jstor.org/stable/4297951

Bosboom, J., & Stive, M. (2021). *Coastal dynamics*. TU Delft OPEN Publishing. https://doi.org/10.5074/T.2021.001

Bowen, A. (1980). Simple models of nearshore sedimentation, beach profiles and longshore bars, 1–11.

Brutsche, K., Rosati, J., Pollock, C., & McFall, B. (2016). *Calculating depth of closure using wis hindcast data* (No. VI-45). U.S. Army Engineer Research, Development Center (Coastal, and Hydraulics Laboratory).

Bruun, P. (1954). *Coast erosion and the development of beach profiles*. Beach Erosion Board, U.S. Army Corps of Engineers. Washington, D.C.

Bruun, P. (1962). Sea-level rise as a cause of shore erosion. *Journal of the Waterways and Harbors division*, *88*. https://doi.org/https://doi.org/10.1061/JWHEAU.0000252

Bujan, N., Cox, R., & Masselink, G. (2019). From fine sand to boulders: Examining the relationship between beach-face slope and sediment size. *Marine Geology*, *417*, 106012. https://doi.org/https://doi.org/10.1016/j.margeo.2019.106012

CoastSnap. (2022). *CoastSnap: Community Beach Monitoring*. Retrieved June 3, 2024, from https://www.coastsnap.com/map

Cooper, J., & Pilkey, O. (2004). Sea-level rise and shoreline retreat: Time to abandon the bruun rule. *Global and Planetary Change*, *43*(3), 157–171. https://doi.org/https://doi.org/10.1016/j.gloplacha.2004.07.001

Dai, Z., Du, J., Li, C., & Chen, Z. (2007). The configuration of equilibrium beach profile in south china. *Geomorphology*, *86*(3), 441–454. https://doi.org/https://doi.org/10.1016/j.geomorph.2006.09.016

Dean, R. (1977). *Equilibrium beach profiles: U.S. atlantic and gulf coasts*. University of Delaware. Newark.

Dean, R. (1991). Equilibrium beach profiles: Characteristics and applications. *Journal of Coastal Research*, *7*(1), 53–84.

Grasso, F., Michallet, H., Barthélemy, E., & Certain, R. (2009). Physical modeling of intermediate cross-shore beach morphology: Transients and equilibrium states. *Journal of Geophysical Research: Oceans*, *114*(C9). https://doi.org/https://doi.org/10.1029/2009JC005308

Hallermeier, R. (1978). Uses for a calculated limit depth to beach erosion. *Proceedings of the Sixteenth Coastal Engineering Conference*, 1493–1512. https://doi.org/10.1061/9780872621909.090

Hallermeier, R. (1981). A profile zonation for seasonal sand beaches from wave climate. *Coastal Engineering*, *4*, 253–277. https://doi.org/https://doi.org/10.1016/0378-3839(80)90022-8

Haney, R., Kouloheras, L., Malkoski, V., Mahala, J., & Unger, Y. (2007). *Beach nourishment*. MassDEP. Boston.

Hanssen, J., van Prooijen, B., Volp, N., de Vet, P., & Herman, P. (2022). Where and why do creeks evolve on fringing and bare tidal flats? *Geomorphology*, *403*. https://doi.org/10.1016/j.geomorph.2022.108182

Harley, M. D., Turner, I. L., & Short, A. D. (2015). New insights into embayed beach rotation: The importance of wave exposure and cross-shore processes. *Journal of Geophysical Research: Earth Surface*, *120*(8), 1470–1484. https://doi.org/https://doi.org/10.1002/2014JF003390

Harley, M. D., Turner, I. L., Short, A. D., & Ranasinghe, R. (2011). A reevaluation of coastal embayment rotation: The dominance of cross-shore versus alongshore sediment transport processes, collaroy-narrabeen beach, southeast australia. *Journal of Geophysical Research: Earth Surface*, *116*(F4). https://doi.org/https://doi.org/10.1029/2011JF001989

Hartigan, J. (1975). *Clustering algorithms*.

Hastie, T., Tibshirani, R., & Friedman, J. (2001). *The elements of statistical learning* (2nd ed.). Springer series in Statistics.

Hegge, B., Eliot, I., & Hsu, J. (1996). Sheltered sandy beaches of southwestern australia. *Journal of Coastal Research*, *12*(3), 748–760. Retrieved January 17, 2024, from http://www.jstor.org/stable/4298521

Hsu, T., Tseng, I., & Lee, C. (2006). A new shape function for bartype beach profiles. *Journal of Coastal Research - J COASTAL RES*, *22*, 728–736. https://doi.org/10.2112/04-0340.1

IBTrACS. (2022). *2022 major hurricane fiona (2022257n16312)*. Retrieved June 3, 2024, from https://ncics.org/ibtracs/index.php?name=v04r00-2022257N16312

Inman, D., Elwany, M., & Jenkins, S. (1993). Shorerise and bar-berm profiles on ocean beaches. *Journal of Geophysical Research: Oceans*, *98*(10), 18181–18199.

IPCC. (2023). *Climate change 2023: Synthesis report. contribution of working groups i, ii, and iii to the sixth assessment report of the intergovernmental panel on climate change*. IPCC. Geneva, Switzerland. https://doi.org/10.59327/IPCC/AR6-9789291691647

Komar, P., & McDougal, W. (1994). The analysis of exponential beach profiles. *Journal of Coastal Research*, *10*(1), 59–69. Retrieved January 18, 2024, from http://www.jstor.org/stable/4298193

Lee, P. Z. (1994). The submarine equilibrium profile: A physical model. *Journal of Coastal Research*, *10*, 1–17. https://api.semanticscholar.org/CorpusID:55105190

Levoy, F., Anthony, E., Monfort, O., & Larsonneur, C. (2000). The morphodynamics of megatidal beaches in normandy, france. *Marine Geology*, *171*(1), 39–59. https://doi.org/https://doi.org/10.1016/S0025-3227(00)00110-9

Longuet-Higgins, M. (1953). Mass transport in water waves. *Philosophical Transactions of the Royal Society of London. Series A, Mathematical and Physical Sciences*, *245*. https://doi.org/10.1098/rsta.1953.0006

Makaske, B., & Augustinus, P. (1998). Morphologic changes of a micro-tidal, low wave energy beach face during a spring-neap tide cycle, rhône-delta, france. *Journal of Coastal Research*, *14*(2), 632–645. Retrieved January 17, 2024, from http://www.jstor.org/stable/4298817

Masselink, G., & Short, A. (1993). The effect of tide range on beach morphodynamics and morphology: A conceptual beach model. *Journal of Coastal Research*, *9*, 785–800.

Millar, D., Smith, H., & Reeve, D. (2007). Modelling analysis of the sensitivity of shoreline change to a wave farm. *Ocean Engineering*, *34*(5), 884–901. https://doi.org/https://doi.org/10.1016/j.oceaneng.2005.12.014

NASA. (2024). *What is climate change?* Retrieved April 15, 2024, from https://science.nasa.gov/climate-change/what-is-climate-change/

Palha, A., Mendes, L., Fortes, C., Brito-Melo, A., & Sarmento, A. (2010). The impact of wave energy farms in the shoreline wave climate: Portuguese pilot zone case study using pelamis energy

wave devices. *Renewable Energy*, *35*(1), 62–77. https://doi.org/https://doi.org/10.1016/j.renene.2009.05.025

Pasch, R., Reinhart, B., & Alaka, L. (2023). *Hurricane fiona*. National Hurricane Center. USA.

Powell, K. (1990). *Predicting short term profile response for shingle beaches*. Hydraulics Research Wallingford. Wallingford, Oxfordshire.

Ranasinghe, R., McLoughlin, R., Short, A., & Symonds, G. (2004). The southern oscillation index, wave climate, and beach rotation. *Marine Geology*, *204*(3), 273–287. https://doi.org/https://doi.org/10.1016/S0025-3227(04)00002-7

Ranasinghe, R., Symonds, G., Black, K., & Holman, R. (2004). Morphodynamics of intermediate beaches: A video imaging and numerical modelling study. *Coastal Engineering*, *51*(7), 629–655. https://doi.org/https://doi.org/10.1016/j.coastaleng.2004.07.018

Reeve, D., Karunarathna, H., Pan, S., Horrillo-Caraballo, J., Różyński, G., & Ranasinghe, R. (2016). Data-driven and hybrid coastal morphological prediction methods for mesoscale forecasting. *Geomorphology*, *256*, 49–67. https://doi.org/https://doi.org/10.1016/j.geomorph.2015.10.016

Reguero, B., Losada, I., & Méndez, F. (2019). A recent increase in global wave power as a consequence of oceanic warming. *Nature Communications*, *10*(205). https://doi.org/10.1038/s41467-018-08066-0

Reimann, L., Vafeidis, A., & Honsel, L. (2023). Population development as a driver of coastal risk: Current trends and future pathways (14th ed.). *Cambridge Prisms: Coastal Futures*, *1*, 1–23. https://doi.org/10.1017/cft.2023.3

Roelvink, J., & Stive, M. (1989). Bar-generating cross-shore flow mechanisms on a beach. *Journal of Geophysical Research: Oceans*, *94*, 4785–4800. https://doi.org/10.1029/JC094iC04p04785

Schasfoort, F., & Janssen, S. (2013). *Sand nourishments*. STOWA. Netherlands.

Scott, F., Antolínez, J., McCall, R., Storlazzi, C., Reniers, A., & Pearson, S. (2020). Hydro-morphological characterization of coral reefs for wave runup prediction. *Frontiers in Marine Science*, *7*(361).

Senechal, N., & Coco, G. (2024). On the role of hydrodynamic and morphologic variables on neural network prediction of shoreline dynamics. *Geomorphology*, *451*, 109084. https://doi.org/https://doi.org/10.1016/j.geomorph.2024.109084

Seymour, R. (2005). Cross-shore sediment transport. In M. Schwartz (Ed.), *Encyclopedia of coastal science* (pp. 352–353). Springer Netherlands. https://doi.org/10.1007/1-4020-3880-1_104

Short, A. (2009). Decadal scale patterns in beach oscillation and rotation narrabeen beach, australia—time series, pca and wavelet analysis. *Journal of Coastal Research*, *20*, 523–532. https://doi.org/10.2112/1551-5036(2004)020[0523:DSPIBO]2.0.CO;2

Snoddon, R. (2023). How fiona became a record-breaking canadian storm. *CBC*. Retrieved April 15, 2024, from https://www.cbc.ca/news/canada/nova-scotia/weather-snoddon-fiona-recap-1.6976249

Stive, M., Aarninkhof, S., Hamm, L., Hanson, H., Larson, M., Wijnberg, K., Nicholls, R., & Capobianco, M. (2002). *Coastal Engineering*, *47*, 211–235. https://doi.org/https://doi.org/10.1016/S0378-3839(02)00126-6

Ton, A., Vuik, V., & Aarninkhof, S. (2021). Sandy beaches in low-energy, non-tidal environments: Linking morphological development to hydrodynamic forcing. *Geomorphology*, *374*, 107522. https://doi.org/https://doi.org/10.1016/j.geomorph.2020.107522

Travers, A. (2007). Low-Energy Beach Morphology with Respect to Physical Setting: A Case Study from Cockburn Sound, Southwestern Australia. *Journal of Coastal Research*, *2007*(232), 429–444. https://doi.org/10.2112/04-0275.1

Türker, U., & Kabdaşli, M. (2009). The shape parameter and its modification for defining coastal profiles. *Environmental Geology*, *57*(2). https://doi.org/10.1007/s00254-008-1269-1

Turner, I., Harley, M., Short, A., Simmons, J., Bracs, M., Phillips, M., & Splinter, K. (2016). A multi-decade dataset of monthly beach profile surveys and inshore wave forcing at narrabeen, australia. *Scientific Data*, *3*(160024). https://doi.org/10.1038/sdata.2016.24

Wright, L., & Short, A. (1984). Morphodynamic variability of surf zones and beaches: A synthesis. *Marine Geology*, *56*(1), 93–118. https://doi.org/https://doi.org/10.1016/0025-3227(84)90008-2

Wright, L., Short, A., & Green, M. (1985). Short-term changes in the morphodynamic states of beaches and surf zones: An empirical predictive model. *Marine Geology*, *62*(3), 339–364. https://doi.org/https://doi.org/10.1016/0025-3227(85)90123-9

Zwillinger, D., & Kokoska, S. (2000). *CRC standard probability and statistics tables and formulae*. Chapman & Hall.

A
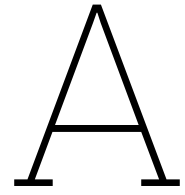
Additional Figures

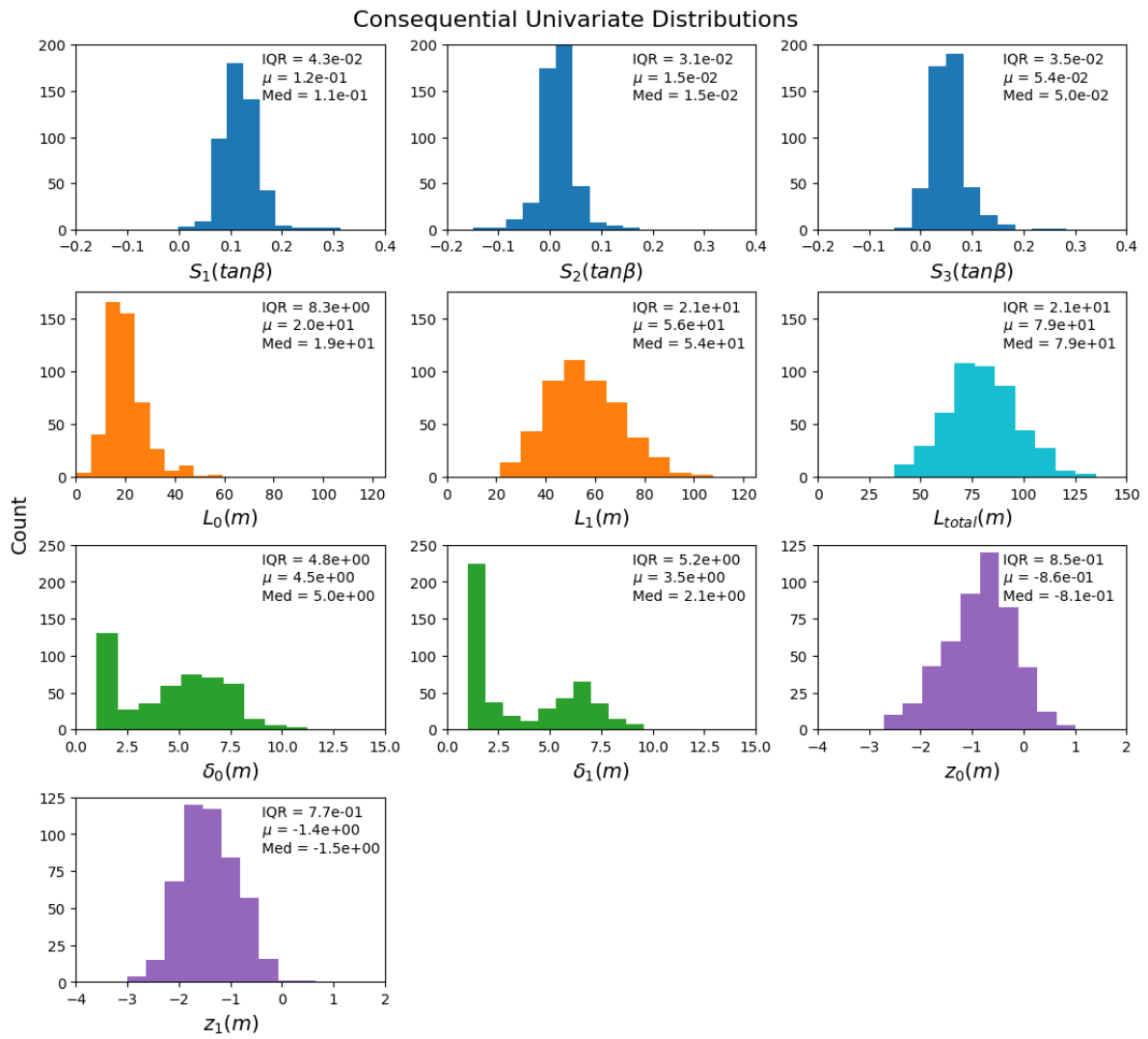# A.1. Parametric Distributions

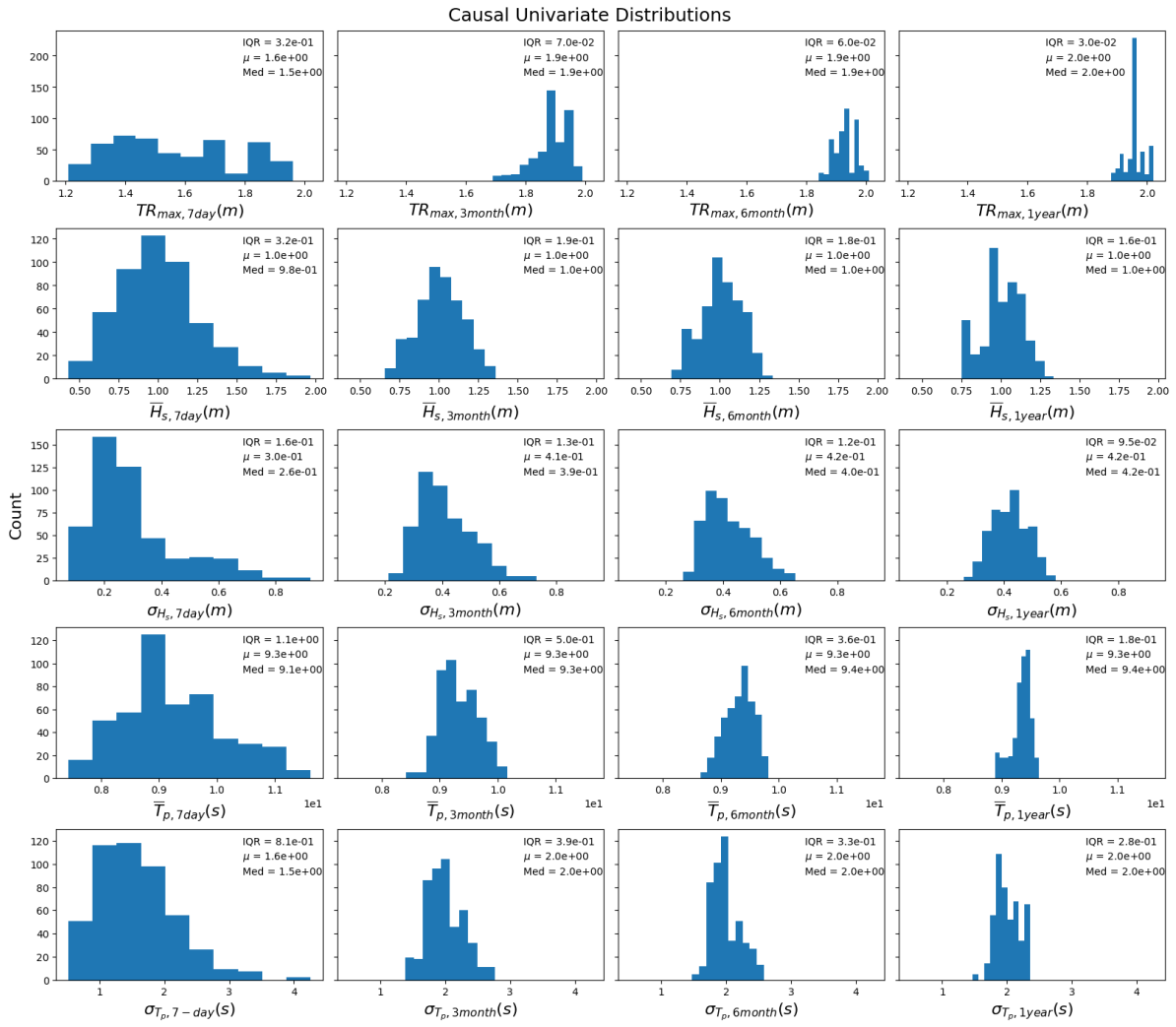**Figure A.1:** Consequential parameter univariate empirical distributions.

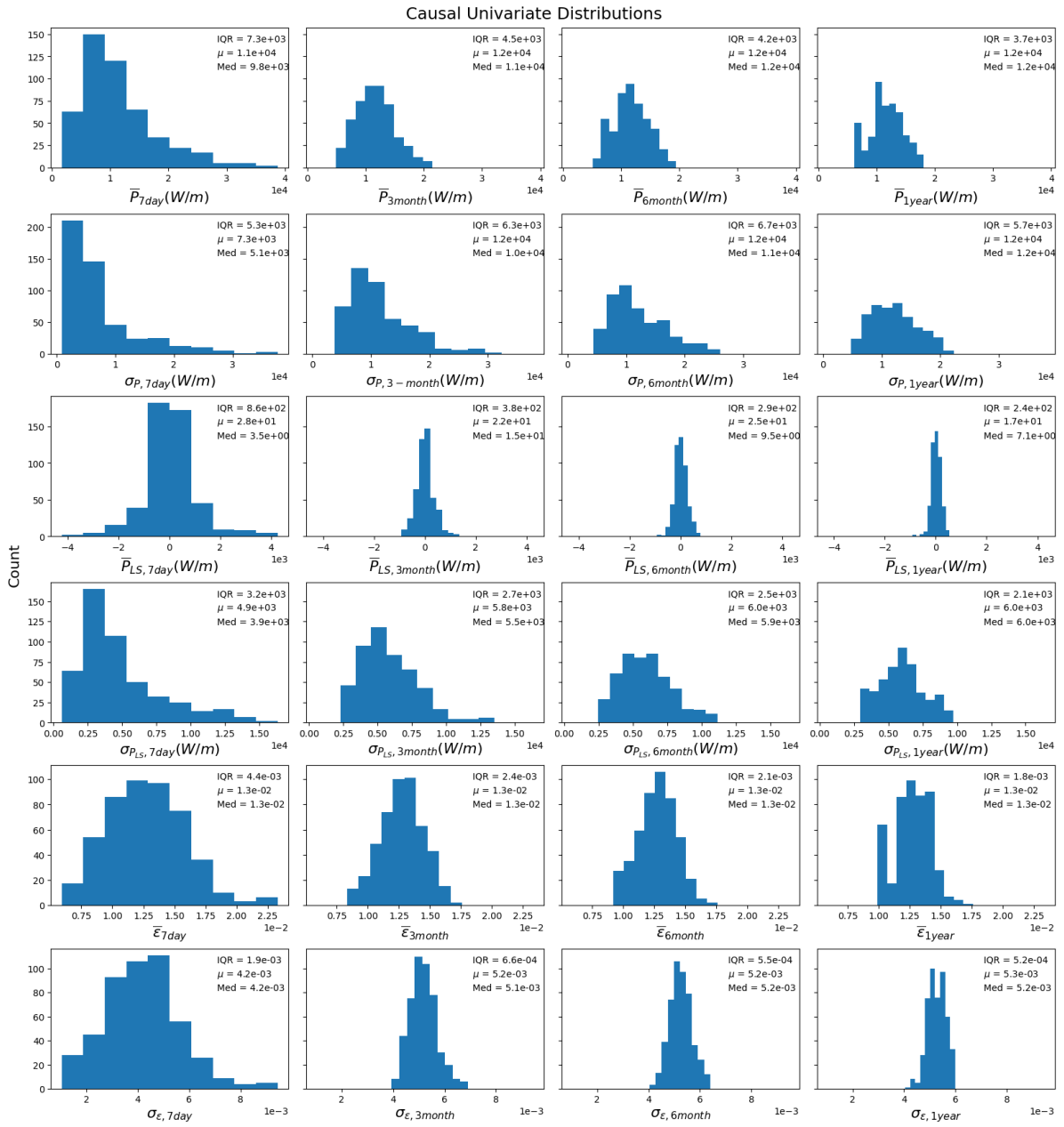**Figure A.2:** Causal parameter univariate empirical distributions (1/2).

Figure A.3: Causal parameter univariate empirical distributions (2/2).
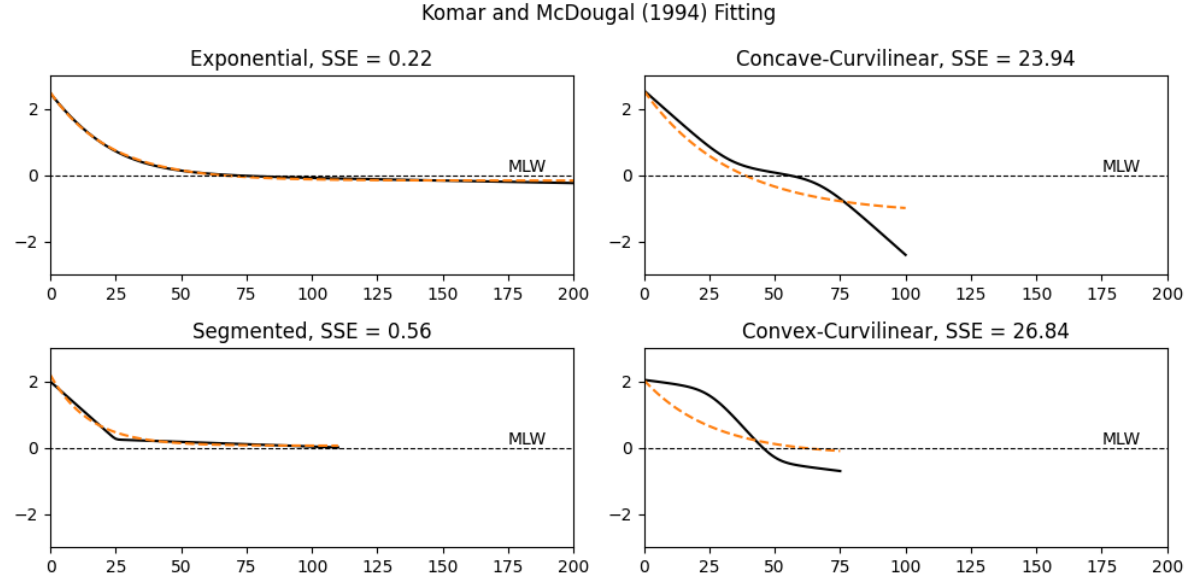
A.2. Parametric Expression Evaluation

Figure A.4: Fit of Komar and McDougal (1994) expression to profile morphotypes from Travers (2007).
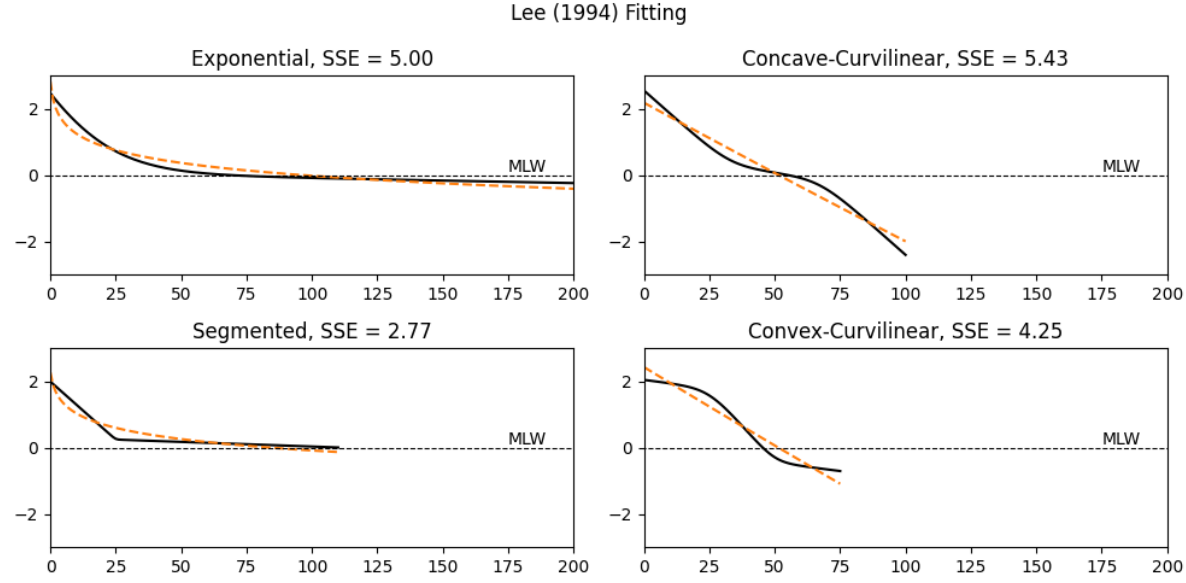
Figure A.5: Fit of Lee (1994) expression to profile morphotypes from Travers (2007).
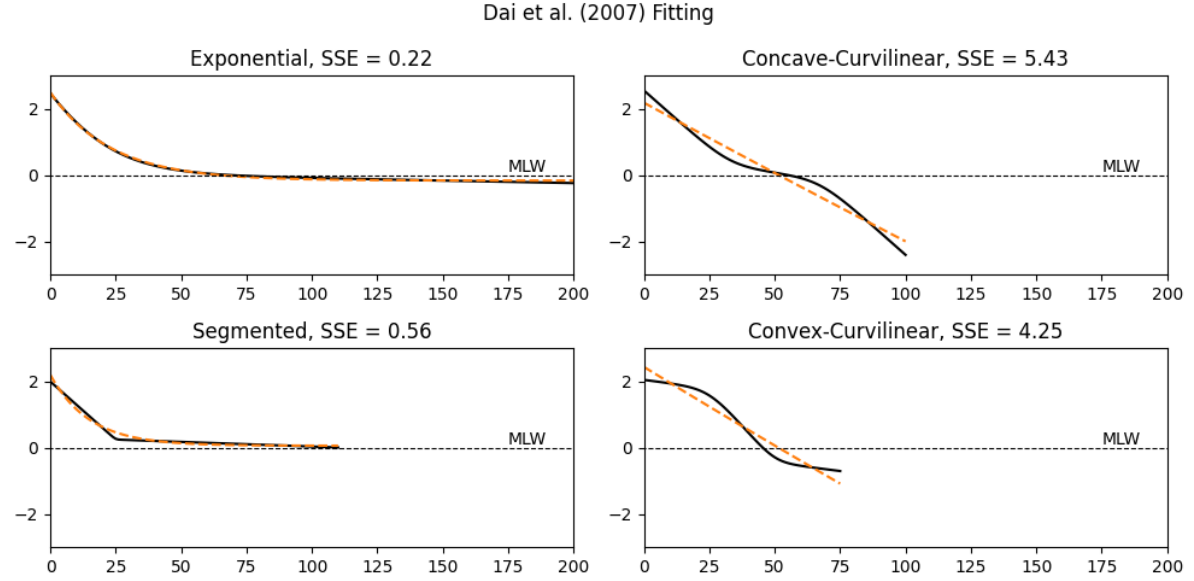
Figure A.6: Fit of Dai et al. (2007) expression to profile morphotypes from Travers (2007).
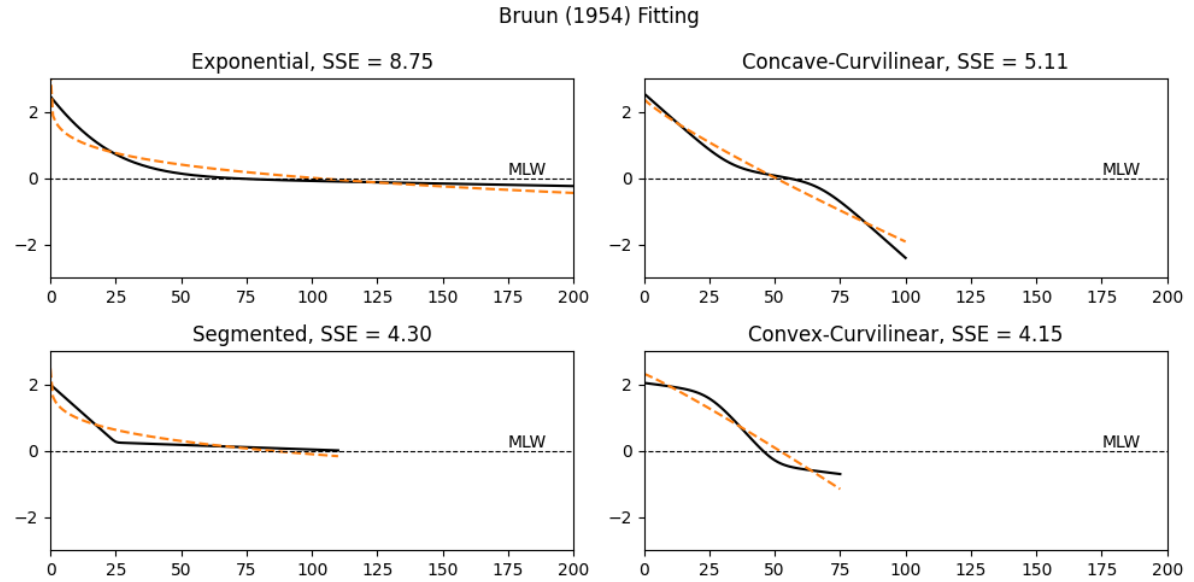
Figure A.7: Fit of Bruun (1954) and Dean (1977) expression to profile morphotypes from Travers (2007).
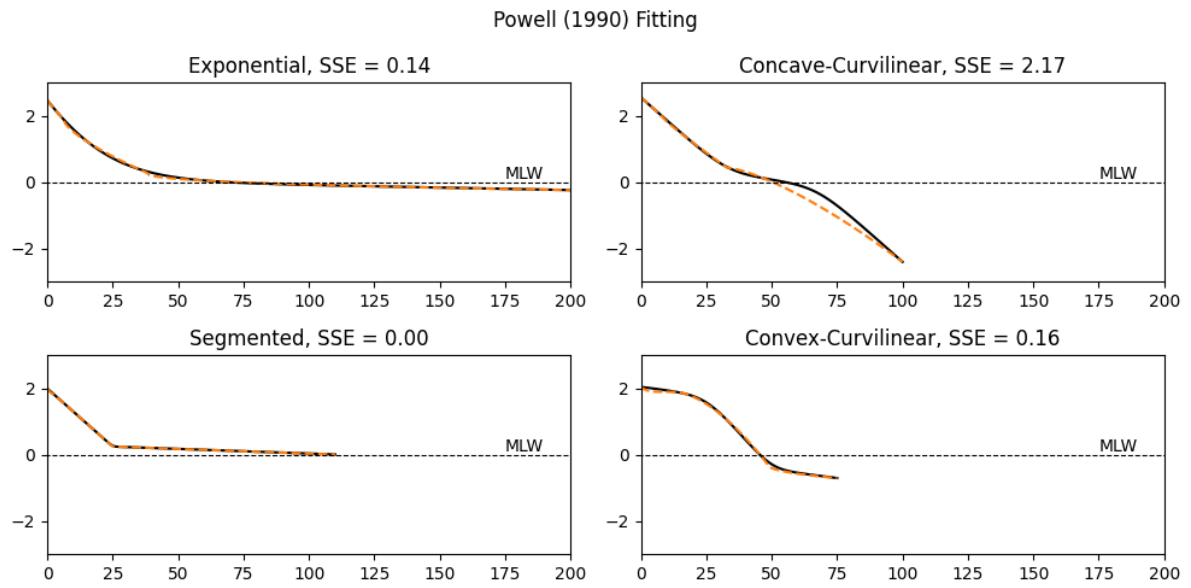
Figure A.8: Fit of Powell (1990) expression to profile morphotypes from Travers (2007).
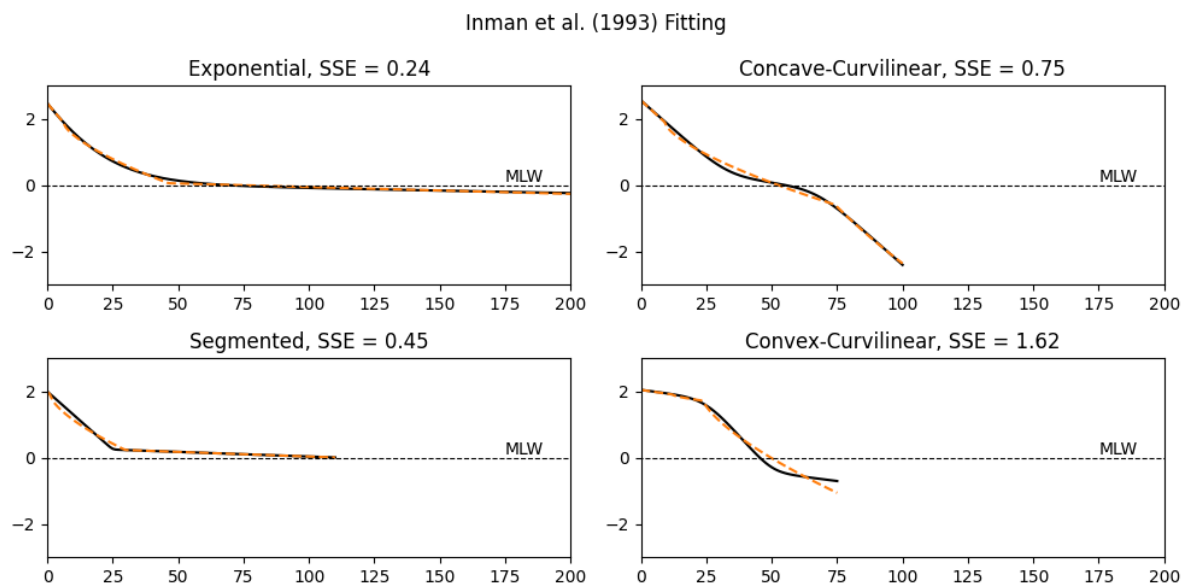

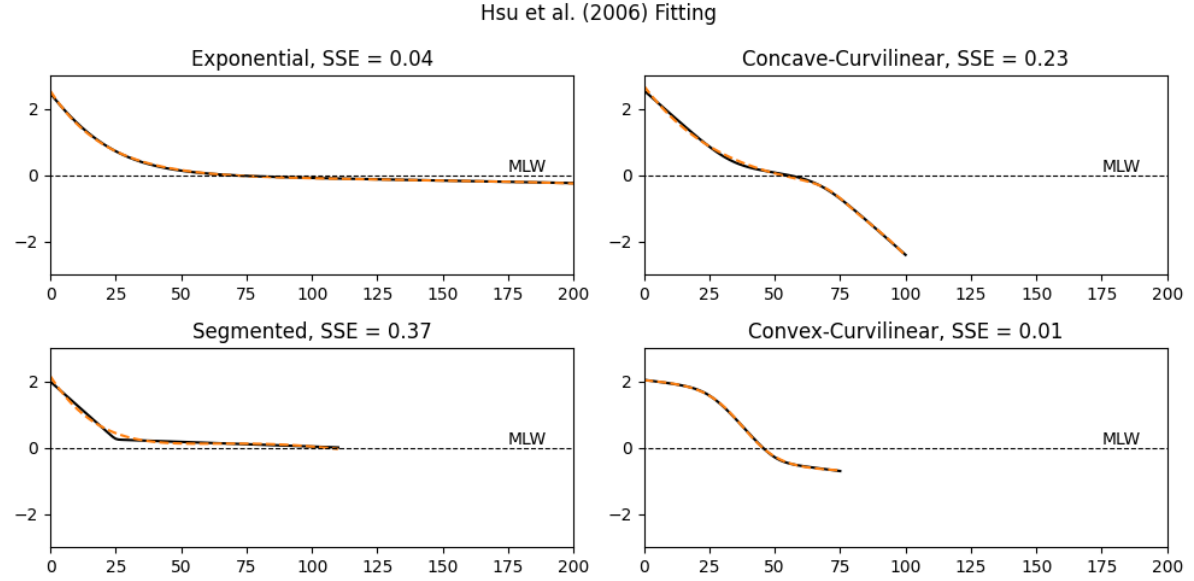**Figure A.9:** Fit of Inman et al. (1993) expression to profile morphotypes from Travers (2007).

Figure A.10: Fit of Hsu et al. (2006) expression to profile morphotypes from Travers (2007).
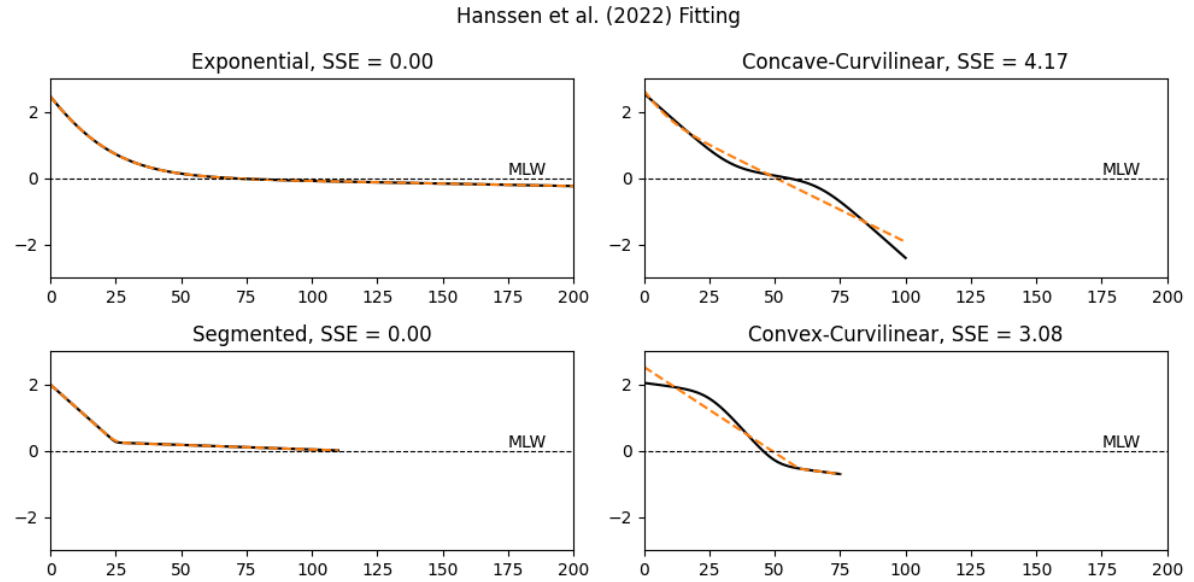

Figure A.11: Fit of Hanssen et al. (2022) expression to profile morphotypes from Travers (2007).
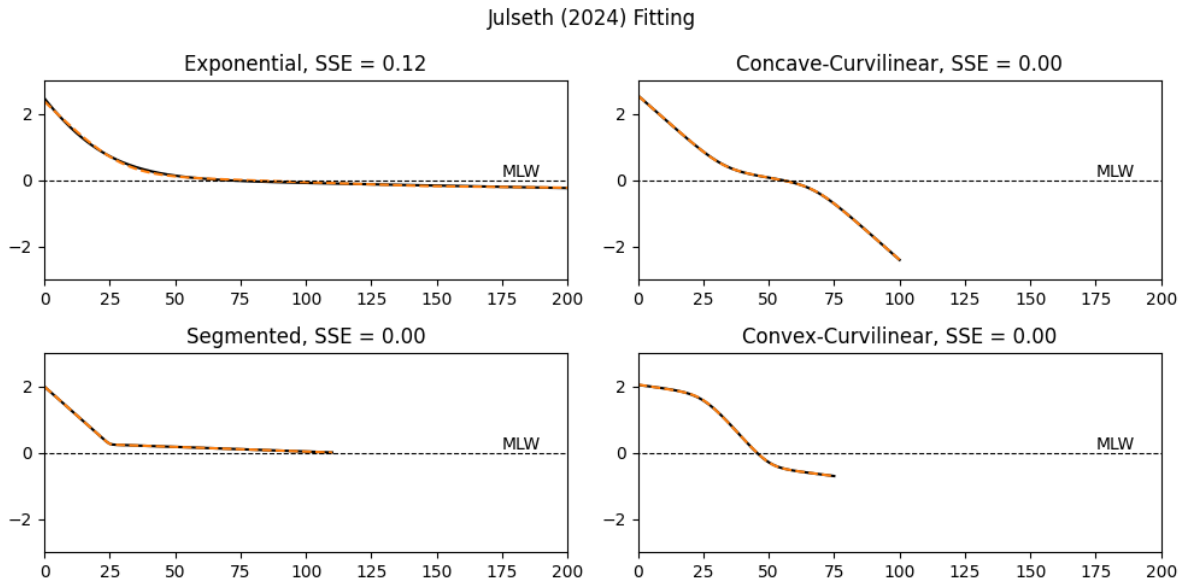
Julseth (2024) Fitting

Exponential, SSE = 0.12

Concave-Curvilinear, SSE = 0.00

Segmented, SSE = 0.00

Convex-Curvilinear, SSE = 0.00

Figure A.12: Fit of Julseth (2024) expression (Section 3.3.1) to profile morphotypes from Travers (2007).

A.3. Profile Characterization

Mild Barred

Mild Unbarred

Steep Barred

Steep Unbarred

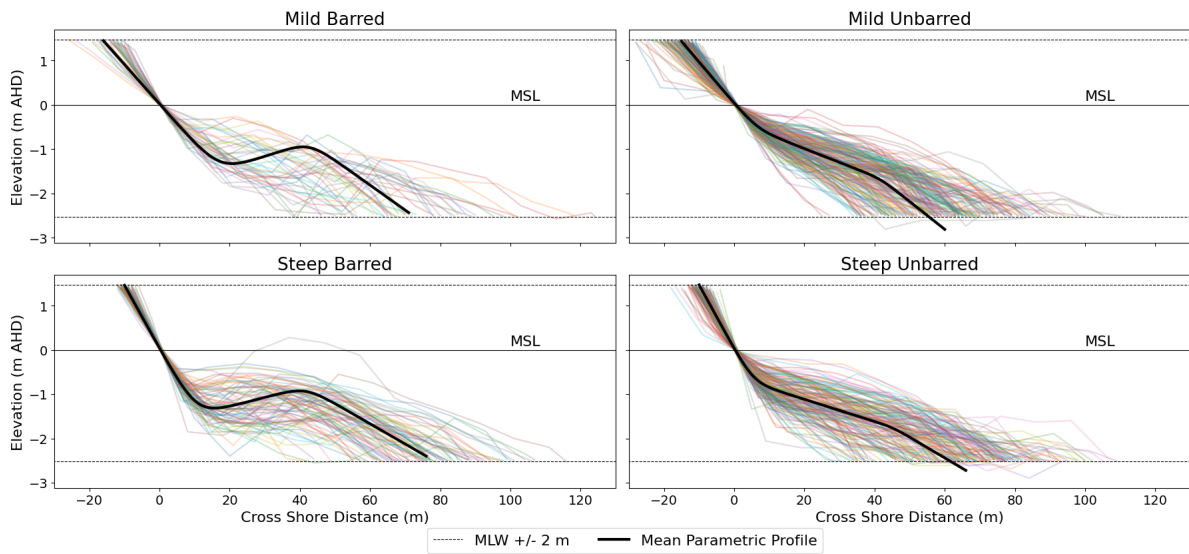······· MLW +/- 2 m ——— Mean Parametric Profile

Figure A.13: Classified measured profiles using the labels defined by the Julseth (2024) parameterization. Coloured lines represent measured profiles, while black bold lines represent the mean parameterized profile associated with each profile class. Labels defined using parameters S_1, z_0, and z_1 following the same rules as in Table 4.2.
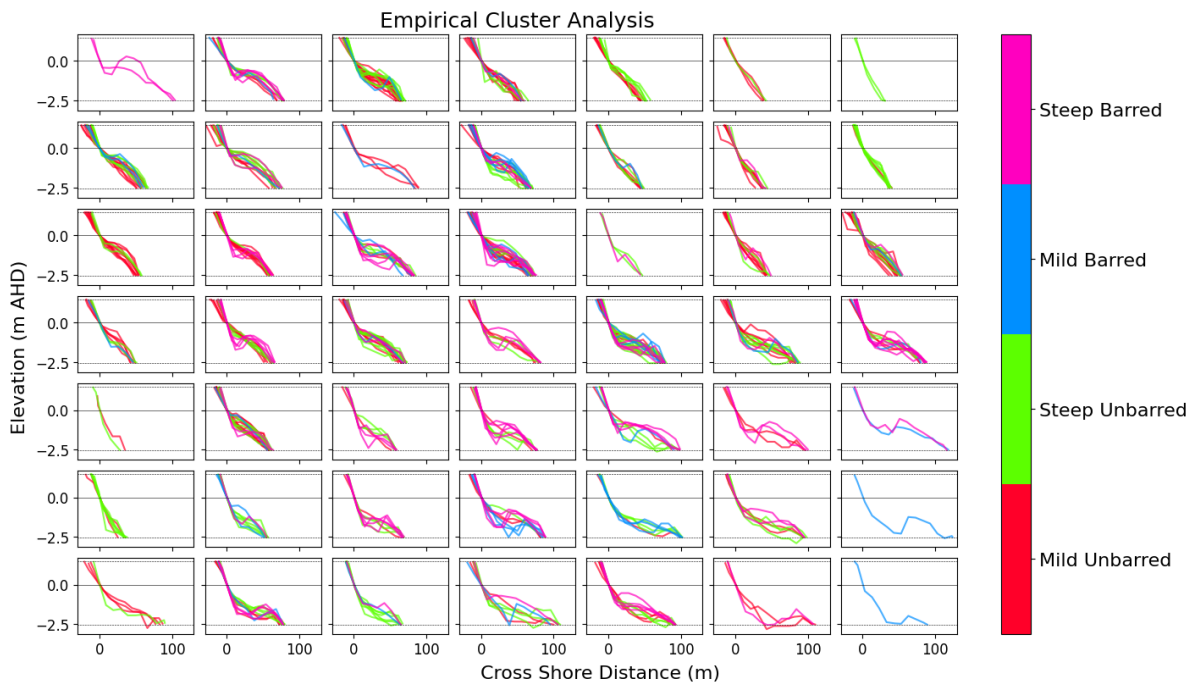
Figure A.14: Measured profiles clustered using empirical measurements, coloured using manual labels.
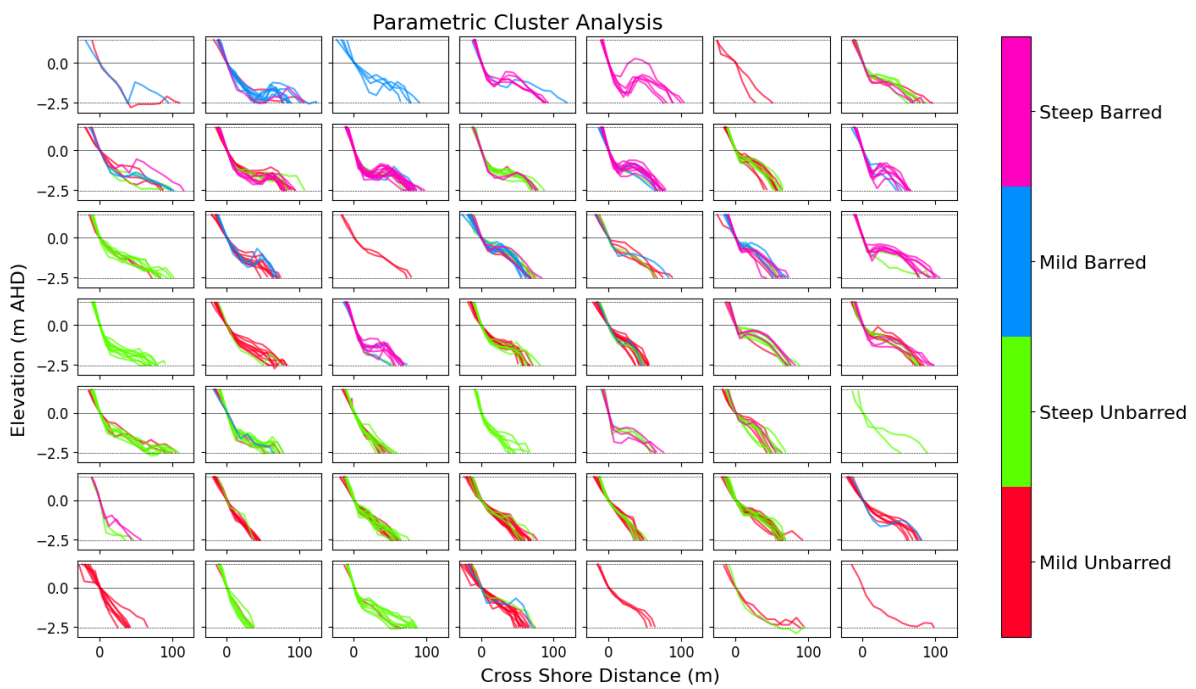

Figure A.15: Measured profiles clustered using parametric representation, coloured using manual labels.
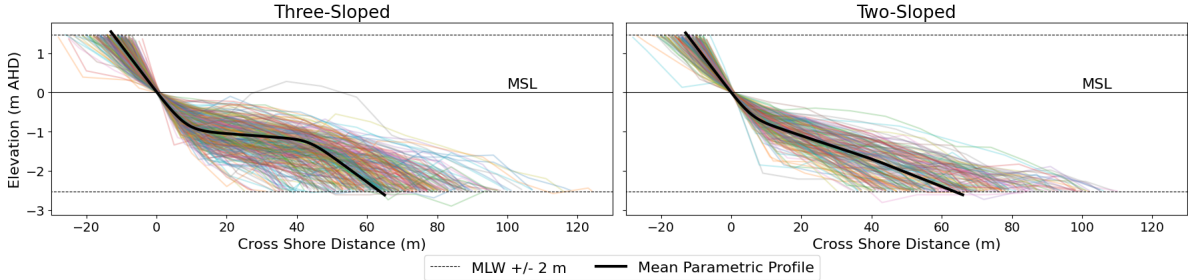
Figure A.16: Classified measured profiles using the labels defined by the Julseth (2024) parameterization. Coloured lines represent measured profiles, while black bold lines represent the mean parameterized profile associated with each profile class. Labels defined using parameters S_2 and S_3, where profiles with less than two degrees of difference between these parameters are classified as two-sloped.
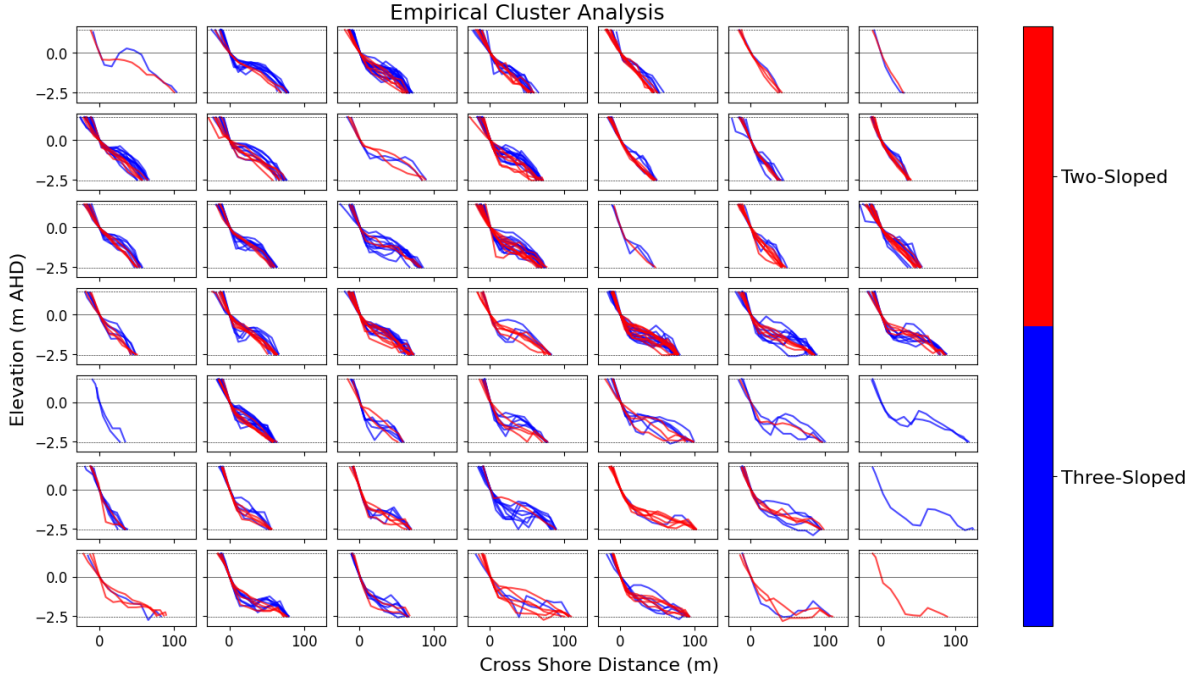

Figure A.17: Measured profiles clustered using empirical measurements, coloured using manual labels.
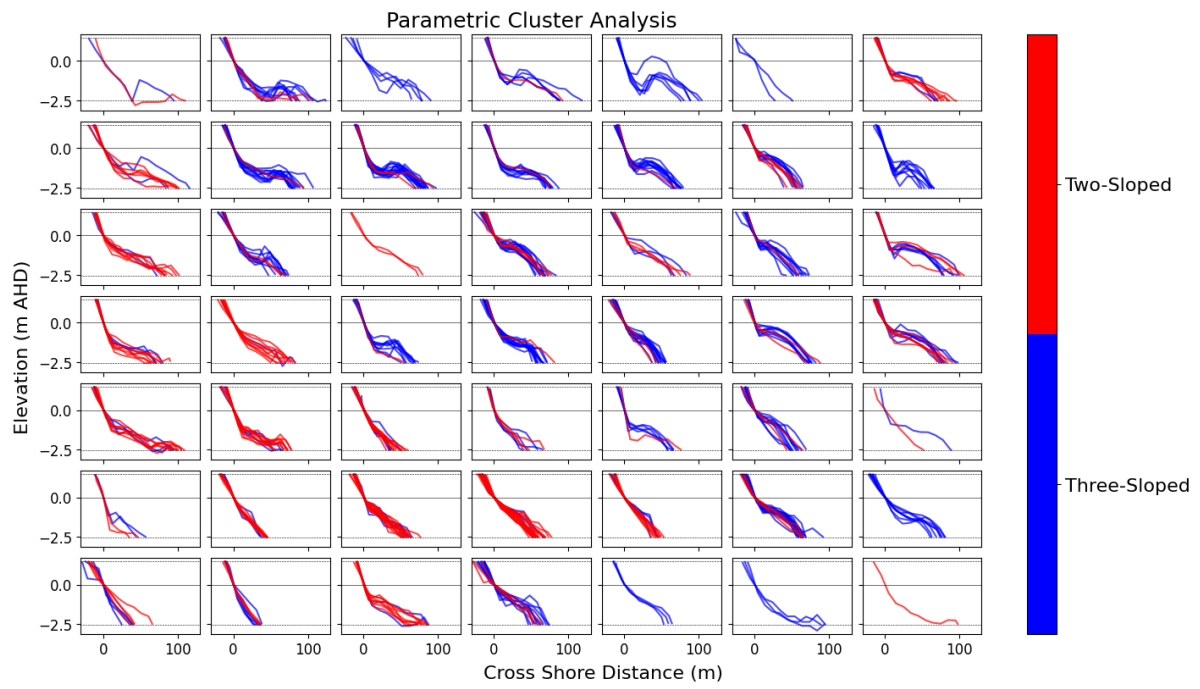
Figure A.18: Measured profiles clustered using parametric representation, coloured using manual labels.

B

Minimization Process

Measured Data
- Cross shore points, X_m
- Measured Elevations $Y_m(x = X_m)$

Parametric Expression
- Predicted elevation, $Y_p=f(\theta, X_m)$
- θ = set of fitting parameters, $[\alpha_1,...,\alpha_i]$
- X_m = cross shore points

Objective Function
- Uses parametric expression to obtain Y_p for some set of θ
- Returns $SSE = \Sigma(Y_m- Y_p)^2$

Initial Guess
- Initial guess for parameters θ

Constraints
- Boundaries: Interval bounds for each parameter α in θ
- Constraints: Bounds for inter-parameter relationships in θ

Minimization Process
- SciPy.optimize.minimize
- Uses Newton-style iteration to minimize the objective function

Optimized Parameters
- Parameters that minimize the objective function
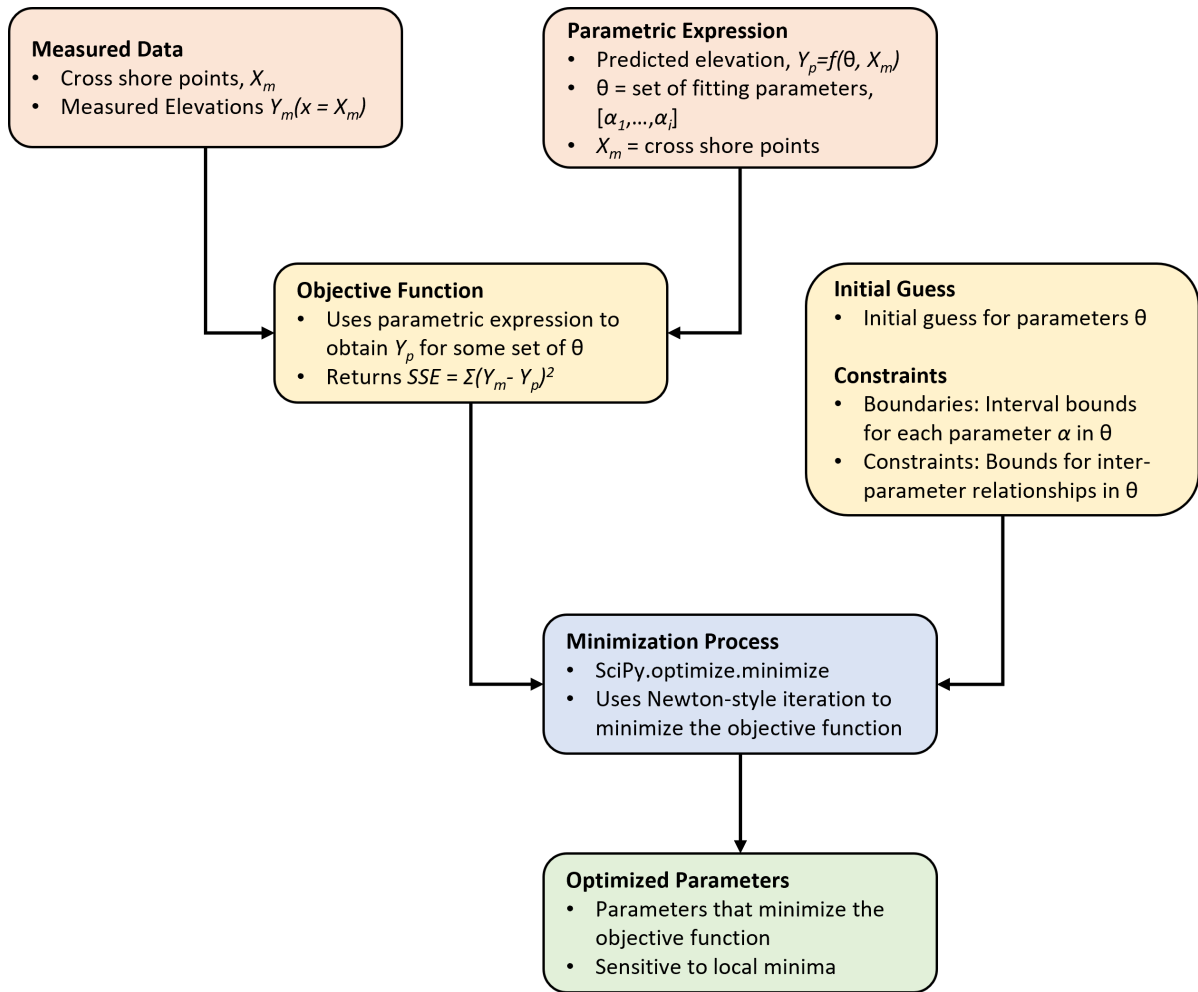- Sensitive to local minima

Figure B.1: An outline of the applied process for parametric expression fitting to profile morphotypes and measured data using minimization.

Table B.1: Applied boundary conditions, constraints, and initial inputs for fitting with each considered parametric expression.

Source	Initial Guess	Boundaries & Constraints
Bruun (1954) and Dean (1977)	$A = 1$ $m = \frac{2}{3}$	$A > 0$ $m > 0$
Powell (1990)	$x_t = xintercept(Y_m)$ $h_t = -1$ $n_1 = 0$ $n_2 = 0$ $n_3 = 0$	$min(X_m) < x_t < max(X_m)$ $min(Y_m) < h_t < 0$ $n_1 > 0$ $n_2 > 0$ $n_3 > 0$ $x_s = xintercept(Y_m)$ $h_s = Y_m(x = 0)$ $x_b = max(X_m)$ $h_b = Y_m(x = max(X_m))$
Inman et al. (1993)	$A_1 = 0.5$ $A_2 = 0.5$ $x_b = xintercept(Y_m) + 1$	$x_b > xintercept(Y_m)$ $x_s = x_b - (\frac{A_1}{A_2}(x_b - S)^m)^{m^{-1}}$ $m = \frac{2}{3}$ $S = xintercept(Y_m)$
Komar and Mc-Dougal (1994)	$m_0 = 0$ $k = 0.1$	$k > 0$
Lee (1994)	$A = 1m$ $B = -1$	$A > 0$ $B < 0$
Hsu et al. (2006)	$A_1 = 1$ $A_2 = 1$ $B_1 = 1$ $B_2 = 1$ $B_3 = 1$ $x_c = \frac{max(X_m)}{2}$ $h_C = Y_m(x = \frac{max(X_m)}{2})$	$-100 < B_2 < 100$
Dai et al. (2007)	$A = 0$ $B = 0$ $C = 0$	$-1 < B < 1$
Hanssen et al. (2022)	$S_1 = 0.1$ $S_2 = 0.1$ $L = \frac{max(X_m)}{2}$ $\delta = \overline{diff(X_m)}$ $z_0 = 1$	$0 < L < max(X_m)$ $\overline{diff(X_m)} < \delta < \frac{max(X_m)}{4}$
Julseth (2024)	$S_1 = 0.1$ $S_2 = 0.1$ $S_3 = 0.1$ $L_0 = \frac{max(X_m)}{4}$ $L_1 = \frac{3max(X_m)}{4}$ $\delta_0 = \overline{diff(X_m)}$ $\delta_1 = \overline{diff(X_m)}$ $z_0 = 1$	$0 < L_0 < max(X_m)$ $0 < L_1 < max(X_m)$ $\overline{diff(X_m)} < \delta_0 < \frac{max(X_m)}{12}$ $\overline{diff(X_m)} < \delta_1 < \frac{max(X_m)}{12}$ $L_1 - L_0 > \frac{\delta_0 + \delta_1}{2}$